RNA binding proteins RBPMS and RBPMS2 regulate alternative splicing and act in ribonucleoprotein granule formation

INAUGURAL-DISSERTATION

zur Erlangung des Doktorgrades der Naturwissenschaften

- Doctor rerum naturalium -

(Dr. rer. nat.)

vorgelegt dem

Fachbereich 08 - Biologie und Chemie der

Justus-Liebig-Universität Gießen

Durchgeführt am Max-Planck-Institut für Herz- und Lungenforschung,

W.G. Kerckhoff-Institut Bad Nauheim

eingereicht von

Shan Lin

(Msc. Biology, Genetics)

(Shandong, China)

Gießen, 2022

Die Untersuchungen zur vorliegenden Arbeit wurden am Max-Planck-Institut für Herz- und Lungenforschung (W. G. Kerckhoff-Institut) in Bad Nauheim unter Leitung von Prof. Dr. Dr. Thomas Braun durchgeführt.

Vom Fachbereich 08 - Biologie und Chemie der Justus-Liebig-Universität Gießen angenommen

Erstgutachter:

Prof. Dr. Dr. Thomas Braun
Abteilung für Entwicklung und Umbau des Herzens
Max-Planck-Institut für Herz- und Lungenforschung
Ludwigstraße 43
D-61231 Bad Nauheim

Zweitgutachter:

Prof. Dr. med. Michael Kracht
Justus-Liebig-Universität Giessen
Biomedizinisches Forschungszentrum Seltersberg (BFS)
Rudolf-Buchheim-Institut für Pharmakologie
3.OG, Raum B322
Schubertstrasse 81
D-35392 Gießen

Ehrenwörtliche Erklärung:

Ich versichere, dass ich meine Dissertation

RNA binding proteins RBPMS and RBPMS2 regulate in alternative splicing and act in ribonucleoprotein granule formation

unter der Leitung von Prof. Dr. Dr. Thomas Braun (Max-Planck-Institut für Herzund Lungenforschung, Bad Nauheim) selbstständig und ohne unerlaubte Hilfe angefertigt und mich dabei keiner anderen als der von mir ausdrücklich angegebener Quellen und Hilfen bedient habe.

Prüfungszwecken gedient.

Gießen,

Shan Lin

Acknowledgements

This research has been performed in the Department I: Cardiac Development and Remodeling at the Max-Planck-Institute for Heart and Lung Research (MPI HLR) in Bad Nauheim, Germany. I was supported by a China Scholarship Council (CSC) fellowship in the first three years and W.G. Kerckhoff-Stiftung fellowship in the following years.

I am grateful for the invaluable opportunity working in such an excellent lab to open the scientific world in my life. First, I would like to thank my supervisor, Prof. Dr. med. Dr. rer. nat. habil. Thomas Braun for all his support in the project processes during my time at MPI HLR. I was deeply supervised and mentored by his outstanding ideas which guidied me to explore different aspects during the research. His open-minded character gave me the opportunity to develop my own views, to solve complicated questions and to open new research fields. I am greatly thanking my PI Dr. rer. nat. André Schneider for his constant help during my work and his suggestions in each stage of the projects, and for patiently discussing with me new experimental results. Thanks to all of my colleagues for providing me the scientific, technological and different knowledge background and supporting me with great enthusiasm. Particular thanks to Marion Wiesnet, Sonja Krüger, Katja Kolditz and Susanne Kreutzer for their technological support. In addition, thanks to Dr. rer. nat. Thomas Kubin, Dr. med. Manfred Richter and Brigitte Matzke from the Kerckhoff Clinic for human diseased heart samples, to Dr. Stefan Günther for RNA-seq and analysis, to Prof. Dr. rer. nat. Christoph Dieterich and Dr. Thiago Britto-Borges (Heidelberg University) for the bioinformatics analysis of alternative splicing, to Dr. rer. nat. Johannes Graumann for Mass Spectrometry analysis. My thanks also go to Silke Kreher for kindly sharing with me the RBM20 mutant mice and Yvonne Eibach sharing with me cultured cardiac bodies. My sincere thanks go to all the members of the Andre Schneider´s Group who have always given me good conversations and supported me in everyday life over the past years. I would like to take this opportunity to thank the other members of my dissertation committee, Prof. Dr. Michael Kracht, Prof. Dr. Katja Sträßer, Prof. Dr. Andreas Krüger, for reviewing my thesis.

Finally, my deepest gratitude goes to my parents and my younger little sister for their greatly confidence of my decision and constantly support me in the past years. I also give thanks for my friends, who gave me the opportunity to get other thoughts and supported me in difficult times. I have a thankful heart for all the things in my life.

Summary

The study reveals that cardiomyocyte (CM) specific ablation of RBPMS and RBPMS2 (RBPMS/2) results in embryonic lethality in conjunction with cardiac malformation. The analysis demonstrates that RBPMS/2 promote alternative splicing (AS), which are essential for heart development and cardiomyocyte identity. Interestingly, overexpression of the dominant isoform RBPMSA induces cardiomyocyte-specific alternative splicing in several non-cardiac tissues. The network of alternative splicing regulated by RBPMS/2 predominantly controls organization and function of the cytoskeleton and sarcomere apparatus, in particular components of M-band and Z-disc, as well as calmodulin binding. Intriguingly, RBPMS/2 deficient cardiomyocytes show multipolar spindle defects and chromosomal mis-segregation, which is causative for an increased frequency of nuclear abnormalities. Furthermore, the study has unraveled that inactivation of a cardiomyocyte specific splicing variant of *Camk2g*, a specific target of RBPMS, results in spindle defects, resembling abnormalities observed in RBPMS/2 double knock out (dKO) cardiomyocytes. In conclusion, the study indicates that RBPMS and RBPMS2 co-regulate alternative splicing in a developmental-stage-specific manner to enable proper sarcomere apparatus and spindle formation.

In addition to the function of RBPMS/2 in alternative splicing, RBPMS operates in the regulation of processing bodies (PBs) and stress granules (SGs) formation in cytoplasm of cardiomyocytes. An interactome screen based on GFP-tagged RBPMS identified interaction partners of the splicing and the RNA stability pathway. Under normal and stress conditions, RBPMS co-localizes with typical RNP-granule markers in the cytoplasm of cardiomyocyte. Inactivation of RBPMS/2 in embryonic cardiomyocyte under physiological conditions results in giant PBs. In contrast, RBPMS/2 deficient embryonic cardiomyocytes fail to form SGs under stress conditions. Furthermore, the formation of RBPMS containing RNP-granules was massively disturbed in DCP1A deficient cardiomyocytes. These results obtained during the course of the study provide first insights in dynamic RNP-granule formation in cardiomyocytes under physiological and pathophysiological conditions.

Zusammenfassung

Die durchgeführte Studie ergab, dass die spezifische Inaktivierung von RBPMS und RBPMS2 (RBPMS/2) in Kardiomyozyten zu einer embryonalen Letalität in Verbindung mit kardialen Missbildungen führt. Es konnte gezeigt werden, dass RBPMS/2 alternative Spleißvorgänge (AS) regulieren, die für die Herzentwicklung und die Kardiomyozyten-Identität wesentlich sind. Interessanterweise führt die Überexpression der RBPMSA-Isoform zu Kardiomyozyten-spezifischen alternativen Spleiß-Veränderungen in verschiedenen nicht-kardialen Geweben. Das durch RBPMS/2 regulierte alternative Spleiß-Netzwerk vermittelt in erster Linie die Organisation und Funktion des Zytoskeletts und des Sarkomer-Apparats, insbesondere Komponenten der M-Banden und der Z-Scheibe-, sowie die Calmodulin-Bindung. RBPMS/2-defiziente Kardiomyozyten zeigten multipolare Spindeldefekte und eine chromosomale Fehlsegregation, die für eine erhöhte Häufigkeit von Kernanomalien verantwortlich ist. Die Studie ergab weiterhin, dass die Inaktivierung einer Kardiomyozyten-spezifischen Spleiß-Variante von Camk2g, einem spezifischen Ziel-Transkript von RBPMS, zu Spindeldefekten führt, vergleichbar den Abnormalitäten in RBPMS/2-defizienten-Kardiomyozyten. Die Studie belegt, dass RBPMS und RBPMS2 alternatives Spleißen auf eine Entwicklungsstadien-spezifische Art und Weise regulieren, um die Ausbildung eines funktionsfähigen Sarkomer-Apparat und mitotischer Spindeln sicherzustellen.

Neben der Funktion von RBPMS/2 in AS wurde entdeckt, dass RBPMS die Bildung von RNP Granula processing bodies (PBs) und Stressgranula (SGs) im zytoplasmatischen Kompartiment von Kardiomyozyten reguliert. Ein Interaktom-Screening auf der Basis von GFP-markiertem RBPMS identifizierte Interaktionspartner des Spleiß-Apparats und des RNA-Stabilitätsweges. Unter normalen und Stressbedingungen ko-lokalisiert RBPMS mit typischen RNP-Granula-Markern im Zytoplasma von Kardiomyozyten. Die Inaktivierung von RBPMS/2 in embryonalen Kardiomyozyten unter physiologischen Bedingungen führt zu stark vergrößerten PBs. Im Gegensatz dazu bilden RBPMS/2-defiziente embryonale Kardiomyozyten im Gegensatz zu normalen Kardiomyozyten unter Stressbedingungen keine SGs. Darüber hinaus ist die Bildung von RBPMS-haltigen RNP-Granula in DCP1A-defizienten Kardiomyozyten massiv gestört. Die Ergebnisse geben erste Einblicke in die dynamische Bildung von RNP-Granula in Kardiomyozyten unter physiologischen und pathophysiologischen Bedingungen.

Table of Contents

Introduction

Post-transcriptional gene regulation

During the past years it has become increasingly apparent that co-transcriptional and post-transcriptional processes play a major role in specifying the transcriptome and proteome of eucaryotes. Regulation can occur at different steps in the life cycle of a mRNA, in particular during splicing, polyadenylation, capping, modification, nuclear export, subcellular transport/localization, translation, and stability (Lipshitz et al., 2017).

These processes are mainly carried out by RNA-binding proteins (RBPs), which can bind specifically to primary RNA sequences as well as to RNA structures, thereby recognizing target mRNAs, recruiting catalytic complexes, and packaging RNA molecules into ribonucleoprotein (RNP) complexes (Balcerak et al., 2019). RBPs not only influence each of these processes, but also interconnect them (Kyburz et al., 2006; Millevoi et al., 2006; Wang et al., 2018a).

Although all RBPs bind RNA, they do so with different RNA-sequence specificities and affinities. This activity is mediated by a relatively small number of RNA binding domains (RBDs), which are further affected by auxiliary domains, regulating interactions of the RBP with other proteins and RNAs. As a result, cells are able to generate numerous RNPs characterized by unique protein and RNA compositions. These RNPs are further remodeled during the course of maturation, export and transport of the mRNA into its functional form. The proper functioning of these complex networks is essential for the coordination of sophisticated post-transcriptional events, which may lead to disease when perturbed (Glisovic et al., 2008). In recent years, numerous proteins lacking conserved RNA binding motifs were identified to bind RNA with low affinity, suggesting an even more dynamic, plastic, and complex function of RNA-protein units (Balcerak et al., 2019).

Different types of RBPs in cardiomyocytes

RBPs comprise a large class of over 2,000 proteins that interact with all types of RNAs in RNA-driven processes (Corley et al., 2020). RBPs typically contain discrete domains which mediate RNA binding. The RNA-recognition motif (RRM), also known as the RNP motif or RNP-type RBD, is the most common and well-studied RNA-binding motif, encompassing an average size of 90 amino acids. It is encoded in a significant number of proteins, involved in almost all aspects of RNA processing and transport. In particular, RRMs are found in virtually all types

of splicing factor families, in single or in multiple copies. RRMs interact with 2–8 nt in single-stranded RNA (ssRNA) commonly through the mode of RNA recognition by RRMs, which involve three aromatic side chains belonging to the two signature sequences of RNP1 and RNP2, and are exposed on the β-sheet surface (Figure 1A) (Maris et al., 2005). The second largest RNA binding domain family is characterized by the K homology (KH) domain, which was first discovered in heterogeneous nuclear ribonucleoprotein K (hnRNPK). The KH domain encompasses 70 amino acids, typically recognizing 4 nt in ssRNA or ssDNA (Valverde et al., 2008).

Many known RRM type RBPs are expressed in cardiomyocyte, including RBM20 (Guo et al., 2012; Li et al., 2013; Maatz et al., 2014), RBM24 (Yang et al., 2014; Liu et al., 2019), muscle blind like splicing regulator (MBNL1) (Dixon et al., 2015; Kalsotra et al., 2008), RBFOX1 and 2 (Wei et al., 2015; Gao et al., 2016), which exert import functions in post-transcriptional processes, in particular alternative splicing.

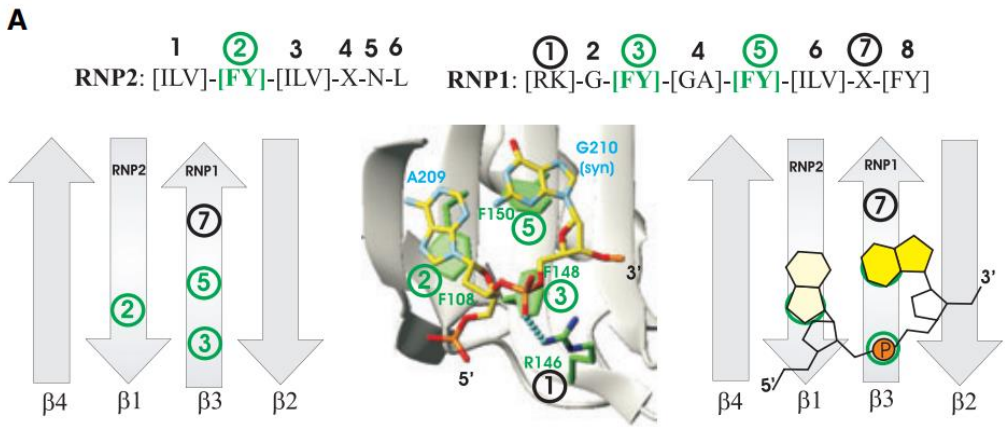

Figure 1. The high versatility of single RRM for mediating interactions with RNA. A. Structure of hnRNP A1 RRM2 in complex with single-stranded telomeric DNA as a model of single-stranded nucleic acid binding (Maris et al., 2005).

RNA splicing

RNA splicing is a post-transcriptional process by which introns, regions of RNA that do not code for proteins, are removed from pre-mRNA and remaining exons are connected to rearrange a single continuous molecule. During this process, newly transcribed precursor messenger RNA (pre-mRNA) transcripts are transformed to a mature mRNA (Chow et al., 2000). Pre-mRNA splicing is executed by the spliceosome, a large and dynamic RNP complex composed of

proteins and small nuclear RNAs (snRNAs), which assembles on pre-mRNA to remove introns. Spliceosome consists of five small nuclear RNAs (snRNAs; U1, U2, U4/U6, or U5), and numerous additional complex-specific proteins (Wahl et al., 2009).

In general, RNA splicing occurs in two different ways, either by constitutive or by alternative splicing (AS). Briefly, constitutive splicing is a process to remove introns from the pre-mRNA, and link the exons together to form a mature mRNA. In contrast, AS is defined as inclusion or exclusion of alternative exons, thereby generating multiple mRNA isoforms from a single pre-mRNA.

Principally, AS encompasses 5 different modes (1) exon skipping, (2) mutually exclusive exon usage, (3) alternative 5´splice site selection, (4) alternative 3´splice site selection, and (5) intron retention (Figure 2A). Exon skipping is the most common form of alternative splicing in higher eukaryotes, where one or more exons (known as cassette exons) and surrounding intronic sequences are included or excluded from a pre-mRNA (Kim et al., 2008). Mutually exclusive exon usage is a specific form of exon skipping, where either one or another exon, but never both, are included in the mature mRNA. Alternative splice site selection can create longer or shorter exons of the same transcript, depending on the usage of different splice acceptor sites at the 5′ end of an exon and splice donor sites at the 3′ end of an exon, respectively. Intron retention represent another form of AS, by which entire or partial intronic sequence will be retained in the mature mRNA transcript. Different AS events can generate multiple proteins with different functions from one primary transcript. First, AS events can occur in the mRNA coding region, thereby altering protein functions, including subcellular localization or posttranslational modifications. Second, AS can install premature stop codons in mRNA isoforms, thereby causing degradation of these isoforms by the nonsense-mediated mRNA decay (NMD) pathway (Lewis et al., 2003). Finally, AS events can occur in 5′ or 3′ untranslated regions (UTRs), which can alter mRNA stability, microRNA accessibility, and mRNA localization.

Beside alternative splicing, two other processes also can generate multiple mRNA transcripts from a single pre-mRNA: alternative polyadenylation and alternative first exon usage (or alternative promoter usage; Figure 2B). Approximately 70% of all human genes generate alternative mRNA isoforms, which differ in length at the 3′ end by a process called alternative cleavage and polyadenylation (Derti et al., 2012). Alternative polyadenylation altered 3´UTR

are differential recognized by microRNAs, thereby fine-tuning protein abundance (Mayr and Bartel, 2009).

Alternative splicing creates diverse mRNA transcripts (isoforms) from a single pre-mRNA to increase transcriptome and proteome diversity. Next-generation-sequencing technologies revealed that the vast majority of mRNAs (>95%) are subjected to alternative splicing (Wang et al., 2008). Disruption of normal alternative splicing patterns can cause or modify human diseases (Faustino and Cooper, 2003).

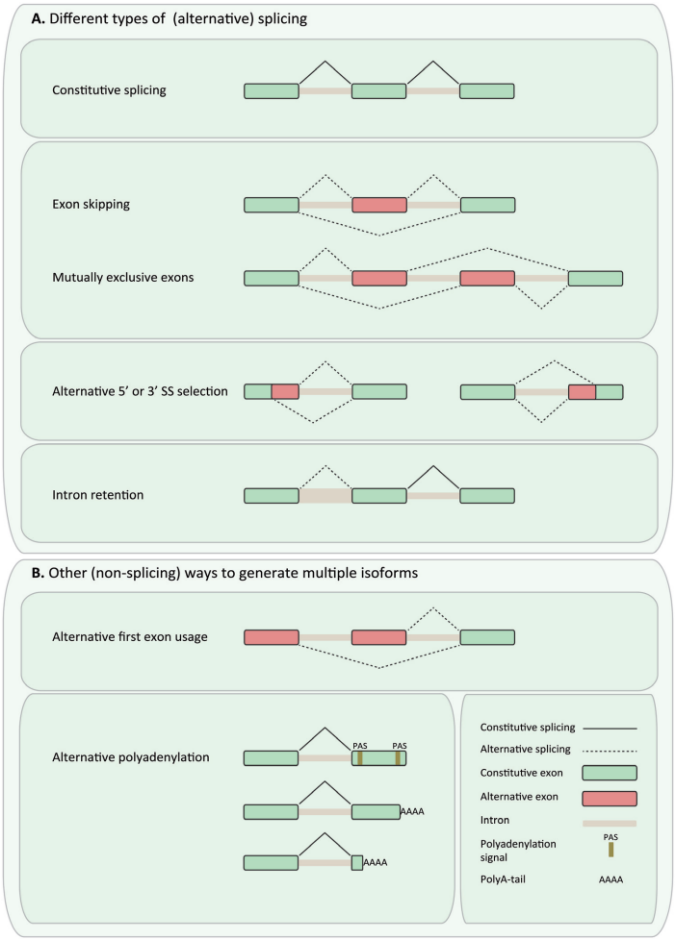

Figure 2. Different types of alternative splicing. A. Different types of (alternative) splicing are depicted. Constitutive splicing is the process of intron excision and exon joining of the majority of all exons in the genomic order. Exon skipping is the inclusion or exclusion of one or more exons (known as cassette exons). Cassette exons can be mutually exclusive. Alternative 5′ or 3′ splice site (SS) selection results in shortened or elongated exons. Intron retention retains part of an intron in the mature mRNA. **B**. Additional ways to generate multiple different mRNA transcripts from a single gene are alternative first exon usage and alternative polyadenylation (van den Hoogenhof et al., 2016).

Regulation of splicing

The extent to which mRNA is either constitutively or alternatively spliced also depends on the usage of strong and weak splice sites. Strong splice sites generally result in constitutive splicing, which are always recognized by the spliceosome. Usage of weak splice sites depends on additional parameters such as splice site sequence, splice site position, and bound splice factors. For example, cis-regulatory sequences known as intronic splicing enhancers, intronic splicing silencers, exonic splicing enhancers, and exonic splicing silencers can be bound by trans-acting RBPs, which in turn recruit spliceosomal components (van den Hoogenhof et al., 2016). Furthermore, numerous tissue-specific RBPs have been described to regulate tissue-specific alternative splicing events (Long and Caceres, 2009).

Alternative splicing (AS) in heart development and postnatal remodeling

Formation of the mammalian heart involves manifold biological signaling, cellular interactions, specification of myocardial progenitor cells, and complex morphological processes like heart tube looping, trabeculation and septation. In particular, transition from fetal to the neonatal circulation is a multiplexed process, accompanied by alteration of physiological, anatomical, and biochemical changes in the cardiovascular system. Postnatal remodeling is mainly mediated by transcriptional and posttranscriptional networks. Developmental mediated AS transitions occur to a greater extent in the heart than in many other tissues. Changes in the generation of alternative isoform that occur before and after birth are particularly important for the adaption of the fetal heart to birth and adult life (Olson, 2006).

Alternative splicing of cardiac troponin T (cTnT; TNNT2) is an important event during heart development and maturation. In the embryonic heart, exon 5 of *Tnnt2* is predominantly included in mRNAs but excluded in the adult heart (Cooper and Ordahl, 1985). Exon 5 inclusion makes embryonic TNNT2-containing myofibrils more sensitive to calcium compared to adult TNNT2 myofibrils lacking exon 5. Depending on the inclusion or exclusion of exon 5, contractile properties of embryonic myocardium differ compared to adults (Godt et al., 1993; McAuliffe et al., 1990). Besides *Tnnt2*, myomesin (*Myom1*) (Schoenauer et al., 2011), titin (*Ttn*) (Lahmers et al., 2004), and LIM domain-binding 3 (*Ldb3*; *Cypher*) (Huang et al., 2003) also play important roles during heart development.

Systematic analysis of alternative splicing during heart development using exon arrays identified multiple AS events, which were associated with enriched motifs for the splicing factors CELF and muscle blind-like splicing regulator (MBNL). Strikingly, CELF expression

decreases during cardiac development, whereas abundance of MBNL increases. Furthermore, inactivation of MBNL in the adult heart results in a shift towards an embryonic splicing pattern (Kalsotra et al., 2008).

Recently, Wang and colleagues investigated genome-wide AS transitions in fetal and adult human hearts (Wang et al., 2016). Here, alternative splicing alterations occurred mainly in protein-coding genes rather than in long non-coding RNAs, among which more than 40% of fetal-specific AS events show significant difference between fetal and adult hearts. Intron retention occurs predominantly in fetal compared to adult hearts, suggesting that this splicing type may affect processes in heart development. Furthermore, alterations in AS in the transition from fetal to adult stage are enriched in cell proliferation and energy-metabolism pathways (Wang et al., 2016).

Aberrant AS results in cardiac diseases

Mutations in RBPs, in particular trans-acting splicing factors as well as cis-acting elements (splicing sites) can result in aberrant AS events, thereby causing cardiac diseases. Several reports suggested, that approximately 60% of all disease-causing mutations results in splicing abnormalities caused by mutations in splice sites or splicing-associated genes (Lopez-Bigas et al., 2005; Pagani and Baralle, 2004; Wang and Cooper, 2007).

Additional reports indicated that the fetal cardiac gene program can be re-expressed in cardiac overload-induced hypertrophy, thereby reconstituting transcriptional features of the embryonic heart (Barry et al., 2008; Olson, 2006; Rajabi et al., 2007). These genes play essential roles in heart development, and mainly function in metabolic and contractile processes of the heart, which are regulated by key transcription factors (Oka et al., 2007; Taegtmeyer et al., 2010). Park and colleges described that the fetal RNA splicing program, accompanied by global mRNA isoform alterations has a major impact on cardiac hypertrophy-induced reactivation of the fetal cardiac gene program (Park et al., 2011). These mRNA isoform alterations result in the expression of protein isoforms encoding protein domains, which are important for adaptation of heart functions under pressure overload (Park et al., 2011). Strikingly, the failing adult heart undergoes a titin isoform transition, characterized by an increase in the fraction of the fetal titin isoform N2BA (Makarenko et al., 2004; Nagueh et al., 2004; Neagoe et al., 2002). Furthermore, re-expression of fetal EH-myomesin is a characteristic feature of dilated cardiomyopathy (DCM) and failing heart, which coincides with a switch in titin isoforms during DCM, suggesting an underlying adaptive program (Schoenauer et al., 2011).

RBPs regulated AS events in heart failure

In recent years, several RBP-regulated AS events have been implicated with heart failure, which includes functions of SC35, ASF/SF2, RBM20 and RBM24. Ding and colleagues described that cardiomyocyte (CM)-specific inactivation of a splicing factor results in heart failure. Embryonic CM-specific inactivation of the SR splicing factor component SC35 caused onset of DCM around 5 weeks of birth, whereas CM-specific postnatal loss of SC35 does not result in DCM like phenotype, suggesting indispensable function in embryonic but not in adult CMs (Ding et al., 2004; Xiao et al., 2007). Similarly, CM-specific knockout of the SR protein family member alternative splicing factor 2 (ASF/SF2) results in the development of DCM by week 6 after birth and rapid progression in heart failure, accompanied by mis-splicing of functionally important genes including calcium/calmodulin dependent kinase II delta (*Camk2d*), *Tnnt2* and *Ldb3*. ASF/SF2 deficient CMs become hypercontractile due to *Camk2d* mis-splicing, resulting in mis-targeting of the kinase to sarcolemma membranes, thereby causing severe excitation contraction coupling defects (Xu et al., 2005).

RNA-binding motif protein 20 (RBM20) is a vertebrate-specific RNA-binding protein encoding two zinc finger (ZnF) domains, one RRM-type RNA-binding domain and an arginine/serine (RS)-rich region. RBM20 mutation causes an early onset of a clinically aggressive form of DCM (Brauch et al., 2009; Li et al., 2010). RBM20 is one of the most frequently mutated genes in DCM (Haas et al., 2015). Studies in human and rodent CMs revealed that RBM20 regulates a large network of AS events by repressing exon inclusion in key regulators of cardiac excitation–contraction coupling such as *TTN*, *CAMK2D*, and ryanodine receptor 2 (*RYR2)* through binding to a UCUU consensus motif in adjacent introns. Specifically, RBM20 regulates AS events of genes involved in calcium handling genes including *Camk2d*, *Ryr2* and calcium voltage-gated channel subunit alpha 1C (*Cacna1c*). Heterozygous loss of *Rbm20* in mice is sufficient to induce a shift in *Camk2d* isoforms, which leads to aberrant calcium handling in cardiomyocytes and increased pro-arrhythmic Ca^{2+} release from the sarcoplasmic reticulum (Guo et al., 2012; Maatz et al., 2014; van den Hoogenhof et al., 2018).

RBM24 represents an RNA-binding protein encoding a single RRM domain. Our group identified RBM24 as a major regulator of muscle-specific splicing during heart and skeletal muscle development (Yang et al., 2014). *Rbm24* knockout mice are embryonic lethal, displaying multiple cardiac malformations, including ventricular septum defects, reduced

trabeculation and compaction, and dilated atria. Specifically, sarcomeres are almost completely lost in RBM24 deficient cardiomyocytes, indicating a crucial role of RBM24 in sarcomerogenesis and heart development, which is in line with analysis of zebrafish RBM24 mutant (Poon et al., 2012). RBM24 regulates multiple splicing events, in particular exon inclusions, which indicate that RBM24 acts a splicing activator. RBM24 splicing targets such as *Naca*, *Fxr1*, *Abcc9*, *Slc25a3*, *Usp25*, and *Usp28*, function in cardiac development and sarcomerogenesis, which strongly suggests that dysregulated AS are causative for cardiac malformations and lack of sarcomerogenesis in RBM24 deficient hearts (Yang et al., 2014). In addition, postnatal RBM24 ablation results in mis-regulated splicing, including *Tnn*, leading to a rapid onset of DCM and postnatal lethality (Liu et al., 2019).

Recruitment of RBPs and function in RNP granule formation

Generation of mature mRNAs requires coordinated processes, including pre-mRNA splicing, 5′-capping and 3′-polyadenylation, followed by subsequent transport to the cytoplasm for translation. In the cytoplasmic compartment, mRNAs are associated with the protein synthesis machinery, which occurs at sites relatively far away from the nucleus (Hermesh and Jansen, 2013). mRNAs are not homogenously distributed throughout the cytoplasm. In neurons, mRNAs are transported to axons and dendrites for local protein synthesis (Gumy et al., 2014). During this process, translation is repressed and mRNAs are protected from degradation (Kindler et al., 2005).

Emerging evidence suggests that liquid–liquid phase separation (LLPS) is instrumental for formation of membraneless organelles in eukaryotic cells. Multivalent macromolecular interactions can mediate transition of proteins into another phase, characterized by different physiochemical properties, essentially creating membraneless organelles (Banani et al., 2017; Wang et al., 2018b). These structures are described as bodies, puncta, granules, droplets, and condensates. As a consequence, membraneless organelles exhibit higher protein density, thereby increasing the rates of biochemical reactions (Bergeron-Sandoval et al., 2016; Shin and Brangwynne, 2017). According to the subcellular localization, condensates are grouped into cytoplasmic and nuclear-localized condensates, where they exert multiple roles in various cellular processes (Wang et al., 2021).

RNP granules are microscopically visible, non-membrane bound compartments formed by RNA molecules and RNA-binding proteins. RNPs have been observed in nuclear and cytoplasmic compartment in all kinds of cells types. Nuclear RNA granule structures (known as nuclear bodies, NBs) include the Cajal bodies, paraspeckles and nuclear speckles.

Furthermore, cytosolic stress granules (SGs) and processing bodies (PBs) contain polyadenylated mRNAs and RNA-related enzymes. SGs are induced under cellular stress conditions in which translation is inhibited and composed of preinitiation complexes and functional mRNAs that can reenter polyribosomes. In contrast, PBs also exist under normal conditions and contain decapping and deadenylation factors as well as RNA exonucleases, mediating mRNA decay (Kedersha et al., 2005). Intriguingly, SG-inducing stress conditions can also initiate a hyperassembly of paraspeckles (An et al., 2019), suggesting a cross-talk between both types of RNP granule (Figure 3).

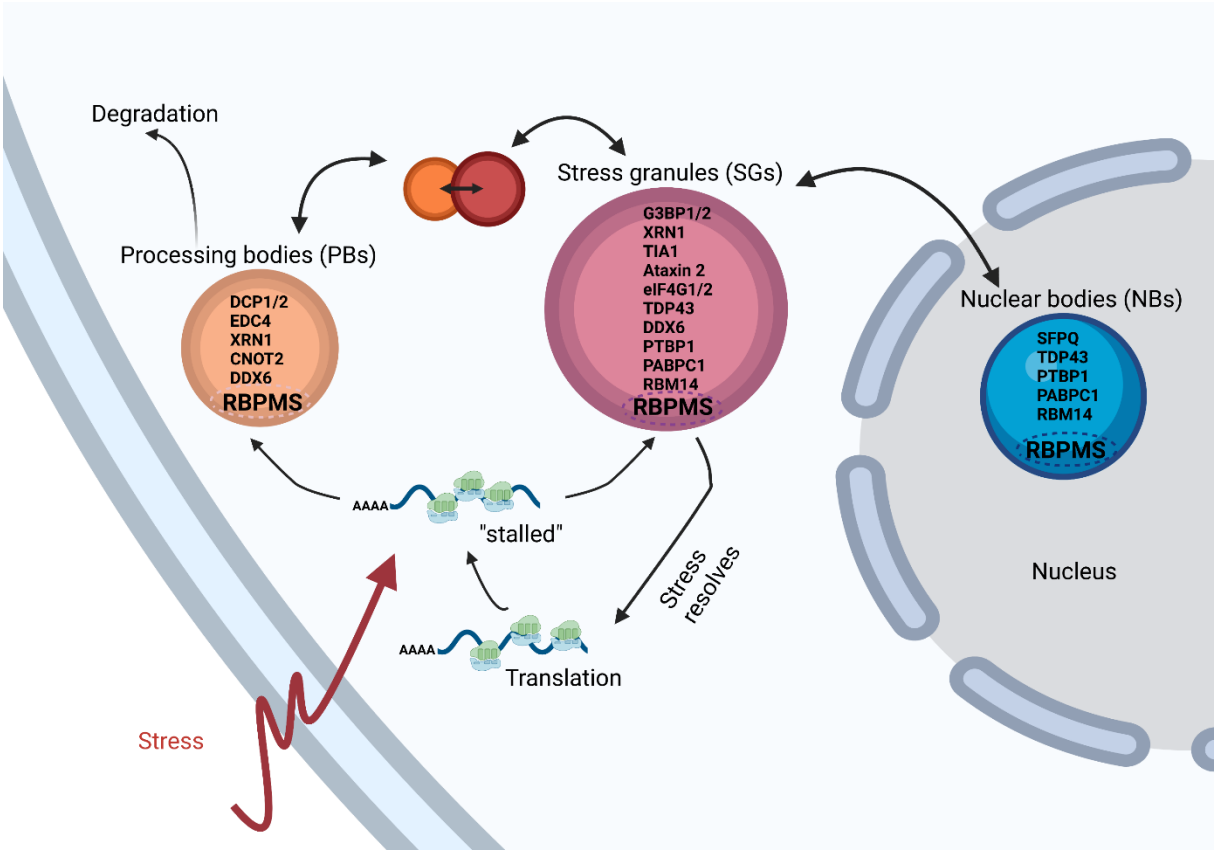

Figure 3. Significant overlap between components of PBs, SGs and NBs. Under cellular stress conditions, the mRNAs can be sequestered to SGs in an RBP-dependent reversible process. Throughout their life-cycle, mRNAs are associated with multiple RBPs, latter act in more than one aspect of post-transcriptional gene regulation, thereby contributing to the complex temporal and spatial regulation of eukaryotic gene expression (An et al., 2019; Li et al., 2013; Zhou et al., 2014). This figure was created with the help of Biorender.

PBs contain RNA processing components such as the RNA decapping machinery (Parker and Sheth, 2007). Canonical mRNA decay is initiated by the removal of the 5′ Cap structure of the mRNA, mediated by the protein-decapping complex, which contains several PB-specific

proteins, e.g. mRNA decapping enzyme subunits 1a or 2 (DCP1A or DCP2, respectively), enhancer of mRNA-decapping protein (EDC3 and EDC4) and one protein – DDX6 – shared with SGs. Knock down of classical PB components decreases the formation of constitutive and stress-induced PBs (Anderson et al., 2015; Ayache et al., 2015; Ohn et al., 2008).

In contrast, SGs contain translation-associated factors and mRNAs. Combined immunofluorescence and RNA FISH in SGs revealed multiple components of the translation initiation complex – e.g. eIF4G1 and poly (A)-binding protein cytoplasmic 1 (PABPC1, hereafter referred to as PABP) (Kedersha et al., 2002; Kedersha et al., 2005). SG-forming RBPs include, among others, Ras GTPase-activating protein-binding protein 1 and 2 (G3BP1 and G3BP2) (Tourriere et al., 2003), T-cell-restricted intracellular antigen-1 and TIA1-related protein (TIA1 and TIAL1, respectively; hereafter referred to as TIA1/R) (Gilks et al., 2004).

Neurodegenerative diseases including Alzheimer's disease, frontotemporal lobar degeneration (FTLD) and amyotrophic lateral sclerosis (ALS) are characterized by pathological protein aggregates that contain core SG-nucleating proteins, such as TIA1/R and G3BP1 (Ash et al., 2014; Vanderweyde et al., 2012). Furthermore, mutations in the RNA-binding proteins TAR DNA-binding protein 43 kDa (TDP-43) and FUS drive pathogenesis of these disorders (Johnson et al., 2009). In degenerating neurons and glia of ALS patients, TDP-43 is depleted from the nucleus and accumulates in large cytoplasmic aggregates. TDP-43 also undergoes several disease-specific posttranslational modifications, including hyperphosphorylation, ubiquitination, and cleavage (Kwon et al., 2007). Intriguingly, many SG and PB associated RNA-binding proteins harbor prion-like domains. For example, TIA1 encodes a prion-like domain that drives SG assembly (Gilks et al., 2004; King et al., 2012).

Recently, dysregulated RNP granules have also been linked to heart failure. Genome-edited pigs homozygous for the pathogenic R636S mutation of human RBM20 develop accumulation of abnormal RNP granules in the sarcoplasm. Dysregulated sarcoplasmic RBM20 RNP granules undergo a liquid–liquid phase separation process and dock along cytoskeletal elements. These results link dysregulated RNP granules to myocardial cellular pathobiology and heart failure in patients with DCM caused by RBM20 mutation. However, detailed analysis of RNP forming processes mediated by mutations of additional RBPs in cardiomyocytes are required to gain deeper insights into molecular mechanisms driving pathogenic RNP granules accumulation resulting in heart failure (Schneider et al., 2021).

Functional analysis of RBPMS family in the myocardium

In total, approximately 400 RBPs have been identified in cardiomyocytes and their functions remain to be explored (Liao et al., 2016). The **R**NA-**b**inding **p**rotein with **m**ultiple **s**plicing (RBPMS) family encodes 2 family members, RBPMS and RBPMS2, which contain a single RNA recognition motif (RRM). Human and mouse RBPMS orthologues exist in multiple proteins isoforms, which are generated by alternative splicing, whereas RBPMS2 is primarily expressed as a single isoform (Shimamoto et al., 1996). Precise RNA recognition element for RBPMS has been defined as tandem CAC segments separated by a spacer of ~1–12 nt, which was also confirmed in corresponding orthologues from Drosophila (Couch Potato) and C. elegans (MEC-8) (Farazi et al., 2014; Ray et al., 2013; Soufari and Mackereth, 2017). Biophysical analysis revealed that the RRM domain of RBPMS forms a symmetrical dimer and thereby binds individually to an entire CAC segment in the RNA bound state (Soufari and Mackereth, 2017; Teplova et al., 2016). A previous study indicated that MEC-8 regulates splicing of *Unc-52* in C. elegans (Lundquist et al., 1996). In addition, RBPMS was found to be a key splicing factor regulating multiple alternative splicing events in smooth muscle cells (SMCs) (Nakagaki-Silva et al., 2019).

During embryonic development, RBPMS is specifically expressed in the developing heart (Gerber et al., 1999). Previous studies in zebrafish indicated that RBPMS2 deficiency causes cardiac stress (Grajevskaja et al., 2018; Kaufman et al., 2018). Very recently, RBPMS has been reported to regulate AS of *Pdlim5*, among multiple other splicing events. Constitutive loss of RBPMS results in a switch of *Pdlim5* isoforms, resulting in pre-mature binucleation and non-compaction cardiomyopathy in a B6C3F1 genetic background (Gan et al., 2022).

Additional studies in HEK293 cells indicated, that RBPMS and RBPMS2 re-localize under oxidative stress conditions to cytoplasmic SGs (Farazi et al., 2014). Furthermore, RBPMS promotes mRNA decay in cytoplasmic PBs by binding CNOT2, a component of CCR4-NOT deadenylation complex (Rambout et al., 2016). RBPMS and RBPMS2 are highly conserved (Shimamoto et al., 1996), which suggests potentially overlapping functions.

The study mainly pursued the following questions:

(i) Exert RBPMS and RBPMS2 fully or partially overlapping functions?
(ii) What are the phenotypic and molecular alterations in mice lacking RBPMS/2?
(iii) Do RBPMS/2 promote cardiac specific alternative splicing events?

(iv) What are the direct RBPMS/2 targets during heart development?

(v) Which is the predominant RBPMS isoform involved in alternative splicing?

(vi) Which molecular functions executed by RBPMS are critical for heart development and function?

(vii) What is the contribution of RBPMS for RNP granule formation, in particular PBs and SGs under normal and cardiac stress conditions?

Material and methods

Material

Table 1 Chemicals and reagents

Chemical	**Company**	**Catalog no.**
Agarose	Carl Roth	2267
Bis-Tris	AppliChem	A1025,0500
Bovine serum albumin (BSA)	Fisher Scientific	BP 1605
DAPI (4', 6-diamidino-2-phenylindole)	ThermoFisher SCIENTIFIC	D1306
Dimethyl sulfoxide (DMSO)	SIGMA-ALDRICH	D-4540
Disodium hydrogen phosphate (Na2HPO4)	Merck	6580.05
1,4-Dithiothreit (DTT)	Carl Roth	6908.2
EDTA	Carl Roth	8040.3
Ethanol (100 %)	Carl Roth	9065.4
Ethidium bromide solution (1 %)	AppliChem	A1152,0100
FSC 22 Frozen Section Compound	Leica	75806-668
Fetal calf serum (FCS)	SIGMA-ALDRICH	F2442
Gelatin from porcine skin	SIGMA-ALDRICH	G1890
Glucose	Carl Roth	X997.2
Glutaraldehyde	SIGMA-ALDRICH	G5882
Glycerin (87 %)	Merck	1.04094.2500
Hydrochloric acid (37 %)	Carl Roth	4625.1
InstantBlue Protein Stain	Expedeon	ISB1L
Isopropanol	Carl Roth	6752.4
Liberase™	Roche	5401151001
Methanol	Carl Roth	4627.5
Nonidet P40	Fluka	74385
Paraformaldehyde	Carl Roth	335.4
Penicillin-Streptomycin (10,000 U/mL)	ThermoFisher SCIENTIFIC	15140122
Phenylmethylsulfonyl fluoride (PMSF)	SIGMA-ALDRICH	P7626
Potassium chloride (KCl)	Carl Roth	6781.3
Potassium bicarbonate (KHCO3)	Merck	1.04854.0500
Potassium dihydrogen phosphate (KH2PO4)	Carl Roth	P018.1
SDS	Carl Roth	2326.3
Skim milk	Fluka	70166
Sodium bicarbonate (NaHCO3)	Merck	1.06329.0500
Sodium chloride (NaCl)	Carl Roth	3957.2
Sucrose	Carl Roth	9097.1
TEMED	Carl Roth	2367.1
Tris	Carl Roth	5429.2
Triton-X 100	Carl Roth	6683.1

TurboFectTM Transfection Reagent	ThermoFisher Scientific	R0531
DharmaFECT 2 Transfection Reagent	Dharmacon	T-2002-01
Tween-20	Merck	822184.05
Xylol	Carl Roth	9713.3

Table 2 List of enzymes and their appropriate reagents

Enzyme	Company	Catalog no.
Proteinase K	Carl Roth	7528.2
0.1 M DTT *	Invitrogen	P/N y00147
T4-DNA-Ligase	Promega	M1801
2 xRapid Ligation-Buffer *	Promega	C6711
Taq Polymerase	Homemade	
REDTaq® ReadyMix™ PCR Reaction Mix	Sigma-Aldrich	R2523
PrimeScript RT Enzyme Mix	Takara	#RR047A
5X PrimeScript Buffer 2 (for Real Time	Takara	#RR047A
RT Primer Mix	Takara	#RR047A
collagenase B	Roche	11088807001
collagenase D	Roche	11088858001
Trypsin-EDTA	Sigma	T4174
Trypsin	Sigma	T0303
EcoR I	Jena Bioscience	EN-113S
10x universal Buffer *	Jena Bioscience	EN-300

Table 3 Buffer solutions

Buffer	**Composition**
Embryonic cardiomyocytes isolation enzymbuffer 10x	8.0 g NaCl; 2.0 g Glucose; 0.2 g KCl; 5.75 mg NaH2PO4xH2O (or 5.0 mg NaH2PO4); 1.0 g NaHCO3 in 100 ml PBS, pH 7.4
Embryonic cardiomyocytes isolation E-cryomix	250 mg Pankreatin; 0.85 g NaCl in 100 ml H2O, 0.2 um filtration, aliguots at -20 ° C
Embryonic cardiomyocytes isolation enzymbuffer complete	A: Predigestion 50 ml Enzymbuffer 1x; 1 m BDM (2.5g/50 ml); 10 ml E-cryomix B: Digestion 50 ml Enzymbuffer 1x; 1 m BDM; 10 ml E-cryomix; Liberase (0.7 ml/25 ml)

Embryonic cardiomyocyte cell culture medium	DMEM 4.5g; 10 % FCS; 1 % P/S; 0.1 % NEAA
Cardiomyocyte isolation calcium-free buffer	113 mmol L-1 NaCl; 4.7 mmol L-1 KCl; 0.6 mmol L-1 KH2PO4; 0.6 mmol L-1 Na2HPO4; 1.2 mmol L-1 MgSO4 x 7H2O; 12 mmol L-1 NaHCO3; 10 mmol L-1 KHCOS; 10 mmol L-1 HEPES; 30 mmol L-1 taurine; 10 mmol L-1 2,3-butanedionemonoxime; 5.5 mmol L-1 glucose
Cardiomyocyte isolation enzyme buffer	0.25 mg·mL-1 Liberase™ DH; 0.14 mg·mL-1 trypsin; 12.5 µmol L-1 CaCl2 in calcium-free buffer
Cardiomyocyte isolation stop buffer 1	10% FCS; 12.5 µmol L-1 CaCl2 in enzyme buffer
Cardiomyocyte isolation stop buffer 2	5 % FCS; 12.5 µmol L-1 CaCl2 in enzyme buffer
Cardiomyocyte cell culture medium	M199 cell culture medium supplemented with 5 mmol L-1 creatinine x H2O; 2 mmol L-1 L-carnitine x HCl; 5 mmol L-1 taurine; 25 mmol L-1 HEPES; 1 % penicillin/streptavidin; 10% fetal calf serum; 1% insulin-transferrin-sodium selenite media supplement, pH 7.3.
Electron Microscopy fixation buffer	1.5 % glutaraldehyde; 1.5 % paraformaldehyde in 0.15 mol L-1 HEPES
Immunofluorescence blocking buffer	2 % FCS; 2 % BSA in 1x PBS
Mass Spec Buffer A	0.1 % formic acid
Mass Spec Buffer B	80 % acetonitrile; 0.1 % formic acid
5 % Immunoblot blocking solution	Dilute 5 g skim milk in 100 mL 1 x TBS-T

10 x PBS, pH 7.4	Dilute 80 g NaCl; 2 g KCl; 14.4 g Na2HPO4; 2.4 g KH2PO4 in 800 mL Aqua dest.; adjust pH to 7.4; refill to 1000 mL with Aqua dest.
1 x PBS, pH 7.4	100 mL 10x PBS + 900 mL Aqua dest.
5 % BSA	Dilute 5 g APS in 100 mL 1 x TBS-T
10 % APS	Dilute 10 g APS in 100 mL Aqua dest.
10 % SDS	Dilute 10 g SDS in 100 mL Aqua dest.
Extraction buffer	100 mmol L-1 Tris-HCl, pH 8.0; 10 mmol L-1 EDTA; 10% SDS
RIPA lysis buffer, pH 8.0	50 mmol L-1 Tris, pH 7,4; 150 mmol L-1 NaCl; 1 % NP-40; 0.5 % sodium deoxycholate; 0.1 % SDS; protease inhibitors (2 mg mL-1 aprotinin, 2 mg mL-1 leupeptin, 1 mol L-1 Na3VO4, 1 mol L-1 NaF, 0.2 mol L-1 PSMF)
Lysis buffer, pH 7.5	20 mM Tris/HCl; 100 mM NaCl; 1 mM EDTA; 1 % NP-40 add Milli Q H2O
Dilution buffer, pH 7.5	20 mM Tris/HCl; 100 mM NaCl; 1 mM EDTA add Milli Q H2O
50 x TAE	Dilute 242 g Tris Base; 57.1 mL acetic acid; 100 mL 0.5 mol L-1 EDTA, pH 8.0 in 1000 mL Aqua dest.
10 x TBS, pH 7.6	0.2 mol L-1 Tris, 1.4 M NaCl
1 x TBS	100 mL 10 x TBS + 900 mL Aqua dest.
1 x TBS/T	100 mL 10 x TBS + 900 mL Aqua dest. + 0.1 % Tween®20
TENS lysis buffer	1 mol L-1 Tris/HCl, pH 8.0; 0.5 mol L-1 EDAT, pH 8.0; 4 mol L-1 NaCl; 20 % SDS

10 x TE	100 mmol L-1 Tris-Cl; 10 mmol L-1 EDTA, pH 8.0
1 x TE	100 mL 10 x TE + 900 mL Aqua dest.
20 x Transfer buffer	Dilute 163.2 g Bicine; 209.6 g Bis-Tris; 12 g EDTA in 1000 mL Aqua dest.
1 x Transfer buffer	250 mL 20 x transfer buffer; 1000 mL methanol; 3750 mL Aqua dest.
1 M Tris, pH 6.8	Dilute 12.1 g Tris in 80 mL Aqua dest.; adjust pH to 6.8; refill to 100 mL with Aqua dest.
1.5 M Tris, pH8.8	Dilute 18.17 g Tris in 80 mL Aqua dest.; adjust pH to 8.8; refill to 100 mL with Aqua dest.

Table 4 Primers used for genotyping

Primer	Sequence
RBPMS1 loxP-for	5'-GCC CCT TTG CTC TTT AGG AGA-3'
RBPMS1 loxP-rev	5'-CCC AGT TTC GAC TTT CCT GAA CC-3'
RBPMS2 loxP-for	5'-CTCAGGTTAACTGCTGGCATGG-3'
RBPMS2 loxP-rev	5'-TCACACTCCTGGTTTCCTCCAG-3'
Cre-for	5'-TAA ACT GGT CGA GCG ATG GAT TTC C-3'
Cre-rev	5'-CAT ATC TCG CGC GGC TCC GAC ACG G-3'
aMyHC-Cre-for	5'-CAG GCA CTT TAC ATG GAG TCC TG-3'
aMyHC-Cre-rev	5'-AGG CTA AGT GCC TTC TCT ACA C-3'
Rosa-CAGG-for	5'-CTT GCT CTC CCA AAG TCG CTC TGA G-3'
Rosa-CAGG-rev	5'-ACC GTA AGT TAT GTA ACG CGG AAC TCC-3'
Rosa-WT-rev	5'-CTT TAA GCC TGC CCA GAA GAC TCC C-3'
DCP1A loxP-for	5'-GGT AGT GGA GGG AGA CAG TAG TTG AG-3'
DCP1A loxP-rev	5'-GTGAGTCACACTTCTGCCACACTGG-3'

Table 5 Genotyping protocols

PCR	Primer	Program	Fragment size
RBPMS1 loxP	RBPMS1 loxP-for	95°C 5:00	Wildtype 160bp
	RBPMS1 loxP-rev	95°C 0:30	Transgene 260bp
		57°C 0:30	
		72°C 0:30	
		Go to 2, repeat 35x	
		72°C 5:00	

		12°C ∞	
RBPMS2 loxP	RBPMS2 loxP-for RBPMS2 loxP-rev	95°C 5:00 95°C 0:30 57°C 0:30 72°C 0:30 Go to 2, repeat 35x 72°C 5:00 12°C ∞	Wildtype 250bp Transgene 400bp
Cre	Cre-for Cre-rev	94°C 4:00 94°C 0:30 63°C 0:30 72°C 0:45 Go to 2, repeat 35x 72°C 5:00 12°C ∞	Transgene 244bp
aMyHC-cre	aMyHC-for aMyHC-rev	94°C 5:00 94°C 0:30 55°C 0:30 72°C 0:70 Go to 2, repeat 36x 72°C 5:00 12°C ∞	Transgene 1000bp
ROSA-CAGG	ROSA-CAGG-for ROSA-CAGG-rev ROSA-wt-rev	94°C 3:00 94°C 0:30 57°C 0:30 72°C 0:30 Go to 2, repeat 35x 72°C 5:00 12°C ∞	Wildtype 249 bp Transgene 325 bp
DCP1A-loxP	DCP1A loxP-for DCP1A loxP-rev	94°C 4:00 94°C 0:30 63°C 0:30 72°C 0:30 Go to 2, repeat 35x 72°C 5:00 12°C ∞	Wildtype 300bp Transgene 370bp

Table 6 TaqMan assay qRT-PCT probes

Name	Assay ID	Species
Acta1	Mm00808218_g1	Mouse
Acta2	Mm00725412_s1	Mouse
Nppa	Mm01255748_g1	Mouse
Nppb	Mm01255770_g1	Mouse

Table 7 Antibodies

Primary antibodies			
Primary antibodies for immunoblotting			
Primary antibody	Dilution	Catalog no.	Company
anti-GAPDH	1:1000	2118	Cell Signaling
anti-RBPMS	1:1000	HPA056999	Sigma
anti-DCP1a	1:1000	WH0055802M6	Sigma
anti-DDX6	1:1000	H00001656-M01	Abnova
Secondary antibodies for immunoblot analysis			
Secondary antibody	Dilution	Catalog no.	Company
goat-anti-mouse IgG, HRP	1:1000	31430	ThermoFisher
goat-anti-rabbit IgG, HRP	1:1000	31460	ThermoFisher
Primary antibodies for immunofluorescence staining			
Primary antibody	Dilution	Catalog no.	Company
anti-α-tubulin	1:1000	T6074	Sigma-Aldrich
anti-G3bp	1:1000	ab56574	Abcam
anti-RBPMS	1:1000	HPA056999	Sigma
anti-DCP1a	1:1000	WH0055802M6	Sigma
anti-DDX6	1:1000	H00001656-M01	Abnova
anti-a-sarc.- Actinin	1:1000	A7811	Sigma
anti-Camk2g	1:1000	SAB1400039	Sigma
Cardiac Troponin I Polyclonal antibody (Rabbit / IgG)	1:1000	21652-1-AP	Proteintech
Troponin T Polyclonal Antibody, FITC Conjugated	1:500	bs-10648R	Biossusa
anti-Phalloidin-FITC	1:1000	P5282	Sigma
Anti-Cardiac Troponin T antibody	1:500	ab105439	Abcam
Secondary antibodies for immunofluorescence staining			
Secondary antibody	Dilution	Catalog no.	Company
Goat anti-Mouse IgG (H+L) Cross-Adsorbed Secondary Antibody, Alexa Fluor 488	1:1000	A-11001	ThermoFisher
anti-rabbit Cy3	1:400	711-165-152	Dianova
anti-mouse Cy5	1:400	715-175-150	Dianova

Table 8 Composition of gel electrophoresis 9 % Bis-Tris Polyacrylamid gel (PAA)

Separation gel:	**9%**
Rotiphorese® Gel 30 (37.5:1) (Roth, 3029.1)	2.1 mL
3.5 x bis-Tris pH 6.5 – 6.8	2 mL
Milli-Q H2O	2.9 mL
10 % Ammoniumperoxodisulfat (APS – Merck, 1.01201)	25 µL

TEMED (Roth, 2367.1)	7 µL
Stacking gel:	**5%**
Rotiphorese® Gel 30 (37.5:1) (Roth, 3029.1)	0.29 mL
3.5 x bis-Tris pH 6.5 – 6.8	0.5 mL
Milli-Q H2O	0.96 mL
10 % Ammoniumperoxodisulfat (APS – Merck, 1.01201)	8 µL
TEMED	3 µL

Table 9 Ready to use buffer solution

Buffer			Company	Catalog no.
NuPAGE™ Running Buffer	MES	SDS	ThermoFisher SCIENTIFIC	NP000202
NuPAGE™ Running Buffer	MOPS	SDS	ThermoFisher SCIENTIFIC	NP000102
TaqMan™ Expression Master Mix		Gene	Applied Biosystems™	10525395

Table 10 Marker

Marker	Company / Composition
Protein Marker VI (10 - 245) prestained BC	PanReac AppliChem
PUC Marker	Homemade

Table 11 Primers for isoforms

Name	Exon	Sequence
Camk2d	14-15-16	F> CGAGAAATTTTTCAGCAGCC
		R1< CTCAGTTGACTCCTTTACCCC
		R2<GCTCTCAGTTGACTCCATCATC
		R3<ACAGTAGTTTGGGGCTCCAG(Xu et al. 2005)
Camk2g	14-15	F>CCTCACAACCATGCTTGTCTCCAGGAA
		R<TCTTCGTGTAGGCCTCAAAGTCCCCAT
Ldb3	4 or 5-6-7	F> AGTCCCCGCTGCCAGTG
		R<AGAGGCGCTGTCCACCG (Xu et al. 2005)
Tpm2	6a	CATTGAAAACCGGGCCATGAAGG
		GGGCTTCCAGGGATTTCAAGTTG
	6b	CTTCGAACCATGGACCAAGC

		AAGAGAGGAGAGAAAGGGGC
Popdc2	5' AS	CAACCACCAACTTTCCCGTG
		TGGGATCTGGACATAACTTGAGA
Bnip3l	6	GACCACAGCTCTCAGTCAGA
		TCACAGGCCACACGAATTTC
Map3k7	12	CTTCCGAGGGCAAGAGGATGAGTG
		CATTCTGACACTAGGGCTGGATGACC
Mfn2	3	GGGCCAACCTGGACCTGAATCAGCA
		CACTTCAGCCATGTGTCGCTTATCC
Sptan1	51	CAAGCTGCGCCAAGAATTTG
		GTTCCCGACTCTTCCACCAT
Sbf2	29	TCAGAAACTCAGAGGCAGCAGTAC
		GGATGTCGGGGAGCTGATCAAACG
Myo9a	27	CCTCAAGCCCACAAACAAGATG
		CTCCTTGTTTCCCTTTGGCCCAG
St7	7	GATCATCTTCGCCCTGCAGATGC
		CGCCAAGAGAATGTACGCAGTTG
Arhgap21	7	CCTGGAGCTCAGTGTAATGCCCA
		GATGGCAACCAGGGATAGCAAAC
GYK	5	CCATTGGTGTCAGCAACCAGAGG
		AGTAGACTGGGTTCTTAGGTCA
Pdlim7	5 or 6	CAGCCTGTTCAGAGCAAACCACA
		GCCAGTCTTCGGTATCCTCCATC
Mlf1	3	AACCTCTTGGAAGAGACTTGCTCAG
		TTGCCATCATCCGATCCATTGTCTG
Tnnt2	5	GGAGGTGGTGGAGGAGTACGAGGA
		GTCTCAGCCTCACCCTCAGGCTCA (Dixon et al.2005)
Myom1	18	CATGGACTGACGACTGCTCAGAGC
		CTGCATCGCTGACGGCCTTGATG (Dixon et al.2005)
Mini-reporters		CCACCATGGATTACAAGGATGACGACG
		GAGATCCATTGTGCTGGGGCGCG

Methods

Transgenic mice

Animal experiments involve in this study were performed in full agreement with institutional guidelines and with approval of the Committee for Animal Rights Protection of the State of Hessen (B2/1125). All animals were housed in individual ventilated cages accompanied with environmental enrichment under sterile appropriate conditions in the Animal House Facility of Max Planck Institute for Heart and Lung Research, Bad Nauheim, Germany. For individual

experiments age-matched littermates were used as controls. The number of animals used in each experiment is label in the corresponding figure legends.

Generation constitutive RBPMS/2 deletion mouse

The constitutive *RBPMS*-lacZ knock out allele was generated by an in-frame fusion of a LacZ-LoxP-PGK-neo-LoxP cassette to exon 4 of RBPMS (ENSMUSE00000210994) using homologous recombination, thereby generating a targeted deletion of RBPMS.

The constitutive *RBPMS2*-lacZ knock out allele was generated by an in-frame insertion of a LacZ-LoxP-PGK-neo-LoxP cassette in the second coding exon of RBPMS2 (ENSMUSE00000532570) using homologous recombination, thereby generating a targeted deletion of RBPMS2.

Generation of mice with cardiomyocyte-specific RBPMS/2 deletion

Conditional RBPMS/2 mutant mice (*RBPMS*$^{flox/flox}$ / *RBPMS2*$^{flox/flox}$) carrying Exon 1 flanked by loxP sites, which disrupts all isoforms of RBPMS and RBPMS2. The crossing of conditional RBPMS/2 mutant mice with deleter mouse strain carrying cell-type specific Cre-recombinase resulted in nonfunctional RBPMS/2 protein in a cell-type specific manner. Conditional, Cre-recombinase mediated RBPMS/2 deletion in cardiomyocytes was achieved by cross-breeding of *RBPMS*$^{flox/flox}$ / *RBPMS2*$^{flox/flox}$ with either XMLC2-Cre (Breckenridge et al., 2007) or αMyHC-Cre (Agah et al., 1997; de Lange et al., 2004) deleter mouse strains to facilitate deletion in early embryonic stage (E7.5) or late embryonic stage (E9.5) cardiomyocytes, accordingly. Heterozygous mice were crossed to obtain homozygous embryos for analysis. Genotyping was performed by PCR using primers (Table 4 and 5). The global deletion of RBPMS was tested by using primers For-CGCCTCGCCTCCTCGGTCTC and Rev-GCTCTCGGGGCTTGATGTCCAG (Product size 332bp).

Conditional overexpression (OE) of RBPMSA tagged by GFP

Transgenic mice conditionally overexpressing RBPMSA isoform in the myocardium were generated in house, using a modified ROSA26 targeting locus by which the SA-site of pBigT was replaced by a synthetic CAG promoter (Srinivas et al., 2001). RBPMS cDNA was amplified from RNAs extracted from embryonic hearts and cloned into the pBigT-CAG vector. The generated pBigT-CAG-RBPMSA-GFP cassette was cloned in PacI and AscI site of the pRosa26-PA construct. The final construct was electroporated into V6.5 F1 hybrid ES cells and

targeted stem cell clones were selected by G418 treatment and screened by Southern blotting with 5' genotyping by EcoRV. Positive ES cell clones were injected into C57BL/6 (B6) blastocysts. Mice carrying the targeted allele were genotyped by PCR as described in Table 4 and 5.

Extraction of genomic DNA from mouse tails

The mouse-tail or ear notches were digested in 500 µL TENS-buffer (Table 3) with 5 µL Proteinase K (10 mg/mL Proteinase K; Roth) at 56°C overnight. The next day, the samples were centrifuged at 14000 rpm for 10 min and decanted into a new tube containing 500 µL isopropanol. Genomic DNA was precipitated by inverting the tubes. After centrifugation at 14,000 rpm for 20 min, supernatants were removed, and the genomic DNA-containing pellets washed in 500 µL 70% ethanol, followed by centrifugation at 14,000 rpm for 5 min. Genomic DNA was air dried at RT for 1-2 h, resuspended in 300 µL sterile 1x TE buffer, and dissolved by incubation at 56°C overnight. Genotyping PCRs were performed with self-designed primers, as indicated in Table 4 using appropriate cycling conditions (Table 5).

Polymerase Chain Reaction and genotyping protocols

Polymerase chain reaction (PCR) was performed using extracted genomic tail DNA, to determine corresponding genotypes. Blue taq PCR Reaction Mix (Vazyme) were used for total 25 µL reaction system. The master mix using for one PCR reaction was prepared as followed:

Reagent	Volume
Blue PCR Reaction Mix	12 µL
Primer 1 (for)	0.5 µL
Primer 2 (rev)	0.5 µL
ddH2O	11 µL
Genomic DNA	1.0 µL
	25 µL

PCR products were loaded on a 1-2% agarose gel (LE Agarose, Biozym, 840004), supplemented with ready-to-use ethidium bromide solution, and separated by TAE (Tris-acetate- EDTA) buffer (Table 3) depending on the size of the gel. Double-stranded DNA was visualized under UV light and gels were imaged using a BioDoc analyzer (BioDocAnalyze - Biometra).

RNA isolation and reverse transcription (RT)-PCR

RNA from embryonic hearts or cultured cell was extracted utilizing the Direct-zol™ RNA Kit according to the manufacturer's protocol and subsequently 1µg RNA was revere transcribed into cDNA using PrimeScript™ RT reagent Kit (Takara, Cat. #RR037A) as followed:

Reagents	Volume	Final conc
5X PrimeScript Buffer (for Real Time)	2 µl	1X
PrimeScript RT Enzyme Mix I	0.5 µl	
Oligo dT Primer (50 µM)*1	0.5 µl	25 pmol
Random 6 mers (100 µM)*1	2 µl	200 pmol
total RNA		
RNase Free dH2O		
Total	10 µl	

Reaction mixture was incubated at 37°C for 15 min*3 (Reverse transcription), thereafter reverse transcriptase was inactivated by heat treatment at 85°C for 5 sec and cDNA was stored at -80°C before usage. PCRs were performed using 50ng cDNAs as template combined with corresponding oligonucleotides (Tabel 11) to detect different mRNA splicing isoforms.

TaqMan® Gene Expression Assays for quantitative real-time polymerase chain reaction

To do quantitative real-time polymerase chain reaction (qRT-PCR), the synthesized cDNA (from last step) was used for TaqMan® Gene Expression Assays (Applied Biosystems) using specific TaqMan probes (Table 6) combined with a StepOnePlus Real-Time PCR System.

The master mix for one qRT-PCR reaction was prepared as followed:

Reagents	Volume
TaqMan™ Gene expression master mix	5.0 µL
TaqMan™ gene specific probe (FAM-dye)	0.5 µL
TaqMan™ gapdh probe (VIC-dye)	0.5 µL
cDNA (diluted 1:100)	4.0 µL
	10 µL

Thermocycler condition was used as followed:

Steps	Temperature (°C)	Time	Number of cycles
1	50	2 min	
2	95	10 min	

1	95	15 sec	40x
2	60	1 min	

Each sample run was performed in technical triplicates. The calculated fold changes (RQ-values) of the examined samples were based on the $\Delta\Delta$Ct values and normalized to *Gapdh* as an internal house-keeping control.

RNA-seq analysis

In summary, total RNA was extracted from three biological replicates of RBPMS/2 double knockouts mediated by XMLC2-Cre and αMyHC-Cre, respectively for RNA-seq. Isolated hearts were lysed with TRI-reagent and total RNA purified by Direct-zol purification column (Zymo Research) followed by DNase treatment to avoid contamination by genomic DNA. RNA and library preparation integrity were verified by Labchip GX Touch (Perkin Elmer).

Library preparation of early heart samples using *RBPMS*$^{flox/flox}$ */ RBPMS2*$^{flox/flox}$ / *XMLC2-Cre vs*. Control littermates was performed by SMARTer Stranded Total RNA Sample Prep Kit - HI Mammalian (Takara Bio) with 400ng total RNA as input. Sequencing was performed on the NextSeq500 instrument (Illumina) using v2 chemistry with 1x75bp single end setup.

Library preparation of late heart samples was performed from 500ng total RNA of *RBPMS/2*$^{flox/floxp}$ */ aMyHC-Cre vs*. Control littermates using Truseq Stranded mRNA Library preparation combined with the low sample protocol (Illumina). Sequencing was performed on the NextSeq500 instrument (Illumina) using v2 chemistry, with 2x75bp paired end setup.

Differential splicing analysis and GO term annotation

Adaptor sequences and low-quality 3′ bases were removed with Flexbar (v3.5) (Dodt et al., 2012). Next, short reads from the rRNA locus were subtracted by mapping against the *Mus musculus* ribosomal RNA precursor using Bowtie2 (Langmead and Salzberg, 2012) (v2.3.5.1) and then discarded. The remaining reads were aligned to the *Mus musculus* genome (Ensembl transcriptome Annotation GRCm38 v96) with STAR (v2.7.3a).

Differential splicing analysis was conducted with rMATS turbo (v4.1.0) with the `--allow_clipping` parameter (Shen et al., 2014). Data analysis was performed as described by Nakagaki-Silva et al. (2019). Sashimi-plots were generated by rmats2sashimiplot

(https://github.com/Xinglab/rmats2sashimiplot) and RNA maps (Gohr and Irimia, 2019). Gene Ontology enrichment analysis were generated by TopGO (Alexa et al., 2006) (version 2.34.0) and AnnotationDbi (version 1.44.0). Alternative splicing events identified by rMATS were validated by RT-PCR in the same manner as described in the RT-PCR section.

Protein extraction and immunoblot analysis

For protein extraction, tissue samples were collected, lysed by homogenization in EB/LB-Buffer (Table 3) buffer, supplemented with protease inhibitors (Table 3), and sonicated for 20 sec at cycle 3, power 30%. In contrast, cardiomyocyte samples were homogenized in RIPA buffer, supplemented with protease inhibitors, and sonicated for 20 sec at cycle 3, power 30%. After incubation on a rotating wheel for a minimum of 30 min at 4°C, cell and tissue homogenates were centrifugated at 14,000 rpm for 20 min at 4°C to separate the supernatant for concentration measurement using Bradford Method. Proteins fraction in the supernatant was diluted with a corresponding dilution buffer and denatured by 1 mol/L DTT (4 µL per 100 µL sample) and subsequently heated to 99°C. Samples were stored at -20°C before usage.

For western blot analysis, 20-30 µg of proteins were loaded on SDS-PAGE gel (Table 8) and blotted onto nitrocellulose membranes (AmershamTM ProtranTM 0.45 µm NC - GE Healthcare, 10600002). Using Transfer Buffer (Table 3) to transfer protein in 30 mV for 2 hours (Power Pac 200 - Bio-Rad) in a blotting chamber (NOVEX® X Cell IIä Blot Module - Invitrogen; EI9051), followed by RedAlert™ to check loading efficacy. The nitrocellulose membrane was washed away using ddH_2O and blocked in 5% skim milk / TBS-T for 1 hour at RT. The blocked membrane was incubated with specific primary antibodies overnight at 4°C, followed by incubation with peroxidase-conjugated secondary antibodies for 1-2 hours at room temperature (RT).

Corresponding protein bands on the membranes were detected and visualized by chemiluminescence using Super Signal® West Femto Maximum Sensitivity Substrate (Thermo Scientific; 34096) combined with the Chemiluminescence Analyzer (ChemiDoc™ MP Imaging System - BioRad, 731BR01764). Thereafter, Image Lab software was used to quantify and normalize the relative protein expression to GAPDH.

Identification of protein interaction partners of RBPMSA

GFP-tagged RBPMS variants were generated as C- and N-terminally tagged versions (RBPMSA-GFP&GFP-RBPMSA) using the pCAG-IRES-Puro vector, which also served to

produce the GFP control construct. Stable polyclonal mouse ES cell clones were generated by electroporation in murine V6.5 ES cells and puromycin selection. Stable expression of GFP-fusion constructs was tested by western blot analysis using an anti-GFP antibody. For GFP pull down experiments, mESCs were cultured on feeder cells and trypsinized for harvesting. To deplete feeder cells, mESC and feeder cells were pre-plated for 1 hour on a 10 cm cell culture dish. Supernatant mESCs were lysed for the mass spectrometry based interactome screen using GFP-Trap® (Chromotek) according to the manufactor´s protocol. Collected magnetic agarose (MA) beads, which bind fusion protein and the corresponding interactome, were analyzed by liquid chromatography–mass spectrometry (LC-MS/MS).

Liquid chromatography/tandem mass spectrometry (LC/MS^2) analysis

Beads were processed using off bead digest, followed by using reductive dimethylation and liquid chromatography/tandem mass spectrometry (LC/MS^2) analysis as described (Deutschmeyer et al., 2019), but forgoing the SAX chromatography step. LC/MS^2 analysis was performed as described (Deutschmeyer et al., 2019), but used version 1.6.0.1 of the MaxQuant suite of algorithms (Cox and Mann, 2008; Cox et al., 2011) and a murine canonical and isoforms uniprot database (The UniProt Consortium, 2007; downloaded 2017/08/17; 90200 entries) (Bairoch et al., 2007). Downstream data analysis and plotting was performed using an R (R Core Team, 2020) and limma (Ritchie et al., 2015) based analysis pipeline (https://github.com/bhagwataditya/autonomics), including a Fisher exact test against the detectome for over-representation with respect to GO (Ashburner et al., 2000) and KEGG (Kanehisa et al., 2012) categories.

Morphological analysis using paraffin embedded hearts

Hearts from different embryonic and adult stages were embedded into paraffin and used for sectioning. The isolated embryo and adult hearts were fixed in freshly prepared 4% paraformaldehyde (PFA - Roth, 0335.4) overnight at 4°C. The following day, the adult hearts were rinsed with PBS for 5 min at RT and further processed in a dehydration series of 70%, 80%, 90% and 100% - ethanol solutions (Rothipuran® Ethanol > 99.8 % (EtOH) - Roth, 9065.4) for 2 h on a shaker at RT for each step. In contrast, embryonic hearts were kept for 1h in each of the different EtOH dilutions. Subsequently, the hearts were transfered to 100% isopropanol for a maximum of 2h (For embryo, maximum 1h) at RT on a shaker and then transferred to 50% isopropanol / 50% paraffin mixture at 56°C, overnight. For better paraffin penetration, the samples were transferred to 100% liquid paraffin for 3h of adult hearts and 1 hour of embryo

hearts at 56°C. Finally, hearts were embedded in paraffin using a tissue embedding center (Leica EG1150C) and adopted to RT overnight. Sections (5 µm) were sectioned with a microtome (Leica RM2125RT) and collected on glass slides (Superfrost Ultra Plus® - Thermo Scientific, J3800AMNZ) using a 42°C water bar. Sections were dried on a heating plate (42°C; HI1220 - Leica) overnight and stored at RT.

Hematoxylin and eosin staining (H&E staining)

For dewaxing, slides with paraffin sections were placed two times in 100% Xylene (Roth, 9713.3) for 5 min each time, followed by rehydration in decreasing EtOH concentration series (100%, 90%, 80% and 70% - EtOH solution) and then rinsed with ddH_2O for 2 min. Afterwards, sections were stained in Mayer's Hematoxylin (Haemalaum, acidic Mayer -WALDECK, 2E-038) for 10 min at RT. Staining solution were rinsed in tepid running tap water for 7 min and sections were counterstained with Eosin (Eosine Solution -WALDECK, 2C-140) for 7 min at RT. Thereafter, the tissue slides were dehydrated in increasing ethanol solution concentration series (70%, 80%, 90% - EtOH) by dipping twice each and subsequent incubation in 100% EtOH for 10 min and 100% xylene (Roth, 9713.3) 2 times for 5 min, mounted in Entellan (Merck-Millipore, 1.07961.0100) and dried overnight. Thereafter, slides were imaged using a Keyence (Keyence BZ- 9000) or Zeiss Axioplan 2 microscope.

Cryosections of embryonic or adult hearts

To perform cryosections from embryonic or adult hearts, hearts were fixed in 4% PFA / 1 x PBS overnight at 4°C. The following day, adult hearts were rinsed with PBS for 5 min at RT and immersed in 30% sucrose / 1 x PBS overnight at 4°C. Thereafter, hearts were rinsed in FSC 22 (Leica) at RT for several mins (30 min for embryo hearts and 45 min for adult hearts), frozen on dry ice, and stored at -80°C before usage. Serial 5-µm thick cross sections were performed using a Leica CM 1950 cryostat and collected on SuperFrost Plus slides, and stored at -80°C for longer immunofluorescence staining.

Immunofluorescence staining of sections and cells

Primary cardiomyocytes as well as cell lines were fixed in 4% PFA / 1 x PBS for 15 min, washed three times with 1 x PBS, permeabilized in 0.1 % Triton X-100 / 1 x PBS for 10 min. To reduce non-specific antibody binding, cells were incubated in a blocking solution containing 2% FCS, 2% BSA in 1 x PBS for 1 h. Cryosectioned tissue specimens, which were already pre-fixed in 4% PFA / 1 x PBS, were fixed again in 4% PFA / 1 x PBS for 5 min and permeabilized

in 0.1% Triton X-100 / 1 x PBS for 10 min. Thereafter, sections or cells were incubated in blocking solution containing 2% FCS, 2% BSA in 1 x PBS for 1 hour. Subsequently, cells or tissue sections were incubated with primary antibodies (Table 7), diluted in the blocking solution as indicated in Table 3, overnight at 4°C. The following day, cells or tissue sections were washed first 3-times in 1x PBS for 5 min each time and then incubated for 2h at RT with secondary antibodies conjugated to Alexa Fluor™ 488, Alexa Fluor™ 594 (Or Cy3) or Cy5 (Table 7) diluted in blocking solution. Thereafter, slides or wells were washed 3-times in 1 x PBS for 5 min and nuclei were subsequently stained with 4',6-diamidino-2-phenylindole (DAPI), 1:1000 diluted in the blocking solution, for 10 min. Sections or cells were again washed in 1 x PBS for three times. Finally, sections or cells were mounted in Mowiol and imaged using a fluorescence microscope (Zeiss Z1.Imager or Leica SP8).

Electron microscopy analysis

To analyze cardiomyocyte-restricted ultrastructural alterations of RBPMS/2 deficient embryonic hearts electron microscopy was used. Embryonic hearts were stored in a fixative containing 1.5% glutaraldehyde (v/v), 1.5% paraformaldehyde (v/w) in 0.15 M HEPES (v/w), pH 8.0 at 4°C until processing for post-fixation in 1% osmium tetroxide. Afterward, samples were stained *en bloc* in 50% saturated watery uranyl acetate, dehydrated by an ascending ethanol series, and embedded in Agar 100. Ultra-thin sections were performed by ultramicrotome at the Institute for Anatomy and Cell Biology, Justus-Liebig-University Giessen, Germany, and image acquisition was used with a transmission electron microscope. All images were captured with a slow-scan 2K CCD camera.

Construction of splicing mini-reporters

In total, 3 splicing reporter minigenes were constructed and further analyzed encompassing St7 (exon 6 to 8), Map3k7 (exon 11 to 13) and Tpm2 (exon 5 to 7). These splicing reporters were generated by overlapping PCRs using C57BL6 genomic DNA as template and subsequently recombined into PacI and AscI site of a modified pCAG-IRES-Puro vector. Hereby, intronic regions were shortened, whereas intron-exon boundaries and exonic sequences remained unaltered. Point mutations of CAC motifs in the splicing reporter minigenes were generated by PCR using oligonucleotides that contained C to T mutation. All constructs were confirmed by sequencing.

Cell culture

Human Embryonic Kidney Cells (HEK293)

HEK 293 cells were cultured in DMEM/10%FCS/1% PSG (1 x Dulbecco's Modified Eagle Medium (DMEM 4.5g/L D-Glucose - Gibco, 42430-025) and passaged at 70-80% confluency. Therefore, cells were incubated with 1xTrypsin-EDTA (Sigma; T4174) in PBS at 37°C for 2 min. After complete detachment of the cell layer, trypsin was inactivated with 2 volumes of pre-warmed complete growth media and cell suspension was transferred to the 15 mL tubes and gently centrifuged (Universal 320R; Hettich Zentrifugen) at 300g for 5 min. After removing the supernatant, cell pellet was gently resuspended in appropriate amount pre-warmed complete growth medium and seeded to a culture dish at a density of 2 x 10^5 cells/100mm.

Transfection of HEK293

The transfection of HEK293 cells with mini-reporter as well as expression constructs was performed by TurboFectTM Transfection Reagent (ThermoFisher Scientific, R053) according to the manufactor´s protocol. The expression constructs (GFP-tagged RBPMS variants) were generated as C-terminally tagged versions (RBPMSA-GFP, RBPMSB-GFP and RBPMS2-GFP) as well as RRM deleted control constructs (RBPMSA-RRM-GFP, RBPMSB-RRM-GFP and RBPMS2-RRM-GFP) using the pCAG-IRES-Puro vector, which also served to generate the GFP control construct. Subconfluent HEK293 cells, cultured in 12 well plates (Greiner bio-one, Cellstar) under humified atmosphere at 37°C and 5% CO2, were transiently transfected with 1 µg of individual plasmid DNA using TurboFect transfection reagent. After 48 h transfection, HEK293 were collected either in ice-cold RIPA buffer for western blot or in TRI-reagent (Zymo Research) for RNA isolation.

Mouse embryonic stem (ES) cell culture, differentiation and selection

ES cell-line harboring a stable integration of an α-myosin heavy chain promoter driven neomycin phosphotransferase gene were used for the *in vitro* differentiation of ES cell derived cardiomyocytes. Therefore, ES cells were cultured on gelatin (0.2%) coated tissue culture dishes and mitomycin treated mouse embryonic feeder cells in DMEM, supplemented with 15% defined FCS, 1% Penicillin & Streptomycin, 0.1mM 2-mercaptoethanol, 0.1mM non-essential amino acids, in a humidified environment containing 10% CO_2 at 37°C. The cells were kept in the undifferentiated state by the addition of leukemia inhibitory factor (1000 U/mL). Trypsin-EDTA was used to detach cells from the culture surface for passaging every second day.

To initiate differentiation, ES cells were dispersed with TrypLE Express into individual cells and inocculated in CERO tubes at a density of 1 x 10^6 cells / 10 ml ES-cell differentiation medium (ES culture medium supplemented with 10% FCS without LIF) and thereafter transferred to CERO - 3D Cell Culture Bench-Bioreactor. After 72 h, culture medium was replaced for the first time, and subsequently replaced daily. At day 9 of differentiation, culture medium was supplemented with G418 (400 mg/mL) to initiate selection of cardiomyocytes, which initiate beating from day 10 onwards.

Isolation of mouse embryonic cardiomyocytes

Timed matings were set up to collect E14.5d wildtype mouse embryo hearts or *RBPMS*$^{flox/flox}$ / *RBPMS2*$^{flox/flox}$ mouse embryo hearts for isolation of cardiomyocytes. Embryos were isolated from placenta and sacrificed using sterile scissors and the chest was opened along the sternum to allow access to the heart. The tissues surrounding the heart were removed and the heart was directly transferred to a new bacterial dish containing PBS on ice. Cardiac cell dissociation was performed using the Neonatal Heart Dissociation Kit (Miltenyi Biotec; 130-098-373) and gentleMACS Octo Dissociator with Heaters (Miltenyi Biotec; 130-096-427) as implemented by the manufacture's protocol. After dissociation, the cardiomyocyte cell fraction was isolated using a mouse Neonatal Cardiomyocyte Isolation Kit (Miltenyi Biotec; 130-100-825) as implemented by the manufacture's protocol (www.miltenyibiotec.com). Subsequently, isolated cardiomyocytes were used either for RNA or protein extraction or culture experiments. For culturing, freshly isolated cardiomyocytes were gently resuspended in DMEM, supplemented with 5% FCS and 1% L-glutamine-penicillin-streptomycin (P/S/G), and seeded on a fibronectin precoated (10 % fibronectin (PromoCell; C-43050) in DPBS) cell culture dish or chamber slides at the density of 1.5 x 10^5 cells per cm^2. Cardiomyocytes were incubated at 37°C and 5% CO2 for manipulation experiments.

Isolation of embryonic cardiomyocytes from single heart

Isolated embryonic heart ventricles were washed 3 times with PBS and thereafter predigested in Enzyme A (3 ml) (Table 3) for 3 x 5 min using a 37°C sharker with 100 rpm, whereas supernatant was discarded. Next, heart lysis was performed in Enzyme B: digestion buffer (Table 3) 6 to 8 times for 10 min at 37°C shaker with 100 rpm. Digestion products were gently resuspended for several times. Remaining heart samples were settled down whereas the supernatant was transferred to a 15 ml falcon tube containing equal amount of culture medium and subsequently spinned down at 1000 rpm for 10 min. The cardiomyocyte pellet of each

digestion round was resuspended in culture medium and pooled in 50 ml tubes at 37°C. Thereafter, cell suspension was filtered through a 100 µm mesh, spinned for 19 min at 1000rpm, resuspend in fresh medium and plate on 1% gelatin. Simultaneously, genotypes of corresponding embryos were performed by PCR from genomic DNA.

Isolation of adult mouse cardiomyocytes

Adult cardiomyocytes were isolated using a method previously described by O'Connell et al. (O'Connell et al., 2007). Mice were anesthetized by intraperitoneal (i.p.) injection of Buprenorphine/Ketamine in 0.9% NaCl with 0.2 mL heparin (Braun, 1708.00.00). The chest was sterilized with 70% EtOH and opened along the sternum to allow access to the heart. The heart was taken out while removing the lung and the aorta by cutting below the aortic arch. Then, the heart was cannulated via the aorta and arrested by retrograde perfusion with calcium-free buffer using a Langendorff perfusion system (Table 3). The cannulated hearts were digested with Enzyme-Buffer by perfusion and removed from the cannula. Atria were divided, and ventricles were minced in stop buffer 1 (Table 3). After gentle pipetting, myocytes were centrifuged at 300 rpm for 1 min. The cell pellets were resuspended in stop buffer 2 (Table 3). Calcium concentration of the cell suspension was then stepwise adjusted to 1 mmol L-1 and after adjustment of Ca^{2+} concentration, the cell suspension was centrifuged at 300 rpm for 1 min. Cell pellets were resuspended in M199 cell culture medium (supplemented with creatinine x H_2O, L-carnitine x HCl, HEPES, penicillin/streptavidin, FCS, and insulin-transferrin-sodium selenite media supplement), and seeded on cell culture dishes or chamber slides pre-coated with laminin (10 µg/µL laminin in MEM media) and incubated at 37°C and 5% CO_2.

Adenoviral infection of embryonic cardiomyocytes

Isolated embryonic cardiomyocytes were infected with a recombinant adenovirus expressing a codon improved Cre-recombinase under the CMV promoter (Ad-CMV-iCre; 10^7 PFU mL^{-1}) (Vectorbiolabs; Cat. No: 1045) to induce site-specific recombination of genomic DNA between the two loxP sites flanking exon 1 of *Rbpms* and *Rbpms2*. An empty adenovirus (Ad-Null; 10^7 PFU m) (Vectorbiolabs; Cat. No: 1300) was used as an appropriate mock control. Cardiomyocytes were incubated with the adenovirus mixture for 6 h and washed five times with 1 x PBS to remove remaining virus particles and thereafter cultured in fresh medium for additional 48 h before collection.

siRNA mediated knockdown in cultured embryonic cardiomyocytes

To study the effects of Camk2g isoforms encoding exon 14 in cultured E14.5 embryonic cardiomyocytes, siRNA mediated knockdown (KD) experiments directed against exon 14 were performed. For this purpose, cultured embryonic cardiomyocytes were transfected with 0.5 µmol/L of appropriate siCamk2g-exon14 (Custom camk2g E14, CTM-504862) as well as siControl (ON-TARGETplus Non-targeting siRNA #1, D-001810-01-05) using Lipofectamine™ RNAiMAX transfection reagent (Thermofisher; #13778030) according to the manufacturer's instruction.

Statistical analysis

Statistical analyses were calculated by Prism 8 (GraphPad). Statistical significance was determined by using two tailed paired and unpaired t tests, $P < 0.05$ was considered significant. *$P < 0.05$;**$P < 0.01$; ***$P < 0.001$; ****$P < 0.0001$.

Results

RBPMS and RBPMS2 are essential for cardiac development

A previous study reported that the RBPMS homologue HERMES (*HEart*, RRM Expressed Sequence) in Xenopus encodes an RNA-binding protein, which is specifically expressed during Xenopus heart development (Gerber et al., 2002). In order to analyze the spatial and temporal expression pattern of both RBPMS family members (RBPMS and RBPMS2) during mouse embryonic development we made use of whole mount in situ hybridization (WISH) as well as LacZ Knock-in reporter strains for both genes ($RBPMS^{LacZ}$ and $RBPMS2^{LacZ}$). Both visualization approaches consistently indicated expression of RBPMS in heart and smooth muscle cells (Figure 1A-C) and expression of RBPMS2 in the heart (Figure 1A and B) during embryogenesis. Furthermore, LacZ staining on cryosection confirmed RBPMS expression in the myocardium and all types of smooth muscle cells including lung, intestine, kidney, bladder and umbilical cord (Figure 1C). The replacement of critical coding exons in both Knock-in reporter strains by LacZ generated non-functional alleles, which allowed breeding of constitutive homozygous single and double mutants for *RBPMS* and *RBPMS2*, enabling functional analysis of both genes. Homozygous $RBPMS^{LacZ/LacZ}$ knock-out mutants (hereinafter referred to as *RBPMS KO*) (Figure 2A and B) as well as homozygous $RBPMS2^{LacZ/LacZ}$ knock-in mutants (data not shown) are viable and do not display gross morphological or ultrastructural changes of the myocardium.

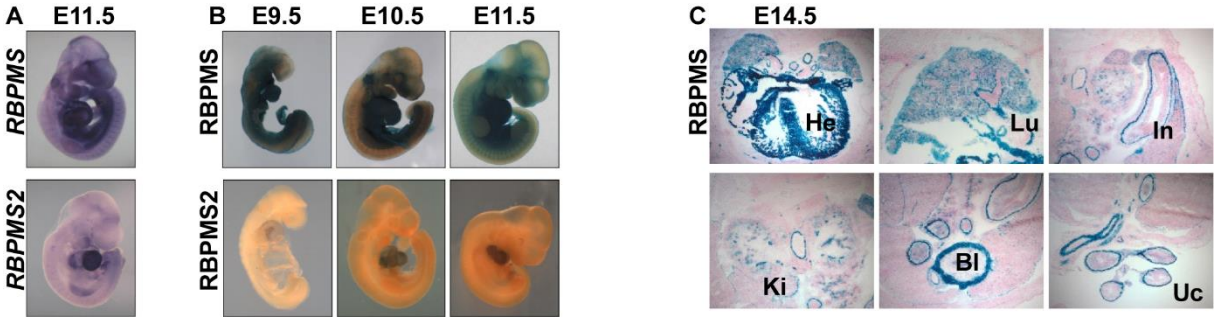

Figure 1. RBPMS is highly expressed in the embryonic heart and smooth muscle tissues.

A. Whole-mount in situ hybridization to detect *RBPMS* and *RBPMS2* mRNA in developing embryos at E11.5. **B.** *X-gal* staining of embryos to visualize $RBPMS^{LacZ}$ and $RBPMS2^{LacZ}$ reporter expression during embryonic stages (E9.5, E10.5 and E11.5). **C.** X-gal staining of frozen cross sections from $RBPMS^{LacZ}$ reporter embryos at E14.5. he: heart; lu: lung; in: intestine; ki: kidney, bl: bladder; uc: umbilical cord.

Since RBPMS and RBPMS2 might have overlapping functions during early heart development, we analyzed constitutive *RBPMS/2* double homozygous KOs (hereinafter referred to as *RBPMS/2 dKO*). Concomitant inactivation of RBPMS and RBPMS2 resulted in early embryonic lethality from E11.5 to E13.5, accompanied by multiple cardiac malformations, including ventricular hypo-trabeculation, ventricular non-compaction and dilated atria (Figure 2C and D), compared to *RBPMS/2* double heterozygous serving as controls.

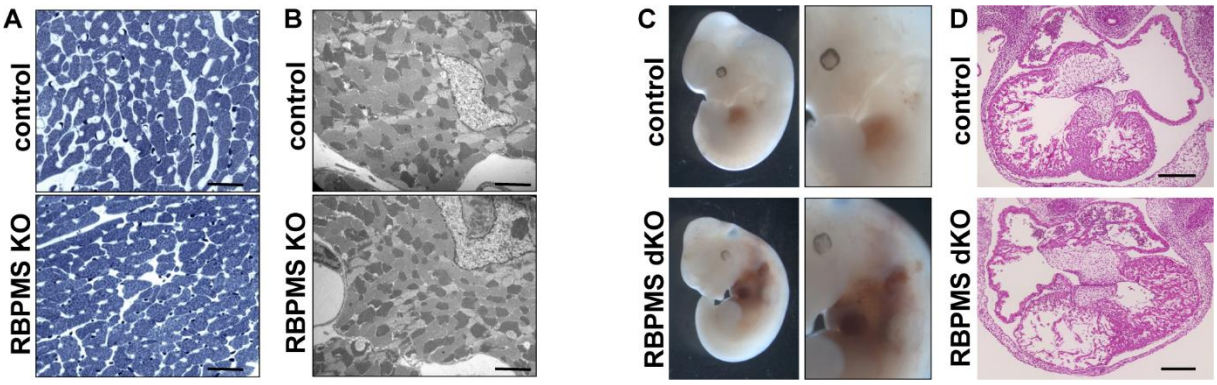

Figure 2. RBPMS and RBPMS2 are essential for cardiac development and survival.

A, B. Normal myocardial ultrastructure. Light microscopy (A) and electron microscopy (B) analysis of control and *RBPMS KO* hearts, respectively. Scale bar, 20 µm (A) and 2 µm (B), respectively. **C, D.** Images of control and constitutive *RBPMS/2 dKO* embryonic hearts (C) and H&E staining of paraffin sections (D) at E12.5. Scale bar, 200 µm.

Since combined constitutive inactivation of RBPMS and RBPMS2 leads to a severe embryonic phenotype both in the heart and in vascular smooth muscle cells, two mouse strains were established in which RBPMS/2 were specifically inactivated in cardiomyocytes. *Xenopus laevis* light chain 2 (XMLC2) promoter CRE mice (Breckenridge et al., 2007) were crossed to *RBPMS*$^{flox/flox}$ / *RBPMS2*$^{flox/flox}$ animals to generate the *RBPMS/2*$^{flox/flox}$ / *XMLC2-Cre* mice line, hereinafter referred to as *XML-dKO* (Figure 3A). In a parallel approach, we crossbred *RBPMS*$^{flox/flox}$ / *RBPMS2*$^{flox/flox}$ mice with animals carrying alpha myosin-heavy chain (*Myh6*) Cre (αMyHC-Cre) (Agah et al., 1997; de Lange et al., 2004), resulting in the *RBPMS/2*$^{flox/flox}$ / *aMyHC-Cre* line, hereinafter referred to as *aMyHC-dKO* (Figure 3C). *XML-dKO* mutant embryos showed reduced myocardial trabeculation and compaction starting at E12.5 and died around E15.5, whereas *aMyHC-dKO* mutant embryos manifest a phenotype around E16.5 and died around birth. Both mutants showed an arrest of cardiac development, including trabeculation and compaction defects (Figure 3A-F) compared to *RBPMS*$^{flox/flox}$ / *RBPMS2*$^{flox/flox}$ littermate control. In order to visualize phenotype progression upon cardiac specific RBPMS

and RBPMS2 inactivation in *αMyHC-dKO* mutants, hearts were isolated from E16.5 to P1 (Figure 4A). During cardiac development, mutant hearts loose the normal apex structure and show decreased ventricular wall thickness as well as a reduced trabeculation (Figure 4B and C).

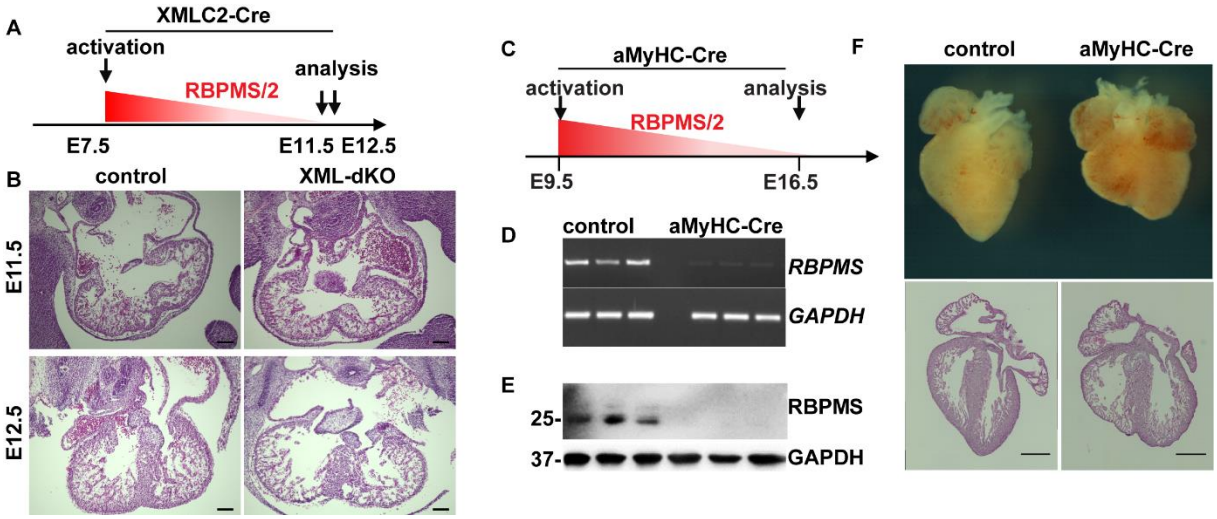

Figure 3. RBPMS and RBPMS2 are essential for cardiac development and survival.

A. Timeline of cardiac-restricted inactivation of RBPMS and RBPMS2 during early heart stage. *RBPMS*$^{flox/flox}$ / *RBPMS2*$^{flox/flox}$ mice were crossbred with the XMLC2-Cre strain mediating recombination in cardiac crescent cells at E7.5 (Breckenridge et al., 2007). **B.** H&E-stained sections of control and *XML-dKO* hearts at E11.5 and E12.5, n = 3 for each group. Scale bar, 100 µm. **C-E.** Timeline of the cardiac-restricted inactivation of RBPMS and RBPMS2 during later cardiac stage. *RBPMS*$^{flox/flox}$ / *RBPMS2*$^{flox/flox}$ mice were crossbred with the aMyHC-CRE line initiating CM specific RBPMS/RBPMS2 inactivation at E9.5 (Agah et al., 1997; de Lange et al., 2004). RT-PCR (D) and Western blot analysis (E) of control and *aMyHC-dKO* embryonic hearts at E16.5. GAPDH was used as loading control. **F.** Images of control and *aMyHC-dKO* hearts and corresponding H&E stained sections at E16.5, n = 3 for each group. Scale bar, 500 µm.

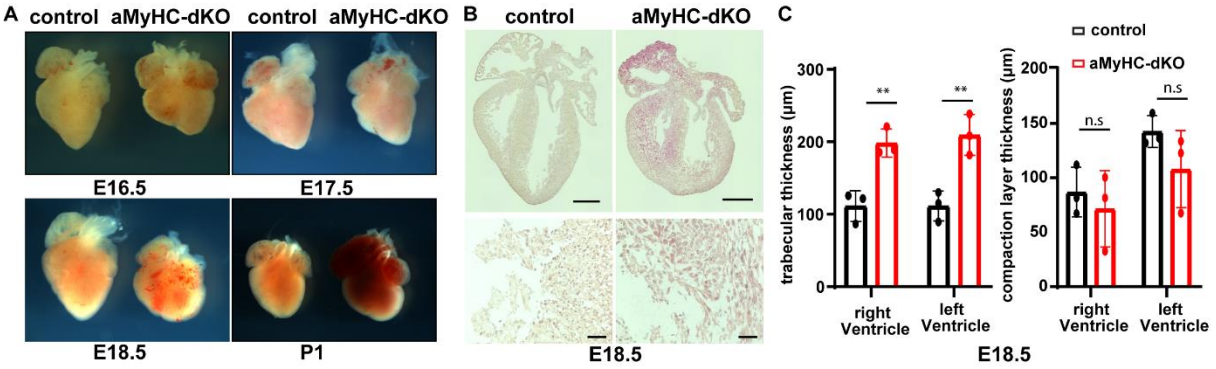

Figure 4. Cardiac-restricted inactivation of RBPMS and RBPMS2 are essential for cardiac development and trabecula formation.

A. Phenotype progression of *aMyHC-dKO* mutant hearts from E16.5 to P1. **B.** H&E-stained sections of control and *aMyHC-dKO* mutant hearts at E18.5, n = 3 for each group. Scale bar, 500 μm (up) and 20 μm (down). **C.** Analysis of myocardial wall thickness of both genotypes at E18.5, n = 3 for each group. Statistical significance was calculated by Student's t-test (**p<0.01).

Cardiac ultrastructure disruption was examined by transmission electron microscopy in the myocardium of E16.5 *aMyHC-dKO*. Here, pathomorphological alterations were observed in majority of *RBPMS/2 dKO* cardiomyocytes, including disruption of sarcomere integrity and nuclear abnormalities (Figure 5A). Furthermore, immunofluorescence staining of cardiomyocyte specific markers α-Actinin and troponin T (cTnT; TNNT2) confirmed sarcomere defects in *aMyHC-dKO* mutants (Figure 5B). In control hearts, RBPMS is present throughout the entire embryonic myocardium and is differentially distributed in subcellular compartments, predominantly in the nucleus (Figure 5B). Of note, complete loss of RBPMS in cardiomyocyte nuclei of *aMyHC-dKO* mutant hearts indicate an efficient inactivation (Figure 5B).

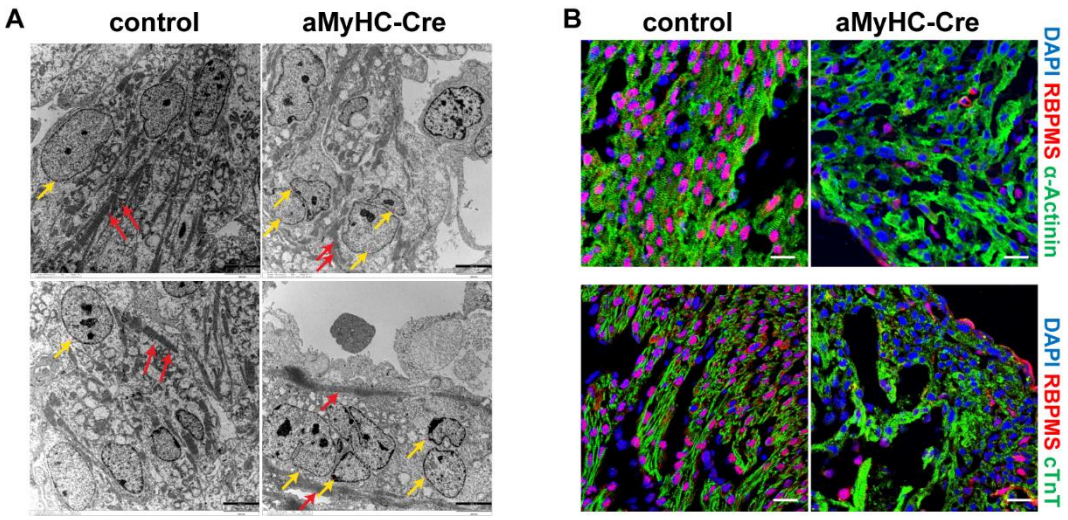

Figure 5. Pathomorphological alterations in cardiac-restricted RBPMS and RBPMS2 inactivated mice.

A. Ultrastructural analysis of control and *aMyHC-dKO* mutant hearts by electron microscopy at E16.5. Scale bar, 5000 nm. Yellow arrows, nuclei; red arrows, sarcomeres. **B.** Immunofluorescence staining of RBPMS, red, α-Actinin, green, cTnT, green, and nuclei (DAPI, blue) of control and *aMyHC-dKO* mutant heart sections. Scale bar, 10 μm.

Surprisingly, RBPMS localizes in the nucleus of isolated embryonic cardiomyocytes kept at low cellular density, but is translocated from the nucleus to the cytoplasm when the cell density is increased (Figure 6A). This observation suggests that RBPMS might alter subcellular localization in a context-dependent manner, e.g., under stress conditions. A well-defined cellular stress model of the adult myocardium is the myocardial infarction model (MI), which combines multiple aspects including hypoxia, necrosis, inflammatory responses as well as dedifferentiation and survival of cardiomyocytes (Prabhu and Frangogiannis, 2016). Interestingly, in the healthy adult myocardium (data not shown) as well as in the border zone of a MI model RBPMS localizes to cardiomyocyte nuclei (Figure 7A), but accumulates in the cytoplasm of cardiomyocytes in the infarct zone (Figure 7B). Additionally, an accumulation of RBPMS positive non-cardiomyocytes, most likely immune cells, was observed in the infarct zone, which was not analyzed any further.

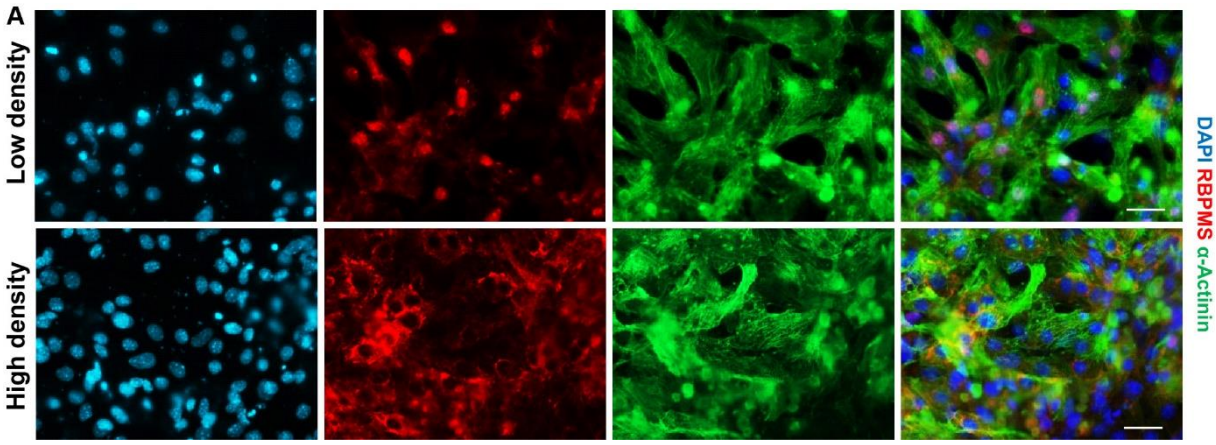

Figure 6. RBPMS undergoes a subcellular localization switch from the nuclear to the cytoplasmic compartment in isolated embryonic cardiomyocytes upon cellular density.

A. Immunofluorescence staining of RBPMS, red, α-Actinin, green, and nuclei (DAPI, blue) in isolated embryonic cardiomyocytes under low density and high density at E16.5. Scale bar, 10 μm.

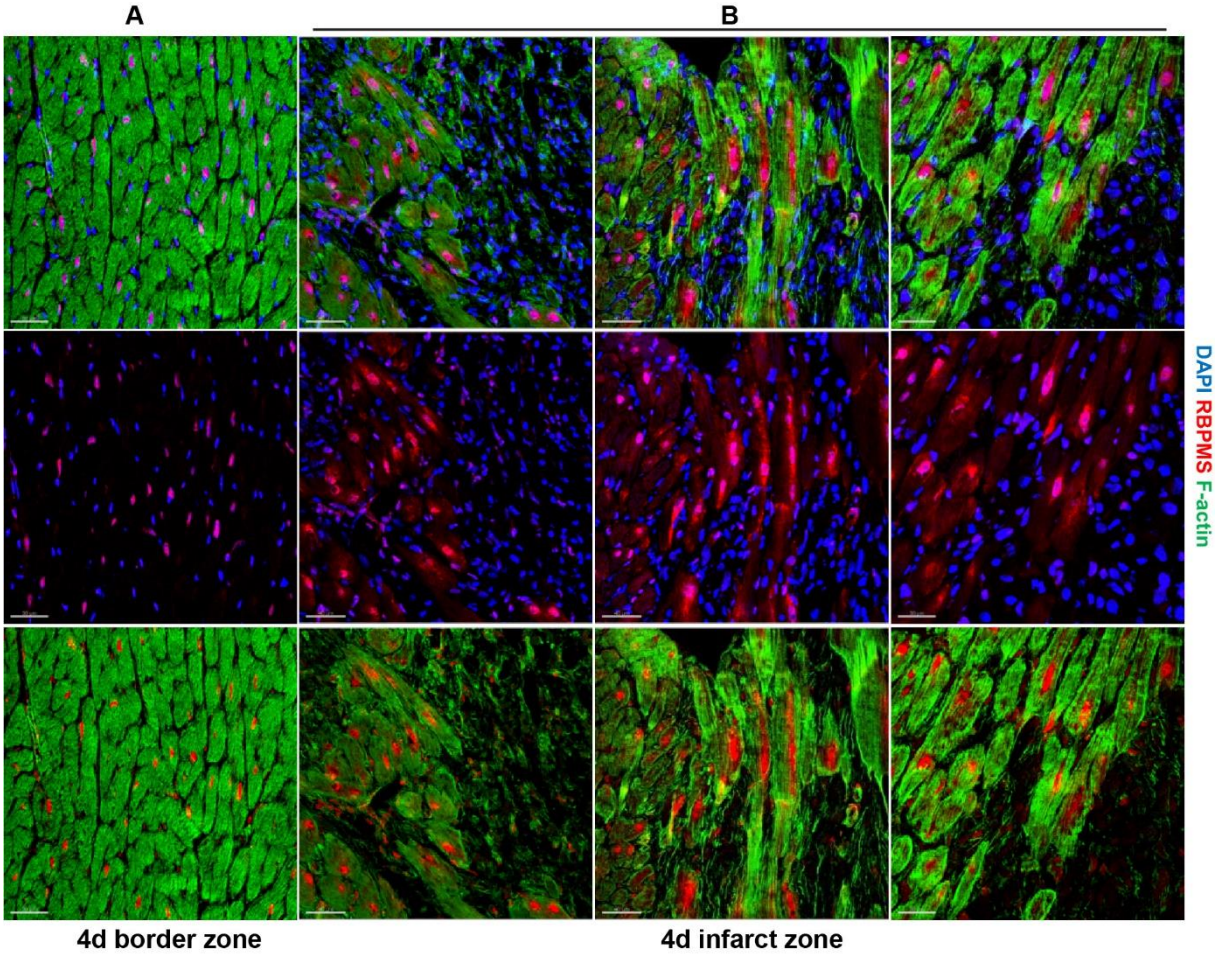

Figure 7. RBPMS undergoes a subcellular localization switch from the nuclear to the cytoplasmic compartment in adult cardiomyocytes of the infarct zone.

A. Immunofluorescence staining of RBPMS, red, F-actin, green, and nuclei (DAPI, blue) in the border zone of heart after myocardial infarction (4d). Scale bar, 10 μm. **B.** Immunofluorescence staining of RBPMS, red, F-actin, green, and nuclei (DAPI, blue) in infarct zone after myocardial infarction (4d). Scale bar, 10 μm.

The human RBPMS gene spans over a genomic region of 230kb and generates multiple mRNA isoforms (four RefSeq and at least 19 transcript variants according to AceView) resulting in multiple protein isoforms (Shimamoto et al., 1996), whereas the RBPMS2 gene produces only a single isoform. In order to correlate the RBPMS subcellular localization with corresponding protein isoforms in mouse, we first investigated RBPMS mRNA isoforms distribution in different mouse organs and murine embryonic stem cell (mESCs) derivatives by semi-quantitative reverse transcription PCR (sqRT-PCR) using 2 specific primer pairs, which detect the altered exons of all predicted isoforms. In total, we detected and validated six distinct RBPMS isoforms by PCR-sequencing, which were differentially distributed in all investigated organs and ES cell derivatives. Among the different RBPMS mRNA isoforms, we identified 2 highly abundant isoforms: *RBPMS-203/-213*, which both encode a 197aa RBPMS variant (named as *RBPMSA*) as well as *RBPMS-202*, which encodes a 220aa RBPMS variant (named as *RBPMSB)* (Figure 8A).

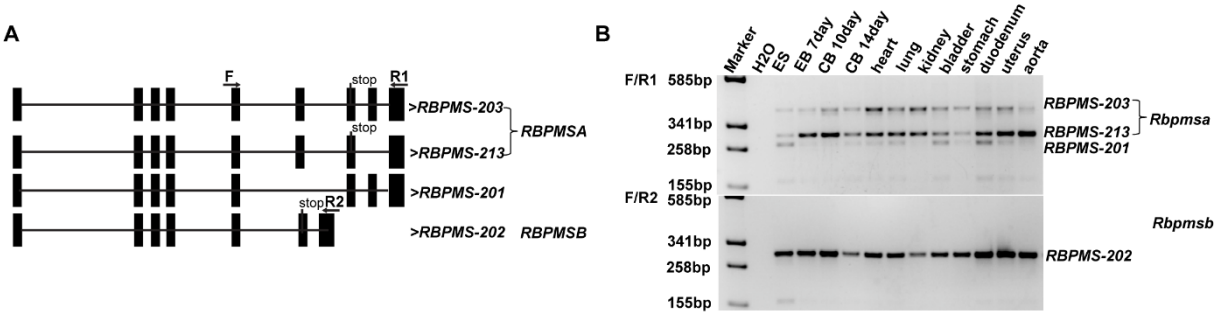

Figure 8. *RBPMS* encodes 6 isoforms generated by alternative splicing at the 3´end.

A. Semi-Q PCR of splicing variants of *RBPMS* in mESCs and mESCs derivatives (embryonic bodies (EBs) and cardiac bodies (CBs)) as well as different mouse tissues. RBPMS encodes 6 isoforms generated by alternative splicing at the 3´end. Two abundant isoforms of *RBPMS* are *RBPMS-203/213* (*RBPMSA*) and *RBPMS-202* (*RBPMSB*) based on Refseq from the Ensembl genome browser 105.

In order to correlate nuclear and cytoplasmic localization of RBPMS, we performed bioinformatical analysis to detect conserved nuclear localization signals (NLS) as well as nuclear export signals (NES) of the two most abundant isoforms RBPMSA and RBPMSB. Using the NES Finder 0.2 pipeline (Brar et al., 2004), we identified a conserved NES (VFCPLLQQIRF) motive in mouse and human RBPMSB, whereas all other pipelines did not detect any conserved NLS or NES sequence (Figure 9A). To test our findings experimentally, we generated overexpression constructs of RBPMSA and RBPMSB fused to a GFP-fluorescence Tag and transfected these constructs in HEK293 cells. The results showed that isoform A is mainly localized in the nucleus while isoform B predominantly accumulates in the cytoplasm (Figure 9B), indicating that the predicted NES signal might be instrumental for cytoplasmic RBPMSB-GFP accumulation. Additionally, RBPMS2-GFP fusion proteins are enrichment in the cytoplasm, similar to RBPMSB (Figure 9B).

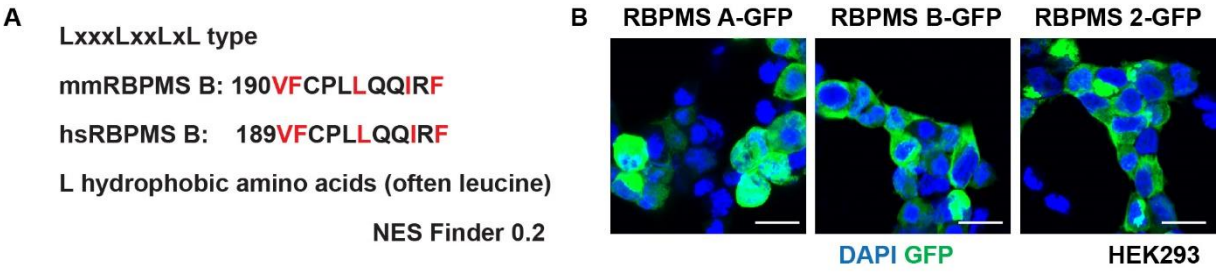

Figure 9. GFP-Tagged RBPMSA, RBPMSB and RBPMS2 displayed a differential subcellular localization, potentially mediated by a conserved nuclear export signal.

A. RBPMSB contains a putative nuclear export signal, which is highly conserved in human and mouse. **B.** Overexpressed RBPMSA-GFP localizes in nuclear and cytoplasm whereas RBPMSB-GFP and RBPMS2-GFP, green, mainly localize in cytoplasm of HEK293 cells. Nuclei (DAPI, blue). Scale bar, 10 μm.

To further analyze RBPMSA localization and function in cardiomyocytes, we generated a Cre inducible RBPMSA-GFP overexpression mouse line in the Rosa26 locus ($R26^{RBPMSA\text{-}GFP}$), which is activated by Cre-mediated removal of the Lox-Stop-Lox (LSL) cassette (Figure 10A). In a first step, we crossbred $R26^{RBPMSA\text{-}GFP}$ with CMV-CRE to generate a ubiquitously activated mice line, hereafter referred to as *RBPMSA OE* (Figure 11A). Global RBPMSA-GFP overexpression was confirmed by western blot analysis in multiple tissues (Figure 11D), which results in lethality around 5 weeks of age (Figure 11A), characterized by a reduced body and organ size (Figure 11B), in particular of the heart, spleen and intestine (Figure 11C). Remarkable, the size of the brain showed only minor alterations (Figure 11C).

In contrast, CM-specific RBPMSA-GFP overexpressing mice (*aMyHC-Cre / R26*$^{RBPMSA\text{-}GFP}$) survive until advanced age without any severe phenotype and display a predominantly nuclear GFP localization (Figure 10B). Thereafter, a RBPMSA rescue line was generated, which combines the following genotypes: *αMyHC-Cre / RBPMS*$^{flox/flox}$ */ RBPMS2*$^{flox/flox}$ */ R26-LSL-RBPMSA-GFP* (hereafter referred to as *RBPMSA*^{Resc}). Cardiomyocyte specific RBPMSA-GFP overexpression prevented the severe embryonic heart phenotype of *αMyHC-dKO* mutants, indicating that the RBPMSA isoform is indispensable for a proper heart development and morphogenesis. Although *RBPMSA*^{Resc} mice survive until adulthood, they show a smaller heart size compared to age matched control littermates (Figure 10C and D). This observation indicates that other RBPMS isoforms, in particular RBPMSB as well as RBPMS2, exert additional functions in post-transcriptional regulation, which might be important for cardiac maturation, maintenance and surveillance mechanisms.

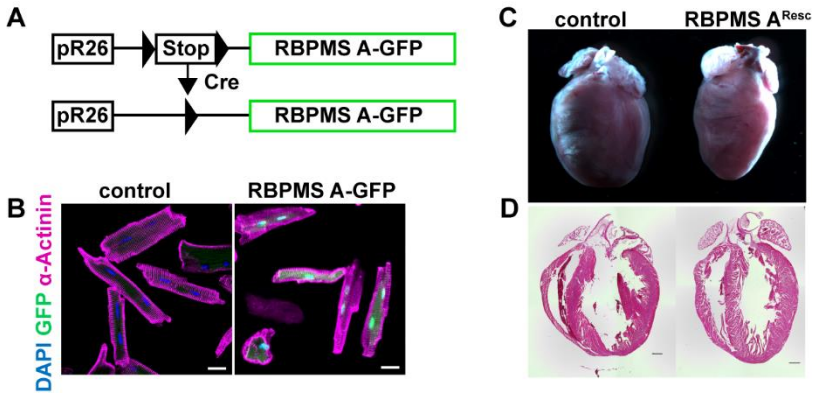

Figure 10. RBPMSA OE recuses the concomitant loss of RBPMS and RBPMS2 in cardiomyocytes.

A. Schematic view of the RBPMSA-GFP OE allele, which enables global or cardiomyocyte specific overexpression of RBPMSA-GFP fusion protein after Cre mediated removal of the stop cassette using aMyHC-Cre. Black triangles represent loxP sites. **B.** RBPMSA-GFP fusion protein, green, localizes to the nucleus of isolated adult cardiomyocytes after aMyHC-Cre mediated activation (10-week-old hearts). α-Actinin, purple, nuclei (DAPI, blue). Scale bar, 20 µm. **C, D.** Images of control and *RBPMSA*^{Resc} hearts (C) and H&E-stained paraffin sections (D) of corresponding hearts at 10 weeks. Scale bar, 500 µm.

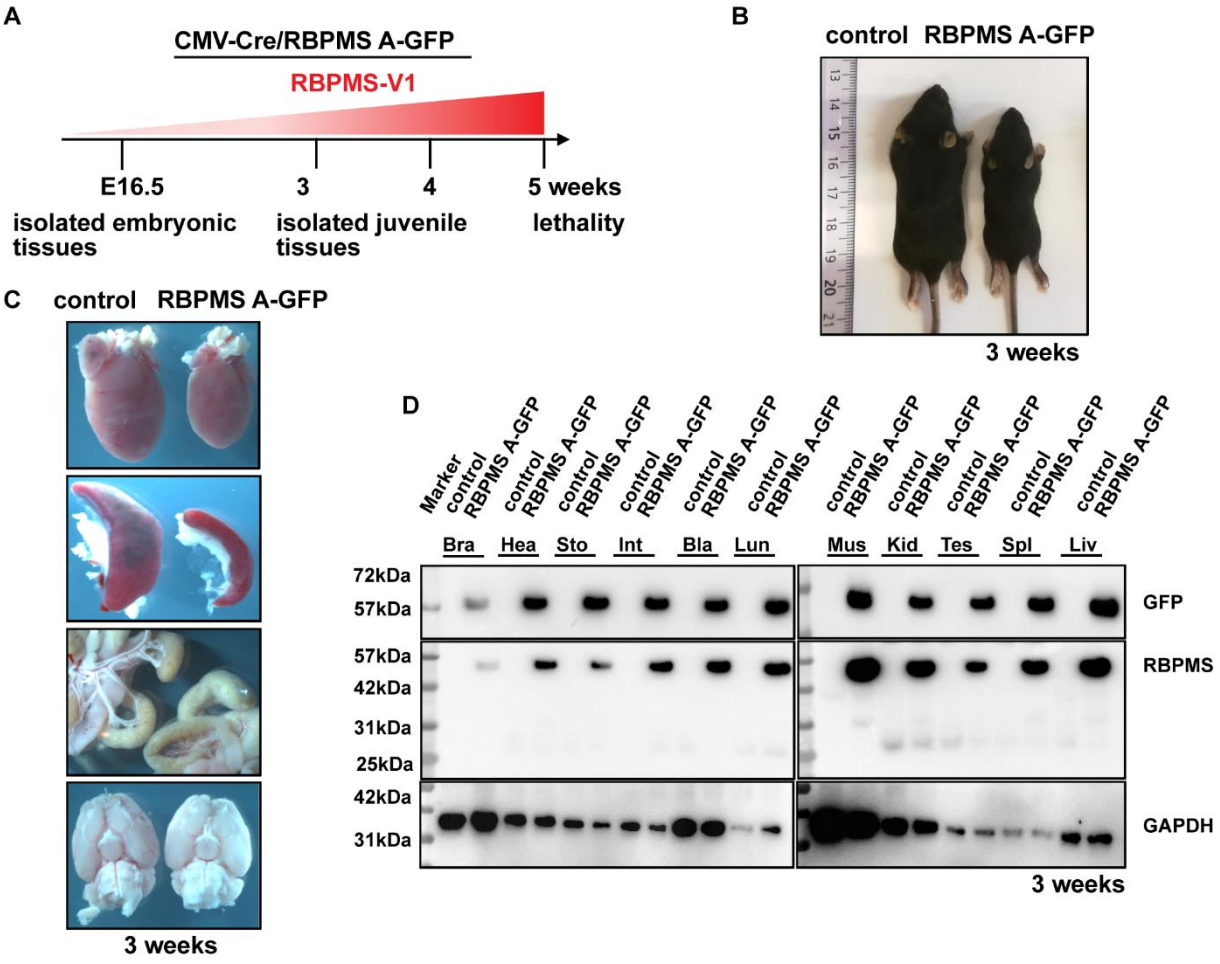

Figure 11. Global RBPMSA OE results in juvenile lethality.

A. Timeline of CMV-Cre mediated global overexpression of RBPMSA-GFP in various tissues. **B.** Images of control and RBPMSA-GFP OE mice at 3 weeks of age. **C.** Different tissues of control and RBPMSA-GFP OE at 3 weeks of age. Tissues: heart, intestine, spleen and brain. **D.** Western blot analysis using RBPMS and GFP specific antibodies in different tissues of control and RBPMSA-GFP OE mice. GAPDH was used as control. Bra: Brain; Hea: Heart; In: intestine; Bla: Bladder; Lun: Lung; Mus: Muscle; Kid: kidney; Tes: Testis; Spl: Spleen; Liv: Liver.

RBPMS/2 regulate cardiomyocyte specific alternative splicing (AS) during heart development

Since RBPMS localizes predominantly to the nucleus of embryonic cardiomyocytes and GFP tagged RBPMS2 is present in the nucleus and cytoplasm, we hypothesized that RBPMS and RBPMS2 might act together to accomplish proper AS during heart development. In order to avoid secondary effects caused by severe cardiac defects RNA-sequencing analysis of hearts was performed using material from both previously mentioned mutant strains at two time points (XML-dKO E11.5: early time point and aMyHC-dKO E16.5: late time point), when the morphological phenotype was not pronounced or initiated (Figure 12A-C). Characteristic cardiac stress markers like *Nppa* and *Nppb* (Man et al., 2018; Sergeeva et al., 2016) are increased in dKO hearts, whereas typical embryonic cardiac markers like *Acta1* and *Acta2* (Ruzicka and Schwartz, 1988; Woodcock-Mitchell et al., 1988) are decreased (Figure 12D). Bioinformatical analysis of AS using rMATs (Nakagaki-Silva et al., 2019; Shen et al., 2014) identified defects in all types of AS events. Skipping of exons (SE) was found to be the most prominently altered AS event, followed by mutually exclusive exons (MXE) (Figure 12E and F), depicted by Sashimi blots (Figure 12G) (Gohr and Irimia, 2019). In detail, approximately one half of all splicing events displayed reduced cassette exon inclusion rates in RBPMS/2 deficient cardiomyocytes (209 up-, 188 down-regulated exons in *XML-dKO*; 255 up- and 226 down-regulated exons in *aMyHC-dKO*) compared to controls (Figure 12E and F). An intersection of the splicing analysis from early and late dKO embryos indicated 99 common candidates (not depicted here). Gene Ontology (GO) enrichment analysis of the differentially spliced genes indicate that RBPMS/2 regulate splicing related to cardiomyocyte structural processes, such as sarcomere organization, actin and cytoskeleton protein binding, calmodulin binding and M band, myosin, Z disc and intercalated disc regulation (Figure 13A).

Selected RBPMS-dependent alternative spliced exons of functional relevant genes were validated by RT-PCR analysis, including both calmodulin binding proteins *Camk2g* and *Camk2d* (Hudmon and Schulman, 2002), actinin binding proteins such as *Tpm2*, *Ldb3*, *Pdlim7*, *Myom1* and *Tnnt2* (Weeland et al., 2015), as well as *Sptan1*, a spectrin binding protein (Bennett and Baines, 2001), and *Popdc2*, an intercalated disc (ICD) binding protein (Swan et al., 2019) (Figure 13B). These examples encompass different splicing types, such as mutually exclusive exons (*Camk2g*, *Camk2d*, *Tpm2*, *Ldb3* and *Pdlim7*) (Figure 13B), alternative 5' SS selection (*Popdc2*) (Figure 13B), exon inclusion (*Sptan1*, *Myo9a*, *Tnnt2*, *Myom1*, *Map3k7*, *Mfn2*, *Sbf2* and *St7*) (Figure 13B and C; Figure 14A) and exon exclusion (*Arhgap21*, *Mlf1* and *Bnip3l*)

(Figure 14B). Particularly, *Gyk* is assigned to two spicing types, exon inclusion of alternative exon 20 and exon exclusion of alternative exon 5, respectively (Figure 14A and B). Among our validated targets, *Myom1*, *Tnnt2* and *Bnip3l*, displayed alternative isoforms alterations from embryonic to neonatal or adult heart (Figure 13C; Figure 14A). The splicing pattern of RBPMS/2 deficient hearts at E11.5 resemble control hearts at E16.5 in respect to *Myom1* and *Tnnt2* exon exclusion. The same holds true for E16.5 RBPMS/2 mutant hearts, which display exon exclusion pattern similar to neonatal control hearts (Figure 13C).

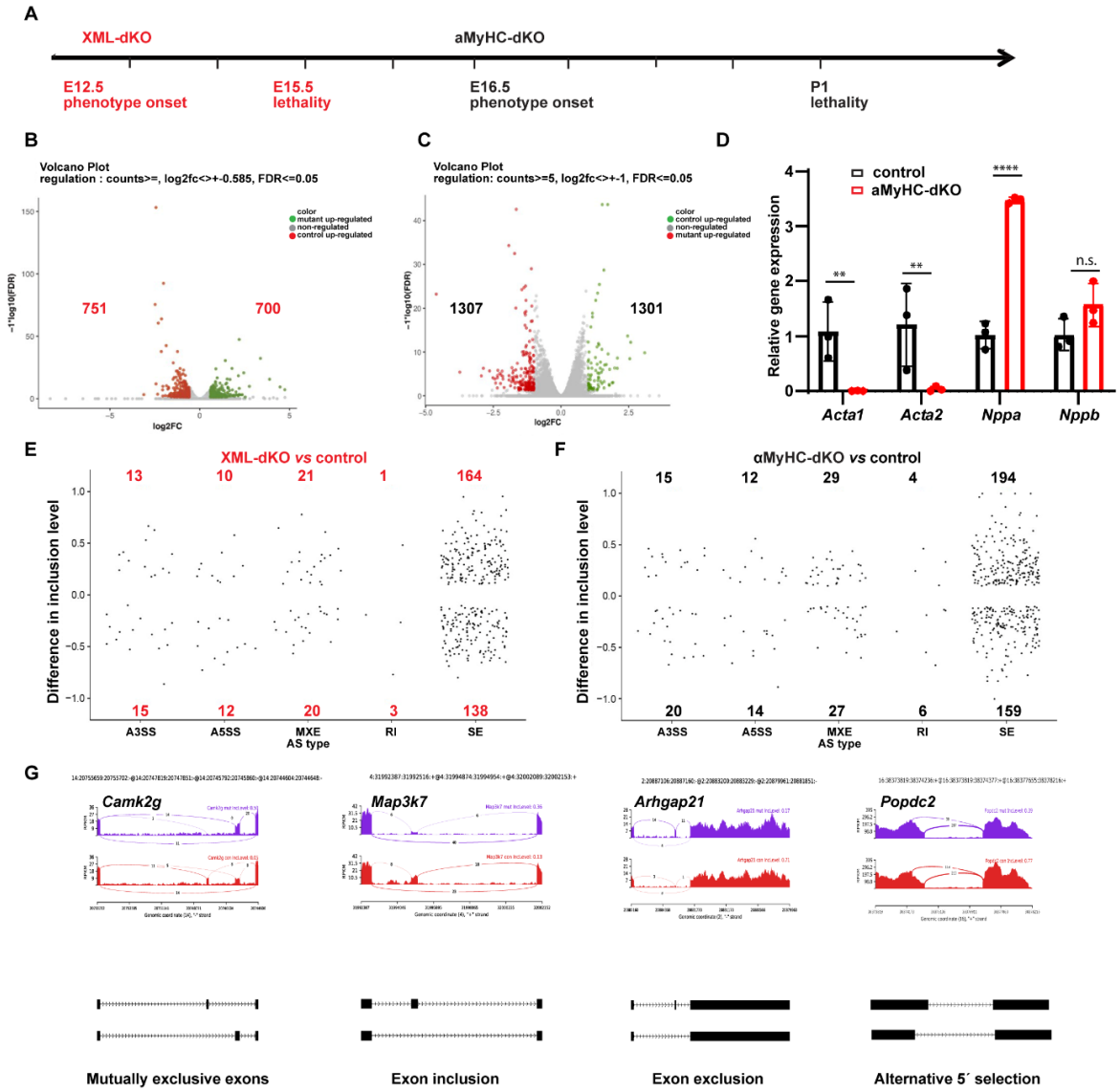

Figure 12. RNA-seq reveals transcriptional changes and alterations of AS in CM-specific RBPMS/2 dKOs.

A. Timeline of *XML-dKO* E11.5: early time point and *aMyHC-dKO* E16.5: late time point during embryonic heart development in respect to phenotype onset and lethality. **B, C.** Volcano blots display numbers of total transcriptional changes based on RBPMS/2 loss at early and late time points. Mutant: *XML-dKO* E11.5: early time point, control: *RBPMS/2*$^{flox/flox}$ (red: down-regulated, green: up-regulated in mutant versus control) (B) and mutant: *aMyHC-dKO* E16.5: late time point, control: *RBPMS/2*$^{flox/flox}$ (red: up-regulated, green: down-regulated in mutant versus control) (C). **D.** Real-time quantification of heart disease and development related markers (*Acta1*, *Acta2*, *Nppa* and *Nppb*) in control and *aMyHC-dKO* hearts. E16.5, n = 3. Statistical significance was calculated by Student's t-test (*p<0.05, **p<0.01, ***p<0.001, ****p<0.0001). **E, F.** AS types are classified (FDR < 0.05 and |IncLevelDifference| > 0.1 were considered statistically significant) in *XML-dKO* (E), and *aMyHC-dKO* (F). AS events were categorized by rMATS into alternative 5' and 3' splice site (A5SS and A3SS), mutually exclusive exon (MXE), skipped exon (SE) and retained intron (RI). Numbers indicate alternative splicing events of different splicing types in *XML-dKO* and *aMyHC-dKO*, respectively compared to control. **G.** Sashimi plots of selected candidates of different AS types. *Camk2g* resembles MXE, *Map3k7* and *Arhgap21* represent SE and *Popdc2* exemplifies an A5SS splicing event. RBPMS/2 act as activators of *Map3k7* exon inclusion as well as a repressor of *Arhgap21* exon exclusion. The numbers depicted on the arches indicate total read numbers mapping to exon-exon junctions. Inclusion Level (IncLevel) values for the alternative splicing events are indicated for mutant, purple, compared to control, red. Schematic view of alternative splicing events and corresponding chromosome coordinates are depicted at the bottom.

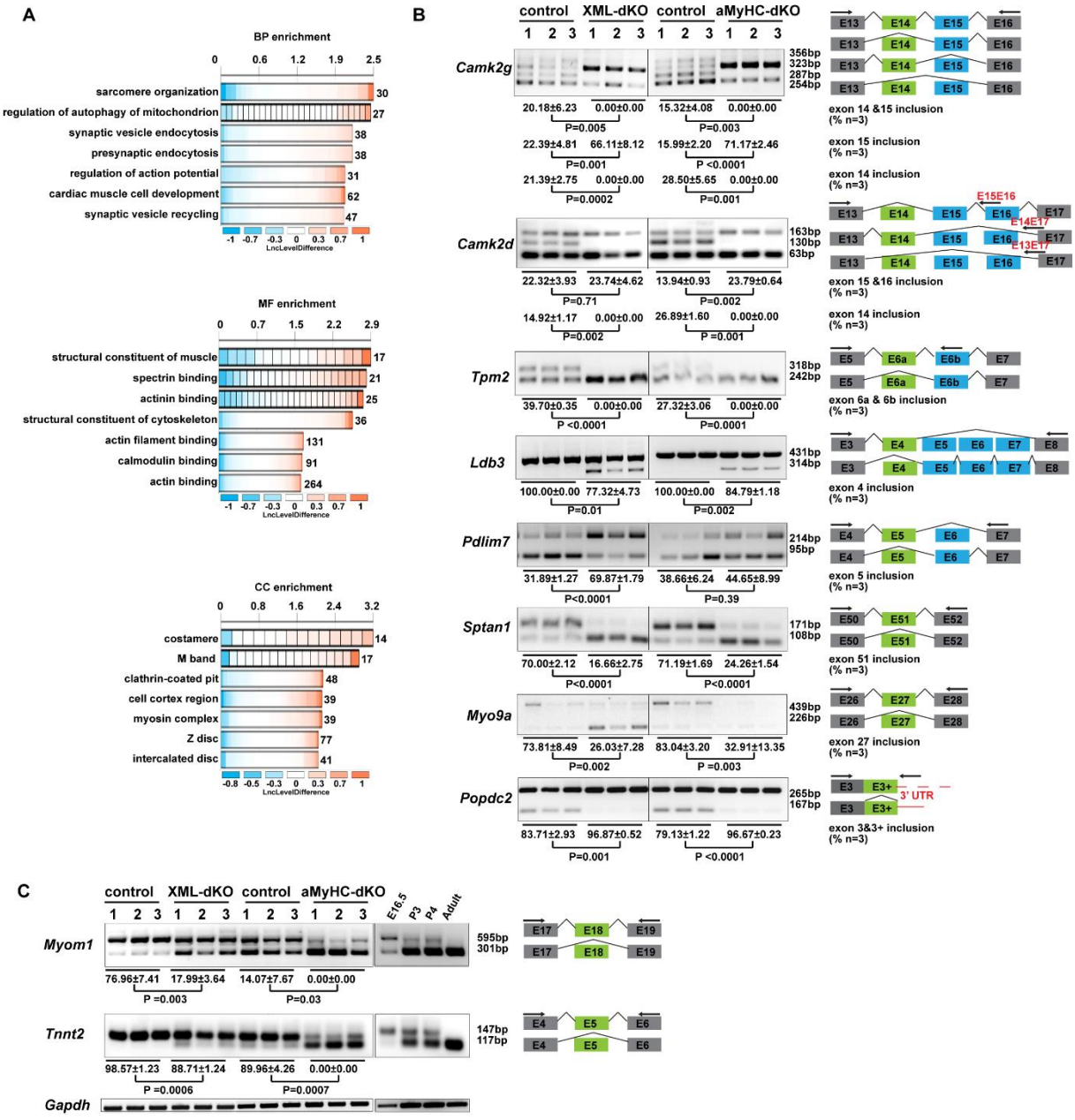

Figure 13. RBPMS/2 are key splicing regulators in heart development.

A. GO analysis of altered AS targets in CM-specific RBPMS/2 dKO hearts. Top 7 significant terms encompassing more than five genes in following three categories: Biological process (BP), molecular function (MF) and cellular component (CC) are depicted. Values on the right site of the bars indicate the total gene numbers in the enriched terms. **B.** RT-PCR analysis of RBPMS/2-dependent AS of genes regulating cytoskeleton and actin pathway in *XML-dKO* and *aMyHC-dKO* mutants at E11.5 and E16.5 with indicated genotypes, n = 3 for each group. **C.** RT-PCR analysis of RBPMS/2-dependent AS of targets related to cardiac maturation in *XML-dKO* and *aMyHC-dKO*. mRNA of embryonic hearts with indicated genotypes was used. *Gapdh* was used as control. Band intensities were quantified by Image J software. Data are shown as

standard error of mean (SEM). P-values were calculated using Student's t-test with significance set at $p \leq 0.05$. Primer positions, exon numbers and calculated band sizes are indicated. Alternatively spliced exons are labeled as green and blue boxes. Exon numbers for all genes are based on Refseq from the Ensembl genome browser 105.

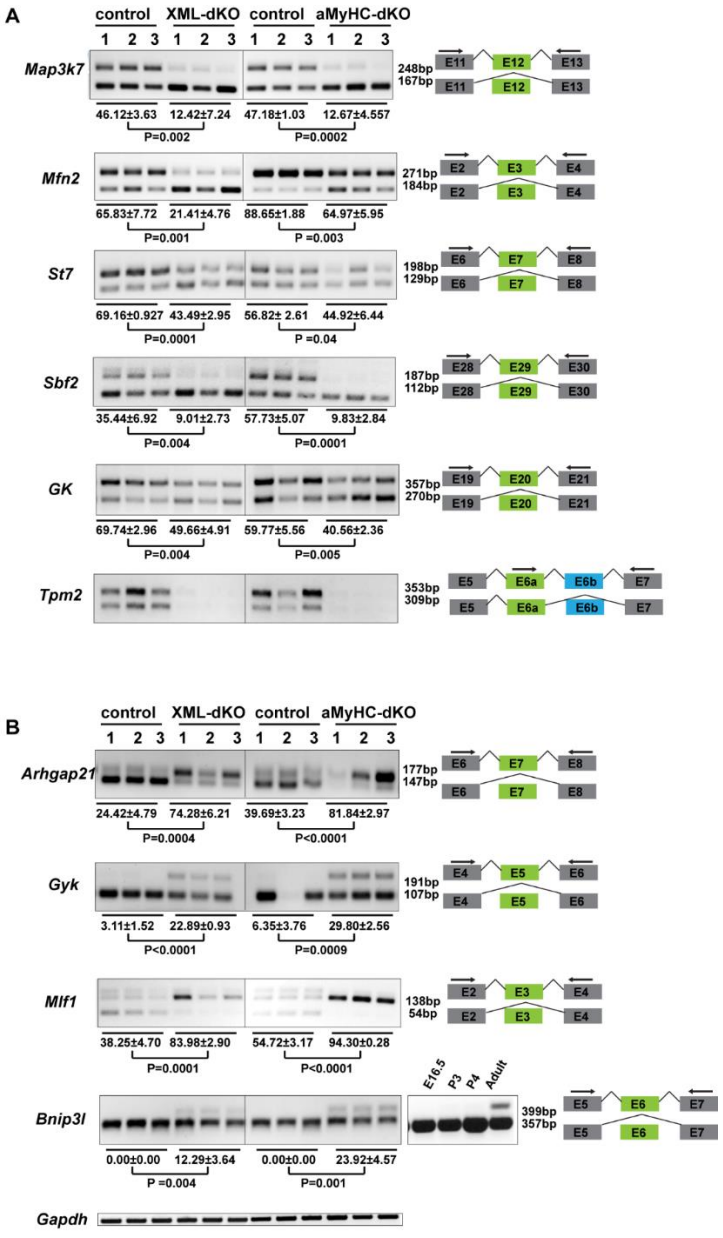

Figure 14. RT-PCR validation of RBPMS/2-dependent AS events regulated in XML-dKO and aMyHC-dKO hearts.

A. Splicing types: Exon inclusion; **B.** Splicing types: Exon exclusion (control *vs XML-dKO* or *aMyHC-dKO*), n = 3 for each group. Band intensities were quantified by Image J software. Data are standard error of mean (SEM). P-values were calculated using Student's t-test with significance set at $p \leq 0.05$. Primer positions, exon numbers and expected band sizes were

indicated. Alternatively spliced exons are labeled as green and blue boxes. Exon numbers for all genes are based on Refseq from the Ensembl genome browser 105.

RBPMSA OE induces CM-specific AS in several tissues and prevents effects caused by loss of RBPMS/2 in cardiomyocytes

Global RBPMSA OE (Figure 11) induces several heart specific splicing events in non-cardiac tissues, including cardiac-specific splicing of *Tpm2, Map3k7*, *Sptan1, St7, Camk2g* and *Bnip3l* (Figure 15A). As previously mentioned, *Tpm2* displays a mutually exclusive AS event incorporating either the cardiomyocyte specific, RBPMS/2 dependent exon 6a or exon 6b (Figure 13B; Figure 14A). Enforced global RBPMSA OE induces enhanced exon 6a expression in embryonic liver, stomach and intestine but not in limbs. However, tibialis anterior (TA) muscles of 3-week-old RBPMSA OE mice showed inclusion of the cardiomyocyte specific exon 6a (Figure 15A). Furthermore, we found that the cardiomyocyte-enriched exon 12 of *Map3k7* is expressed at low levels in embryonic liver and limbs, and completely absent in wildtype 3 week-old muscles. Of note, exon 12 of *Map3k7* is not expressed in embryonic cardiomyocytes of RBPMS/2 dKO mice (Figure 13B). Interestingly, global OE of RBPMSA resulted in a modest upregulation of exon 12 of *Map3k7* in embryonic liver and limb and a strong upregulation in 3-week-old skeletal muscles (Figure 15A). Two additional candidates, *St7* (exon 7) and *Sptan1* (exon 51) respectively, which exhibit a partial loss of cardiomyocyte specific cassette exons in RBPMS/2 dKO hearts (Figure 13B; Figure 14A), showed an increased inclusion of cardiac exons in embryonic limbs of RBPMSA OE mice (Figure 15A). In total, 4 out of 6 selected splicing events in RBPMSA overexpressing tissues are related with exon inclusion, indicating that RBPMS may act as a splice activator, which cooperates with additional splicing factors to exert its function. In contrast, OE of RBPMSA identified 2 candidates, *Bnip3l* (exon 6) and *Camk2g* (exon 15) with decreased exon inclusion in 3-week-old skeletal muscles, indicating that RBPMSA can also act as a splicing repressor (Figure 13B; Figure 14B; Figure 15A).

Based on the regulatory function of RBPMSA in AS in different tissues, we reasoned that OE of RBPMSA might prevent defects in *RBPMS* A^{Resc} hearts by normalizing aberrant AS (Figure 10). RT-PCR analysis indicated that expression of RBPMSA-GFP in RBPMS/2 dKO hearts not only prevented embryonic lethality but partially restored normal splicing pattern, either exon inclusion or exclusion, for all six selected candidates (Figures 15B). The reduced size of

RBPMS A^{Resc} adult hearts (Figure 10 B and C) indicate, that either accuracy of AS ratios or additional post-transcriptional regulatory processes, potentially regulated by RBPMSB or RBPMS2, might be important for cardiac maturation and maintenance.

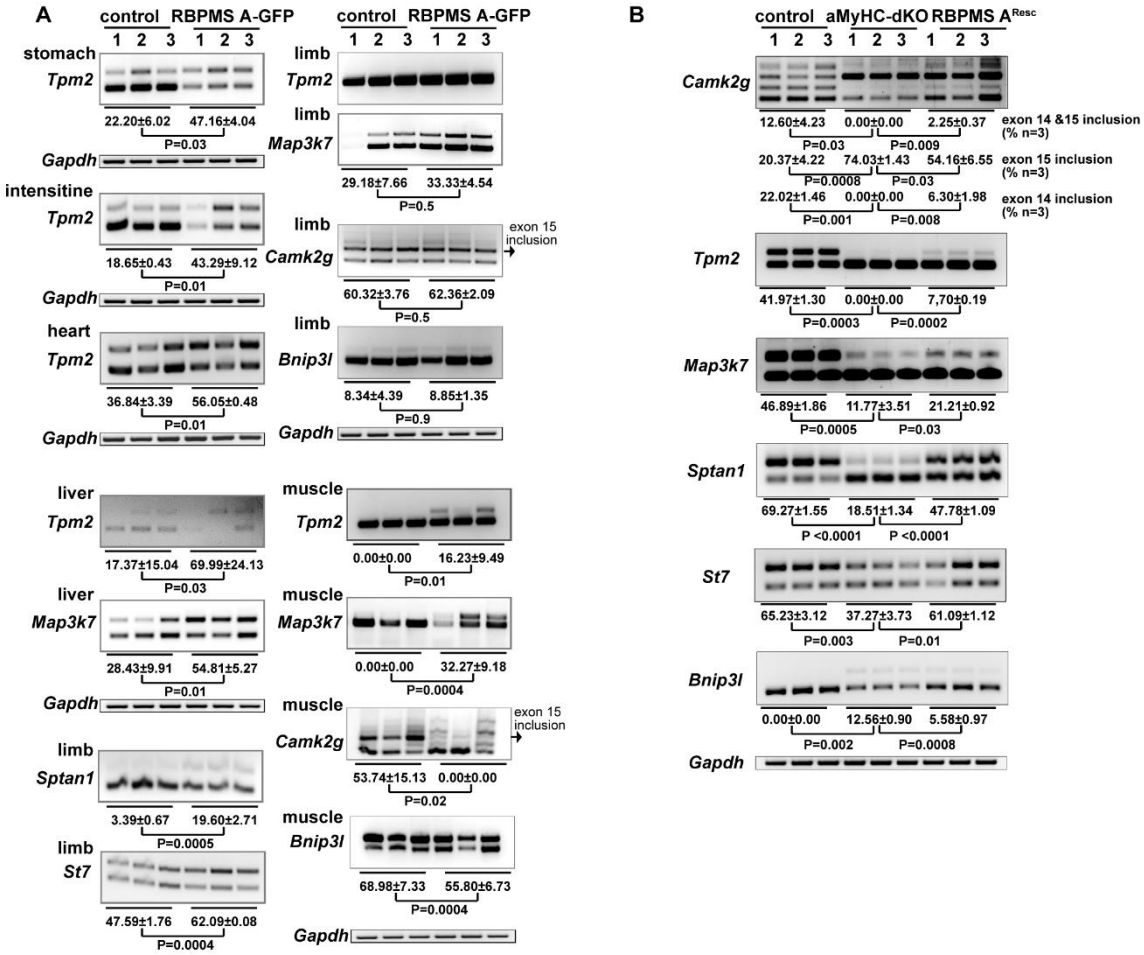

Figure 15. RBPMSA OE promotes cardiac specific splicing events in different tissues and rescues the loss of CM-specific RBPMS/2.

A. RBPMSA OE promotes cardiac specific splicing events in several tissues. RT-PCR analysis of selected RBPMS/2-dependent cardiac specific alternative splicing events in different tissues (mRNA from heart, liver, stomach, intestine and limb at E16.5 as well as skeletal muscle of control and RBPMSA OE, 3-week-old), n=3 for each group. **B.** RBPMSA OE recuses the loss of isoforms regulated by RBPMS/2 in cardiomyocytes. RT-PCR analysis of selected AS candidates from control, *aMyHC-dKO* and *RBPMSA*^{Res} cardiac mRNA with indicated genotypes at E16.5, n=3 for each group. *GAPDH* was used as control. Band intensities were quantified by Image J software. Data are standard error of mean (SEM). P-values were calculated using Student's t-test with significance set at $p \leq 0.05$. *Camkg* exon 14 and 15, *Tpm2*

exon 6a, *Map3k7* exon12, *Sptan1* exon 51, *St7* exon7 and *Bnip3l* exon 6. Corresponding primers are depicted in Figure 13 and Figure 14.

RBPMS/2 regulate CM-specific AS via dispersed tandem CAC motifs

Previous reports suggested that RBPMS directly binds to $CACN_{1-12}CAC$ motifs (Farazi et al., 2014) enriched within or adjacent to target exons, thereby regulating AS in smooth muscle cells (SMCs) (Nakagaki-Silva et al., 2019). In order to gain insights how RBPMS regulates alternative splicing of cardiac targets, we identified corresponding CAC motifs at similar positions in vicinity to RBPMS activated or repressed exons (Figure 16A and B) (Nakagaki-Silva et al., 2019). Exon inclusions suppressed by RBPMS are predominantly characterized by enriched CAC motifs within repressed exons or the adjacent upstream intronic region, while RBPMS activated exons are predominantly correlated with tandem CAC motifs in downstream intronic regions (Figure 16A and B).

As mentioned previously, dynamic isoform shifts of RBPMS/2 targets were observed during embryonic development, which are characteristic for each individual candidate. Since RBPMS/2 are continuously expressed during heart development, the interplay with additional splicing activators as well as repressors might enable fine-tuning of dynamic isoform shifts of regulated targets. In addition, RBPMS/2 binding positions on dispersed CAC motifs adjacent to altered exons might also exert a direct function on exon inclusion/exclusion (Nakagaki-Silva et al., 2019).

In order to shed light on the underlying splicing mechanism, we selected 3 RBPMS targets (*St7, Map3k7* and *Tpm2*), which were dynamically regulated during heart development and displayed more than one tandem CAC motif adjacent to the alternative exons. Among them, *St7* and *Map3k7* represent prototype examples for the inclusion of a single exon, whereas *Tpm2* (Ye et al., 2013) represents a mutually exclusive splicing event. Wildtype and mutant minigene reporter constructs were generated for all 3 candidates based on mouse genomic regions containing constitutive and alternative exons as well as shortened introns carrying intact intron-exon and exon-intron boundaries. Here, we focused on the relative position of $CACN_{1-12}CAC$ motifs in the context of alternative exons (Figure 16C-E, left).

Minigene splicing reporters were co-transfected with GFP-tagged full length RBPMS expression vectors (RBPMSA-GFP, RBPMSB-GFP and RBPMS2-GFP) as well as RRM deleted control constructs (RBPMSA-RRM-GFP, RBPMSB-RRM-GFP and RBPMS2-RRM-

GFP) into HEK293 cells (Figure 16C-E, right), which express endogenous RBPMS at low level (data not show). Co-transfection assays revealed, that RBPMSA and RBPMS2 induce a higher inclusion rate of the *St7* alternative exon 7 and *Tpm2* alternative exon 6a compared to RBPMSB, whereas mock, GFP and RRM-GFP controls did not change inclusion rates (Figure 16C and E). Slightly different results were obtained for *Map3k7*, characterized by a high inclusion rate of alternative exon 12 mediated by full length RBPMSA, RBPMSB and RBPMS2 (Figure 16D). These findings demonstrate that the wildtype splicing reporter faithfully recapitulates endogenous splicing of corresponding target genes. Furthermore, the results clearly indicate that the nuclear RBPMSA isoform represents the dominant AS regulator, and that RBPMS2 exerts a similar function as RBPMSA. In contrast, predominantly cytoplasmic localized RBPMSB is less active in regulating AS.

Next, mutant minigene reporter constructs, in which tandem CAC motifs located up- or downstream of the alternative exons were mutated to TAT, were co-transfected. Individual mutagenesis of 2 downstream located tandem CAC motifs relative to *St7* alternative exon 7 revealed that mutation of the proximal tandem CAC motif strongly abrogates exon inclusion. In contrast, mutagenesis of the distal triple CAC motif only slightly reduces exon inclusion rate compared to the wildtype splicing reporter. As expected, mutagenesis of a tandem CAC motif upstream of constitutive exon 8, which serves as an internal control, did not alter the inclusion rate of alternative exon 7. Of note, mutagenesis of all 3 tandem CAC motifs completely abolished inclusion of *St7* alternative exon 7 (Figure 16C).

The alternative exon 12 of *Map3k7* is flanked by one up- and one downstream located tandem CAC motif, which were mutated individually and concomitantly in the mutant splicing reporters. Mutagenesis of the downstream CAC motif abrogated exon 12 inclusion, indicating that this CAC motif acts as intronic splicing enhancer. However, mutation of the upstream intronic tandem CAC motif effectively increased exon 12 inclusion ratio independently of RBPMS co-transfection, implying that this position acts as an intronic splicing silencer. Concomitant mutations of the upstream and downstream tandem CAC motif nearly completely blocked inclusion of exon 12, indicating that the intronic splicing enhancer overrides the silencer (Figure 16D).

As a third example, the mutually exclusive splicing event of *Tpm2* comprising exon 6a and 6b was investigated, which is regulated by the polypyrimidine tract binding protein (PTB) during heart development (Ye et al., 2013). Here, exon 6a represents the RBPMS induced, cardiac

specific exon, which is flanked by one upstream and 2 downstream intronic tandem CAC motifs. Mutation of the distal downstream tandem CAC motif effectively decreased inclusion of exon 6a, mediated by RBPMSA, RBPMSB and RBPMS2. Strikingly, concomitant mutations of the upstream and both, proximal and distal, downstream intronic tandem CAC motifs completely abolished RBPMS-induced activation of exon 6a (Figure 16E). Based on results from the splicing reporter, it was concluded that two or more tandem CAC motifs adjacent to alternative exons regulate splicing of these targets during heart development and maturation.

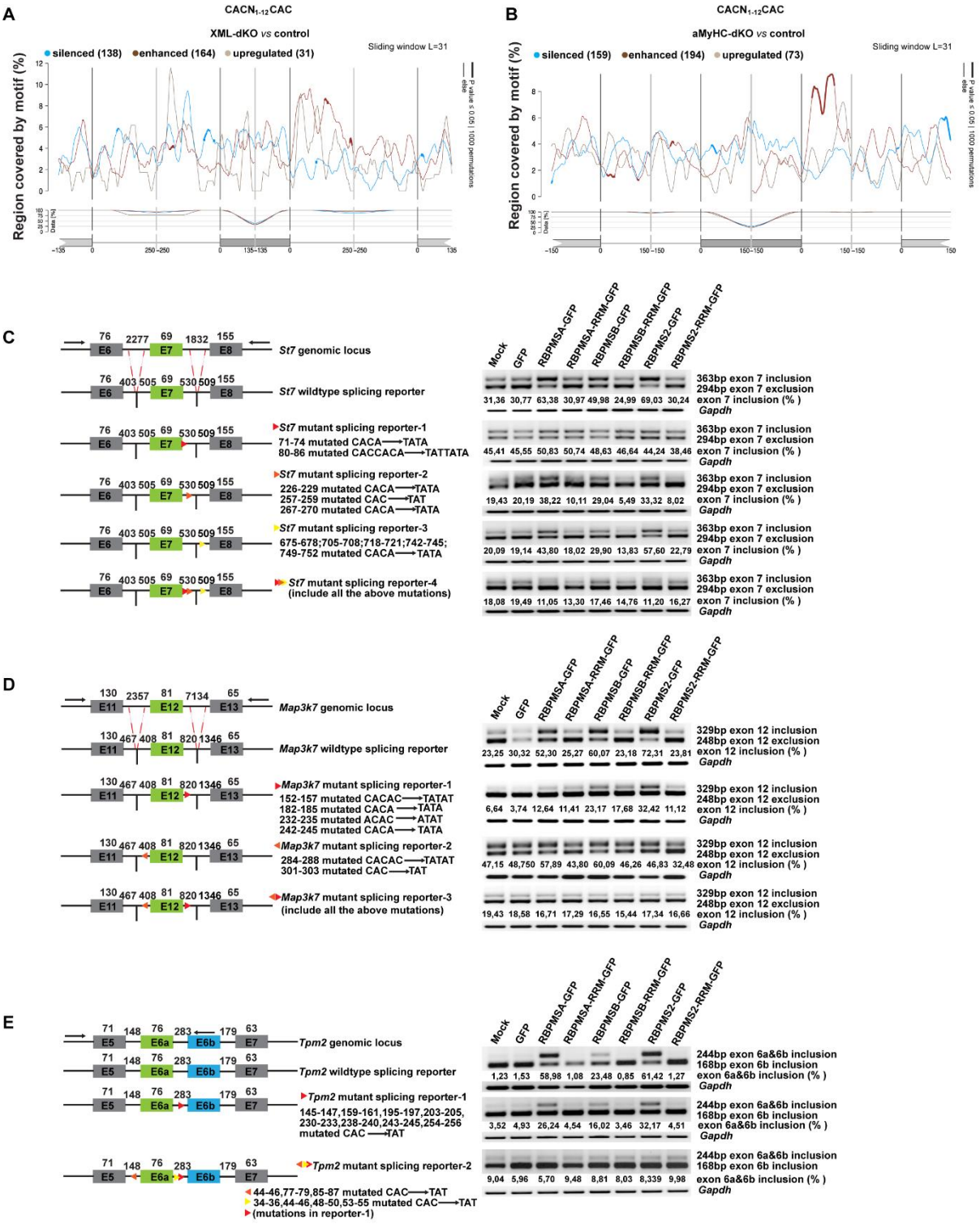

Figure 16. RBPMS and RBPMS2 regulate AS via tandem CAC motifs.

A, B. RBPMS binding motif (tandem CAC motifs) map deduced from altered exons of RBPMS/2 dKO hearts (*XML-dKO* versus *control*, A and *aMyHC-dKO* versus *control*, B). Silenced, blue, enhanced, brown. and unregulated, gray, cassette exons are shown. Statistical significance: p<0.05, 1000 permutations. **C-E.** *St7* exon 7, *Map3k7* exon 12 and *Tpm2* exon 6a

inclusion is mainly mediated by downstream CAC stretches. Left: schematic view of altered exons and shortened flanking introns of wildtype and mutant splicing reporter minigenes for *St7* (C), *Map3k7* (D), *Tpm2* (E). Primer positions to detect the alternative splicing events are labeled by black arrows. Arrowheads indicate the position of upstream or downstream located CAC motifs as well as corresponding mutations. Right: RT-PCR analysis of minigene splicing reporters in HEK293 cells co-transfected with mock (reporter only), GFP (empty vector), RBPMSA-GFP, RBPMSA-RRM-GFP, RBPMSB-GFP, RBPMSB-RRM-GFP, RBPMS2-GFP, RBPMS2-RRM-GFP. Altered alternative exons are depicted in green or blue and constitutive exons are labeled in grey. Band intensities were quantified by Image J.

RBPMS/2 dKO results in nuclear abnormalities of embryonic cardiomyocytes via the loss of a cardiac specific *Camk2g* isoform

Our ultrastructural analysis using electron microscopy indicated an abnormal structure of embryonic cardiomyocytes in *aMyHC-dKO* mice at E16.5 accompanied by sarcomere defects and nuclear abnormalities (Figure 5A). GO enrichment analysis (Figure 13A) as well as validation of selected AS candidates (Figure 13B) suggest that RBPMS/2 orchestrate an alternative splicing program required for sarcomere organization and function, which is further supported by sarcomere defects of RBPMS/2 deficient hearts.

Next, we sought to examine the association between altered alternative splicing and nuclear morphology. Since identification of the nucleation status is challenging in embryonic cardiomyocytes, we combined the early and late CM-specific dKOs with the double-fluorescent mT/mG Cre reporter strain (Figure 17A and B; Figure 18) (Muzumdar et al., 2007) to obtain *RBPMS/2$^{flox/flox}$ / R26$^{dTomato/GFP}$ / XML-Cre*, hereafter referred to as *mTmG XML-dKO* and *RBPMS/2$^{flox/flox}$ / R26^{dTomoato} / aMyHC-Cre*, hereafter referred to as *mTmG aMyHC-dKO*. Non-cardiomyocytes lacking Cre-expression generate a membrane-targeted tandem dimer Tomato (mT), whereas CM-specific expression of Cre switches the labelling to membrane-tethered green fluorescent protein (mG). This approach enables quantitative assessment of normal (mononucleated) and abnormal (multinucleated / micronuclei) cardiomyocytes in corresponding mutants compared to control littermates. Overall, we observed a significant increase of abnormally nucleated cardiomyocytes in RBPMS/2 deficient hearts (Figure 17A and B; Figure18).

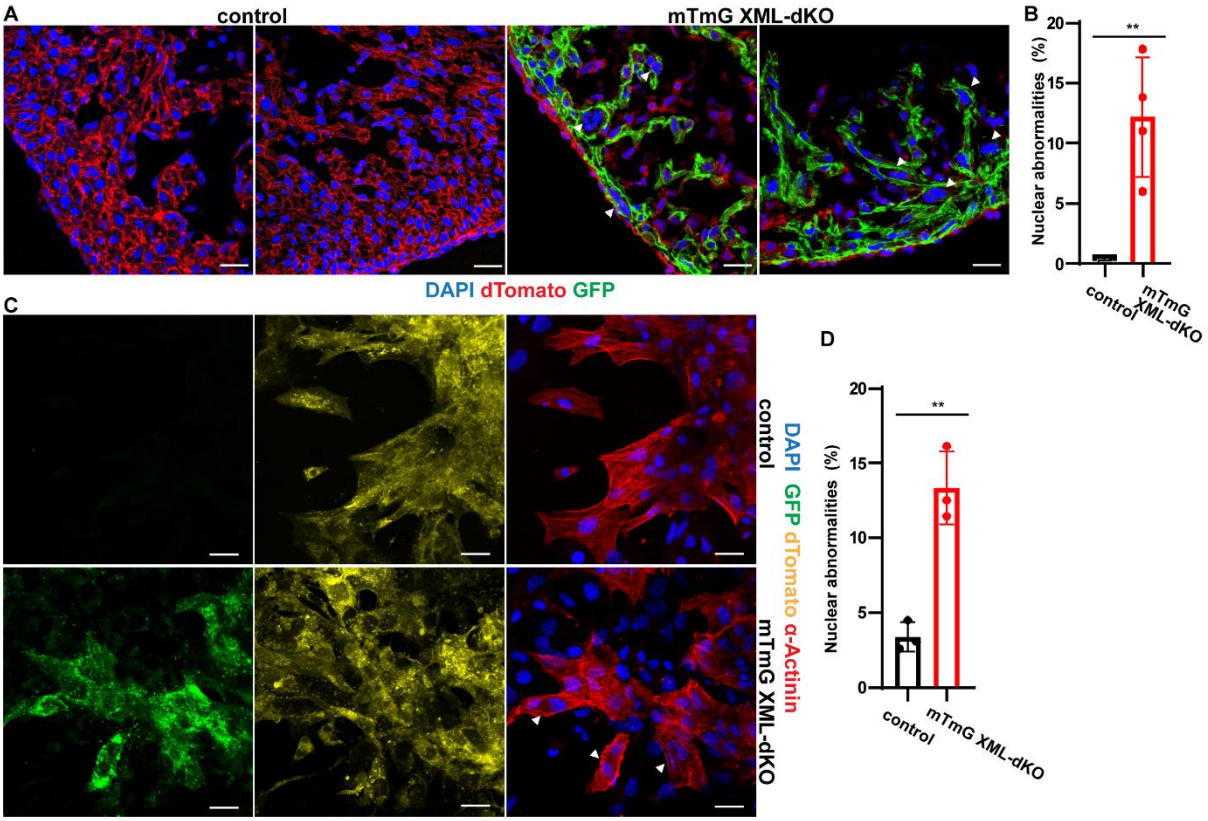

Figure 17. Early myocardial-specific inactivation of RBPMS/2 results in nuclear abnormalities of embryonic cardiomyocytes.

A. Immunofluorescence images of heart sections from control and *mTmG XML-dKO* at E12.5. Scale bar, 20 µm. GFP, green, dTomato, red, and nuclei (DAPI, blue). White arrow labels abnormal nucleated cardiomyocytes. **B.** Quantification of abnormal nucleated cardiomyocytes on heart sections of control and *mTmG XML-dKO* hearts at E12.5 (n = 4 for each group, totally 2219 control *vs* 567 *XML-dKO* cardiomyocytes were analyzed). Statistical significance was calculated using Student's t-test (**p<0.01). **C.** Immunofluorescence images of isolated and cultured cardiomyocytes of control and *mTmG XML-dKO* at E12.5d, n = 3 for each group. Scale bar, 20 µm. GFP, green, dTomato, yellow, α-Actinin, red, and nuclei (DAPI, blue). White arrowheads label abnormal nucleated cardiomyocytes. **D.** Quantification of nuclear abnormalities of control and *mTmG XML-dKO* cultured cardiomyocytes at E12.5d (n = 3 for each group, totally 329 control *vs* 698 *mTmG aMyHC-dKO* cardiomyocytes were analyzed). Statistical significance was performed using Student's t-test (**p<0.01).

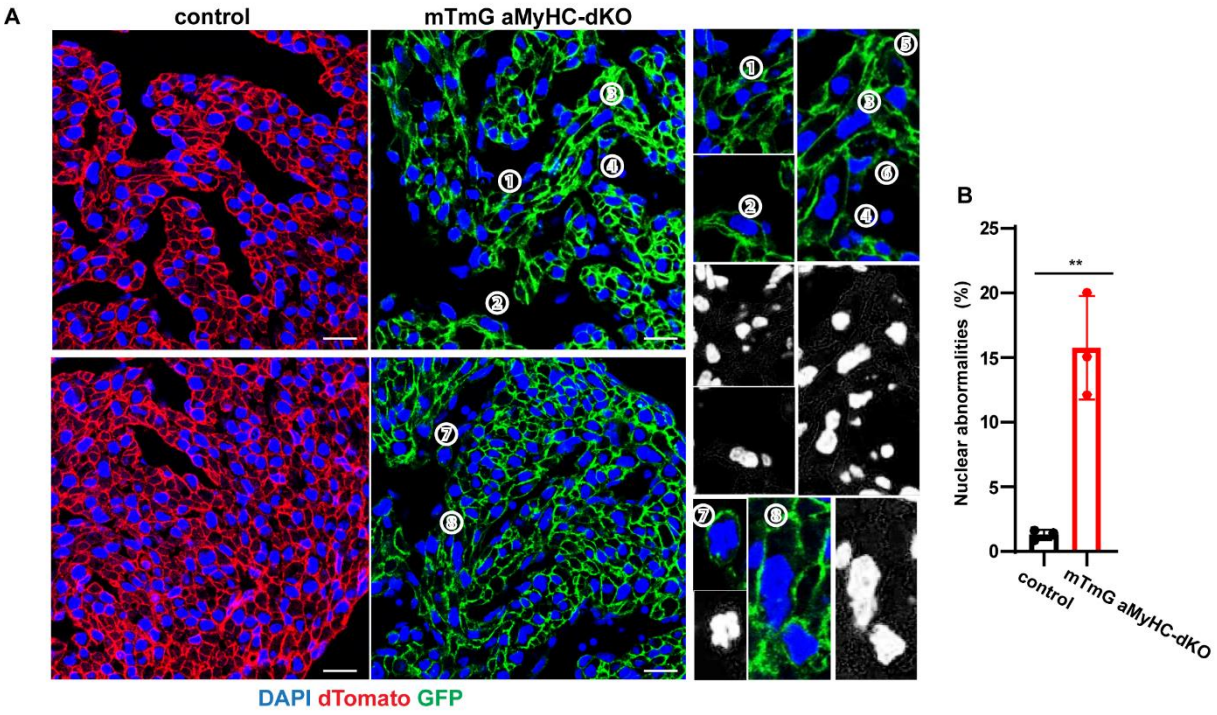

Figure 18. *aMyHC-dKO* mice show nuclear abnormalities in embryonic CMs.

A. Immunofluorescence images of heart sections of control and *mTmG aMyHC-dKO* at E16.5. Scale bar, 20 μm. GFP, green, dTomato, red, and nuclei (DAPI, blue). Number 1 - 8 label selected abnormal nucleated cardiomyocytes, including number 1 to 5 and 7 to 8 label multinucleated cardiomyocytes whereas number 6 labels a micronuclei containing cardiomyocyte. **B.** Quantification of abnormal nucleated cardiomyocytes on heart sections of control and *mTmG aMyHC-dKO* at E16.5 (n = 3 for each group, totally 1223 control *vs* 506 *mTmG aMyHC-dKO* cardiomyocytes were analyzed). Statistical significance was calculated by Student's t-test (**p<0.01).

In addition, TUNEL staining revealed increased apoptosis in *aMyHC-dKO* mutant hearts (Figure 19A and B), while the proliferation (PH3 positive) rate was unaltered (Figure 19C and D). Since quantification of nucleation on sections is error-prone, we next quantified the nucleation state in cultured isolated cardiomyocytes from the *mTmG XML-dKO* and control embryos (E11.5). Cultured cardiomyocytes from *mTmG XML-dKO* displayed an increased ratio of abnormal nuclei compared to control littermates (Figure 17C and D), supporting our results from sections.

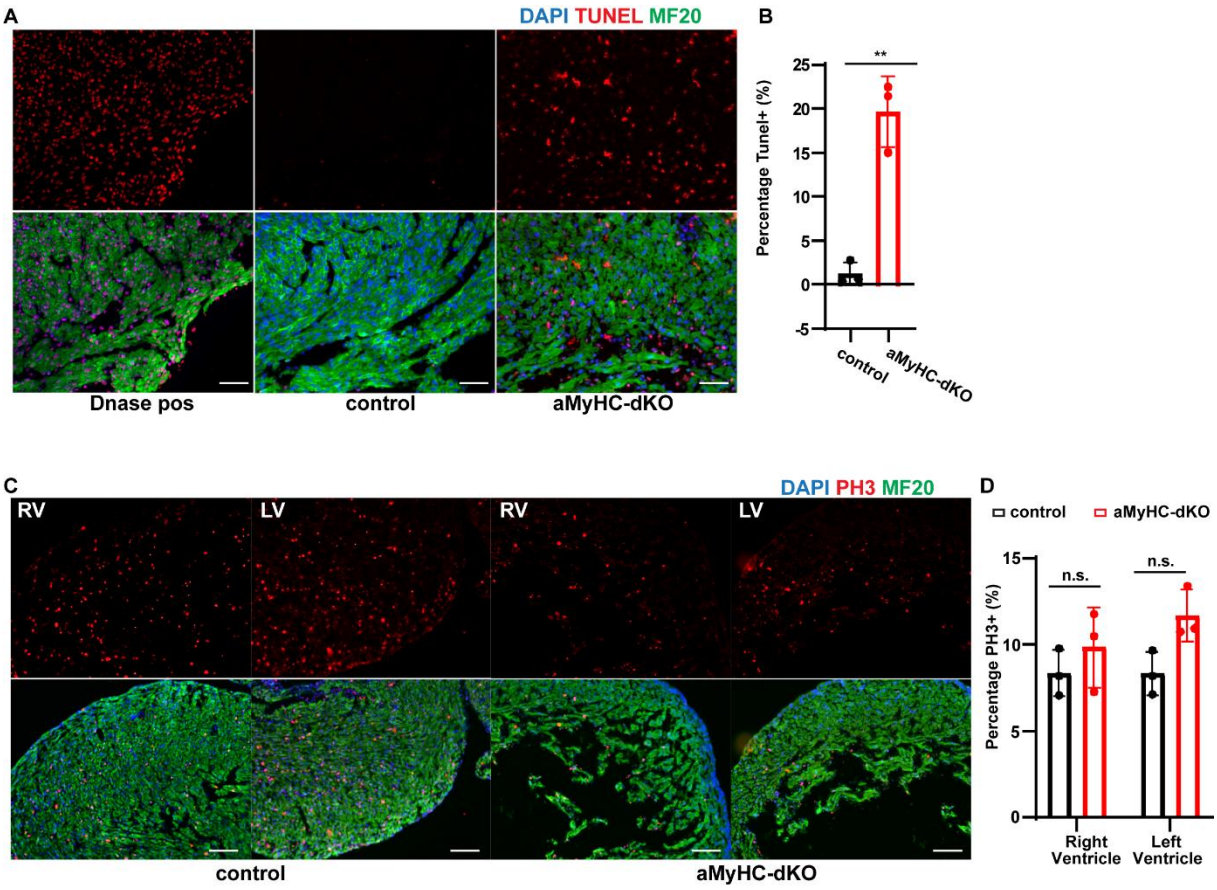

Figure 19. Inactivation of RBPMS/2 in embryonic cardiomyocytes causes apoptosis.

A. TUNEL assay of control and *aMyHC-dKO* mouse heart sections at E18.5. Scale bar, 20 μm. TUNEL, red, MF20, green, and nuclei (DAPI, blue). **B.** Quantification of TUNEL positive cardiomyocyte ratios of control and *aMyHC-dKO* hearts. **C.** Immunofluorescence staining of the proliferation marker PH3 in control and *aMyHC-dKO* mouse heart sections at E18.5. Scale bar, 50 μm. PH3, red, MF20, green; nuclei (DAPI, blue). **D.** Quantification of PH3 positive cardiomyocyte ratios in right and left ventricles, respectively. Statistical significance was calculated by Student's t-test (**p<0.01).

Additionally, we observed a minor fraction of mitotically defective cardiomyocytes in RBPMS/2 deficient hearts (Figure 17A). Nuclear abnormalities usually emerge as a result of errors in chromosome partitioning during mitosis (Holland and Cleveland, 2012). However, mitosis of embryonic cardiomyocytes is rare and defective mitosis in dividing CMs is even rarer, which complicates quantification of abnormally nucleated cardiomyocytes on heart sections (Figure 17A; Figure 18A) or isolated cardiomyocytes of single hearts (Figure 17C). To

overcome this limitation and to systematically categorize different types of mitotic and chromosomal defects arising from concomitant loss of RBPMS and RBPMS2, we performed our analysis in primary embryonic RBPMS/2$^{flox/flox}$ cardiomyocytes, which were infected by Adeno-null (hereafter referred to as *Ad-null*) or Adeno-Cre (hereafter referred to as *Ad-dKO*) virus (Figure 20; Figure 23A). Microtubule immunofluorescence staining by α-Tubulin and chromosome staining by DAPI, enabled visualization of enhanced multipolar spindle formation (red numbers label multipolar spindles in metaphase) and chromosome mis-segregation (yellow arrowheads) in *Ad-dKO* cardiomyocytes (Figure 20A-C). We identified different types of deviant mitotic spindles and chromosome distribution defects in embryonic RBPMS/2 deficient cardiomyocytes. Isolated embryonic cardiomyocytes infected by Adeno-Null, which served as controls, showed proper alignment of condensed chromosomes at the metaphase plate accompanied by bipolar spindle formation and sister chromatids separation (Figure 20A / a). In anaphase control cardiomyocytes, sister chromatids are separated and form equal repartition of chromosomes positioned on both sides of the spindle equator (Figure 20 / h). During telophase, chromosomes in control cardiomyocytes have completed their movement to the spindle poles and the nuclear envelope starts to re-form around each of the two chromosome sets (Figure 20A / m). In contrast, mutant mitotic CMs infected by Adeno-Cre exhibit an increased percentage of unaligned chromosomes (Figure 20A / b-c), multipolar spindle formation (Figure 20A / d-g) in metaphase as well as chromatin bridges (Figure 20A / i) and lagging chromosomes (Figure 20A / j-l) in anaphase (Figure 20B) (Baudoin and Cimini, 2018; Schukken and Foijer, 2018). A detailed characterization of the anaphase indicated that lagging chromosomes arise concomitantly with the formation of bipolar (Figure 20A / j) and multipolar spindles (Figure 20A / k-l). In line with this observation, we also detected cardiomyocytes containing micronuclei in telophase (Figure 20A / n-q). As a consequence, *RBPMS/2* deficient cardiomyocytes show an increased ratio of nuclear abnormalities (Figure 20A / s-v and C), supporting our previous results (Figure 17 and 18).

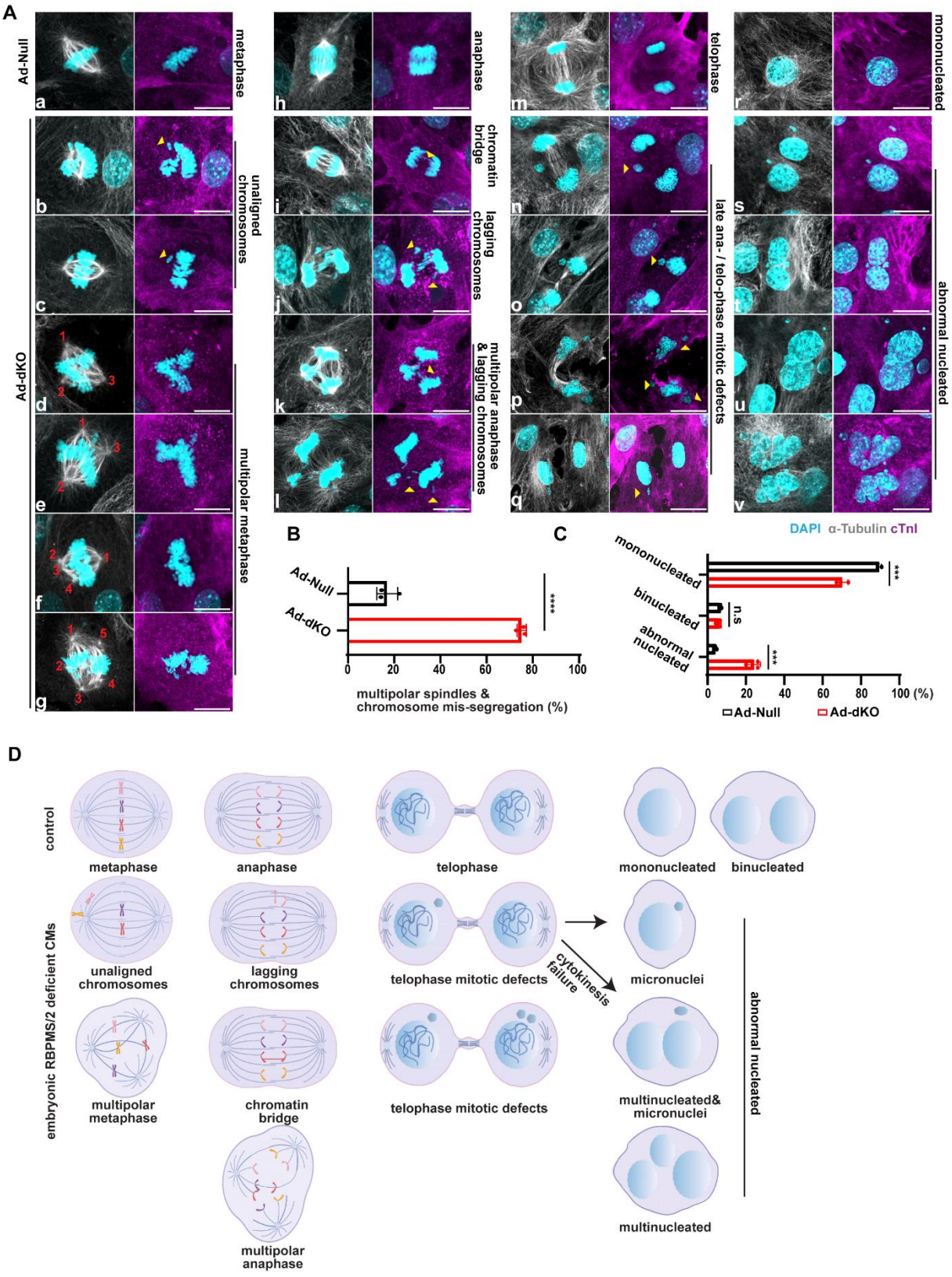

Figure 20. RBPMS/2 inactivation alters nuclearity of embryonic cardiomyocytes and causes spindle and chromosome segregation defects.

A. Immunofluorescence staining of isolated homozygous embryonic *RBPMS/2*$^{flox/flox}$ cardiomyocytes infected by Adeno-Null (control) and Adeno-Cre, respectively at E14.5 and thereafter cultured for 48 hours. Scale bar, 10 µm. Cardiac-specific marker troponin I (cTnI; TNNI3, purple; microtubule marker α-tubulin, grey; nuclei (DAPI, blue). **B.** Quantification of mitotic spindle and chromosome segregation defective embryonic cardiomyocytes were normalized by the number of cardiomyocytes in mitotic phase, E14.5 (n = 3 for each group, 36, 35 and 62 cardiomyocyts for Ad-Null group *vs* 25, 47 and 59 cardiomyocytes for Ad-dKO group were analyzed). **C.** Quantification of abnormal nucleated cardiomyocytes, E14.5 (n = 3 for each group, >350 cardiomyocytes per group were analyzed). Statistical significance was performed using Student's t-test (***p<0.001, ****p<0.0001). Yellow arrowheads label chromosome mis-segregation. Red numbers label multipolar spindles. **D.** Schematic diagram of individual mitotic defects encompassing multipolar spindles, chromosome mis-segregation and failure of cytokinesis. Metaphase chromosomes, colored, mitotic spindles, purple, and nuclei, blue, are indicated.

During the attempts to correlate RBPMS/2 AS targets with formation of multipolar mitotic spindles and defective nuclei, the calcium/calmodulin dependent protein kinase II gamma (*Camk2g*) attracted our attention. RBPMS/2 are required for inclusion of *Camk2g* exon 14 in embryonic cardiomyocytes (Figure 13B). Exon 14 codes for a 11-amino acid nuclear localization domain of *Camk2g*, which only occurs in cardiomyocytes and is not detectable in other tissues except the brain (Figure 21A). Furthermore, during *in vitro* differentiation of embryonic stem cells to embryonic bodies and cardiac bodies, the exon 14-containing isoform of *Camk2g* appears in cardiac bodies and increases during maturation (Figure 21B). Global knockdown of *Camk2g* results in abnormal bipolar spindle formation in immortalized human myelogenous leukemia K562 cells (Holmfeldt et al., 2005), which makes *Camk2g* an attractive candidate to mediate effects of RBPMS/2 AS on spindle formation.

In order to test the function of the cardiac specific *Camk2g* isoform encoding exon 14, we performed a siRNA-mediated knockdown of exon 14 (siCamk2g-exon 14) in E14.5 wildtype cardiomyocytes. In parallel, nonsense scramble siRNA knockdown, abbreviated as siControl, was performed to test potential side effects of siRNA transfection (negative control). Semi-quantitative RT-PCR analysis of *Camk2g* isoforms revealed an efficient knockdown of the exon 14 containing *Camk2g* isoform mediated by siCamk2g-exon 14, whereas siControl did not

interfere with exon 14 abundance (Figure 23B). Quantitative assessment of siCamk2g-exon 14 mediated knockdown cardiomyocytes revealed a strong increase of multipolar spindles and chromosome segregation defects as well as nuclear abnormalities (Figure 22A-C). Similar to RBPMS/2 deficient cardiomyocytes (Figure 20), siRNA mediated knockdown of *Camk2g* exon 14 causes unaligned chromosomes (Figure 22A / b-c), multipolar spindle formation (Figure 22A / d-f) in metaphase as well as chromatin bridges (Figure 22A / h) and lagging chromosomes (Figure 22A / i-j) in anaphase. These results clearly indicate that loss of the exon 14 containing *Camk2g* isoform phenocopies effects of RBPMS/2 inactivation in cardiomyocytes (Figure 20).

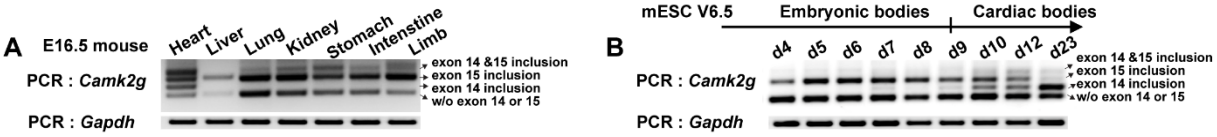

Figure 21. Alternative splicing events of *Camk2g* including exon 14 in different organs.

RT-PCR based detection of *Camk2g* alternative splicing events in different tissues during embryonic development (**A**) as well as embryonic and cardiac bodies derived from mESCs (**B**).

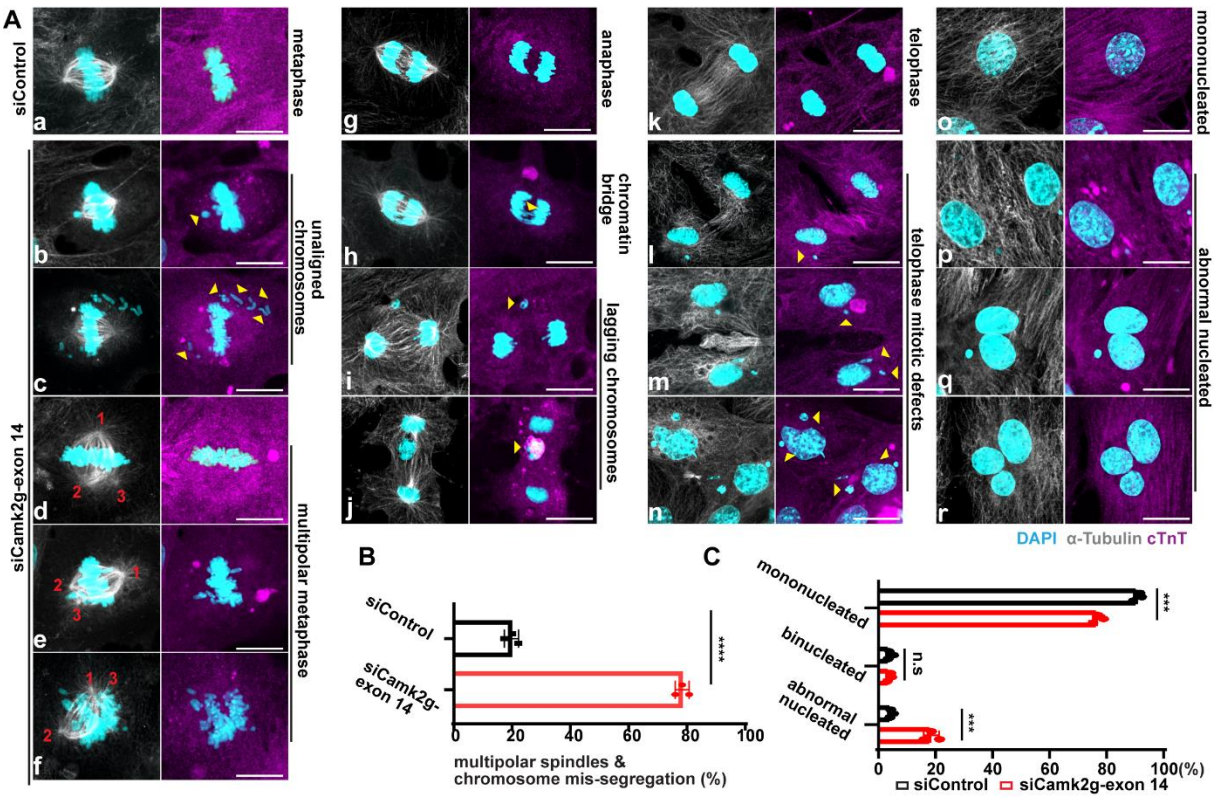

Figure 22. Inactivation of the CM-specific nuclear isoform of *Camk2g* alters nuclearity of embryonic cardiomyocytes and causes spindle and chromosome segregation defects.

A. Knockdown of CM-specific nuclear *Camk2g* isoform phenocopies mitotic spindle and chromosome segregation defects as well as nuclear abnormalities of RBPMS/2 depleted cardiomyocytes. Immunofluorescence staining of siControl and siCamk2g-exon 14 treated isolated embryonic cardiomyocytes at E14.5. Scale bar, 10 µm. cTnT, purple, α-tubulin, grey, and nuclei (DAPI, blue). **B.** Quantification of mitotic spindle and chromosome segregation defective embryonic cardiomyocytes were normalized by number of cardiomyocytes in mitotic phase, E14.5 (n = 3 for each group, 35, 131 and 81 cardiomyocytes for siControl group *vs* 26, 100 and 37 cardiomyocytes for siCamk2g-exon 14 group were analyzed). **C.** Quantification of abnormal nucleated cardiomyocytes, E14.5 (n = 3 for each group, >300 cardiomyocytes per group were analyzed). Statistical significance was performed using Student's t-test (***p<0.001, ****p<0.0001). Yellow arrowheads label the chromosome mis-segregation. Red numbers label the multipolar spindles.

Since the inclusion of exon 14 in *Camk2g* installs a nuclear localization signal (NLS) into this particular CAMK2G protein isoform, we also tested the subcellular localization of CAMK2G by immunofluorescence. In control cardiomyocytes, CAMK2G is found in both, the nuclear and the cytoplasmic compartment. In contrast, siCamk2g-exon 14 knockdown cardiomyocytes were characterized by a strongly decline of nuclear CAMK2G and a general reduction of CAMK2G abundance in the cytoplasm, despite the presence of some CAMK2G-positive dots (Figure 23C and D). These findings suggest, that the presence of the nuclear *Camk2g* isoform is instrumental for normal bipolar spindle formation, preventing multipolar spindle formation and chromosome segregation defects as well as appearance of abnormally nucleated cardiomyocytes. However, it needs to be mentioned that the adenoviral mediated inactivation of RBPMS/2 in embryonic cardiomyocytes resulted in a more severe phenotype compared to siRNA mediated knock down of the cardiac specific *Camk2g* isoform in respect to multipolar spindle formation and chromosome segregation (Figure 20 and 22). These findings strongly suggest that an altered alternative splicing regulatory network caused by loss of RBPMS/2 might involve additional targets required for proper mitotic integrity and chromosome alignment, in addition to *Camk2g*. Such targets might include genes for the actin-cytoskeleton, spindle pole, kinetochore machinery and/or focal adhesion.

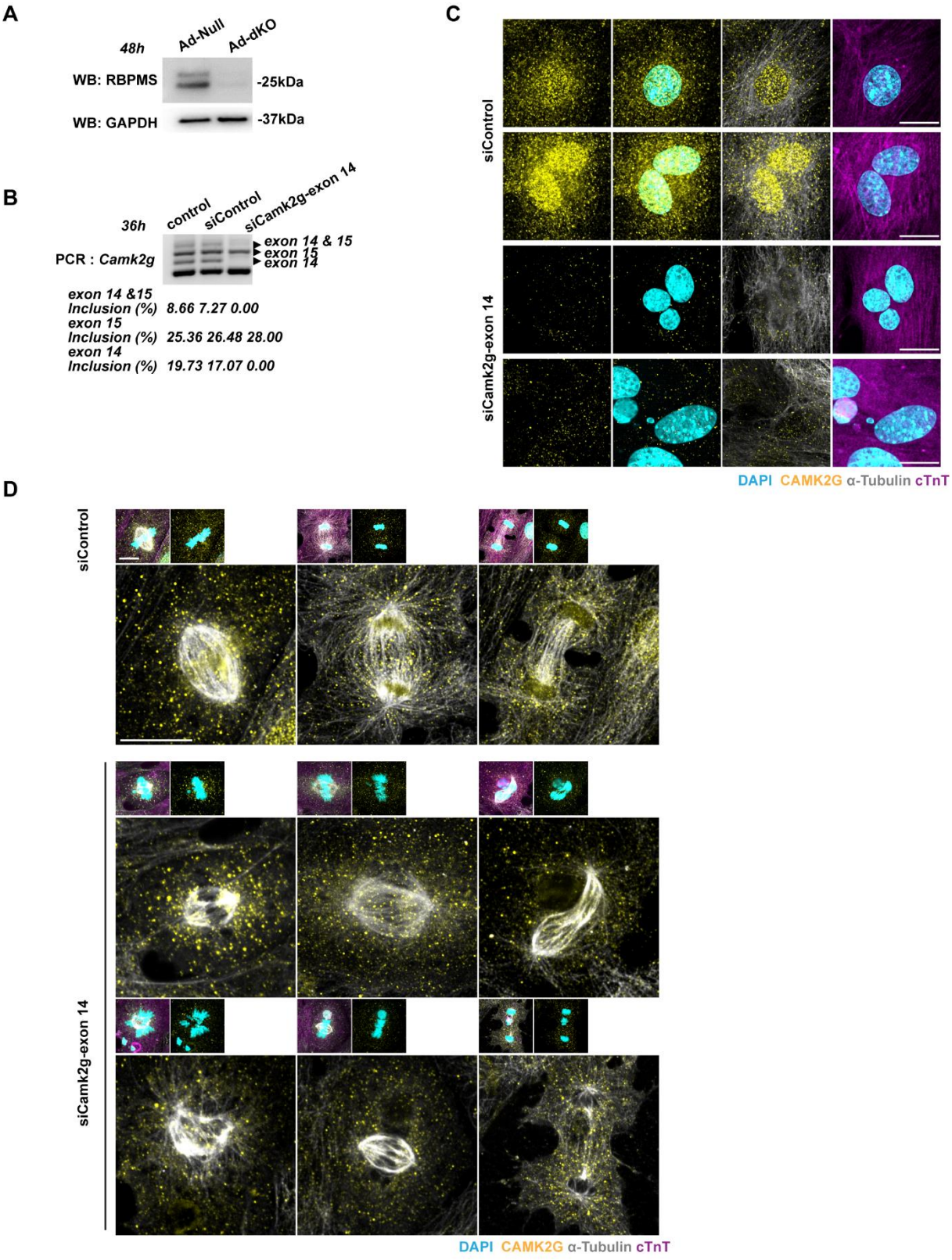

Figure 23. Validation of the knockdown of the CM-specific *Camk2g* isoform.

A. Western blot analysis of isolated homozygous embryonic (E14.5) *RBPMS/2*$^{flox/flox}$ cardiomyocytes infected with Adeno-Null (control) and Adeno-Cre virus. GAPDH was used as a loading control. **B.** RT-PCR analysis of *Camk2g* isoforms in non-transfected control as well as transfected siControl and siCamk2g-exon 14 in isolated wildtype embryonic cardiomyocytes at E14.5. **C.** Immunofluorescence staining of CAMK2G, yellow, α-tubulin, grey, cTnT, purple and nuclei (DAPI, blue) of siControl and siCamk2g-exon 14 treated isolated embryonic cardiomyocytes, E14.5. Scale bar, 10 µm. **D.** Immunofluorescence staining of CAMK2G, yellow, α-tubulin, grey, cTnT, purple, and nuclei (DAPI, blue) of siControl and siCamk2g-exon 14 treated isolated embryonic cardiomyocytes in mitotic phase. CAMK2G positive granules dock along microtubules (spindles) in a highly ordered organization in control cardiomyocytes. Scale bar, 10 µm.

RBPMS/2 and RBM20 inactivation results in a stage specific loss of the NLS-encoding CM-specific exon 14 of *Camk2g* causing nuclear to cytoplasmic localization

RBM20, a well-characterized cardiac master splicing regulator, has been previously reported to regulate multiple alternative splicing events in a rat model, recapitulating consequences of human RBM20 mutations, which cause severe human dilated cardiomyopathy (DCM) (Guo et al., 2012). Although human RBM20 point mutations exhibit rather severe phenotypes, constitutive RBM20 knockout mice are viable (van den Hoogenhof et al., 2018). In the adult rat heart, RBM20 deficiency results in a partial increase of the *Camk2g* isoform harboring exon 15. However, the authors did not comment on altered alternative splicing events encompassing exon 14 (Guo et al., 2012).

Our previous results identified alterations of *Camk2g* isoform in RBPMS/2 deficient hearts as a major driver for defective mitotic spindle formation in embryonic cardiomyocytes. To investigate whether RBM20 has also an impact on splicing of *Camk2g* isoforms, we performed RT-PCR experiments and analyzed the subcellular localization of CAMK2G by immunofluorescence staining in embryonic and adult cardiomyocytes of wildtype, heterozygous and homozygous RBM20 mutant mouse hearts. In embryonic RBM20 mutant hearts, we did not observe changes in inclusion ratios of *Camk2g* exon 14 / exon 15 compared to controls (Figure 24A). In line with this observation, CAMK2G abundance as well as subcellular localization is not altered in wildtype, heterozygous and homozygous embryonic RBM20 mutant hearts (Figure 24B). However, heterozygous and homozygous RBM20 mutant

adult hearts show a decline of exon 14 inclusion and an increased inclusion of exon 15 (Figure 24D). In accordance with the loss of the NLS-encoding exon 14, CAMK2G gradually mis-localizes from the nucleus to the cytoplasm in heterozygous and homozygous RBM20 mutants (Figure 24E). These findings indicate that RBM20 has also an impact on mutually exclusive splicing of *Camk2g* exon 14 & 15. The degree of RBM20-dependent mutually exclusive splicing of *Camk2g* exon 14 & 15 differs among different developmental stages in the heart. The current data suggest that RBPMS/2 have a higher impact than RBM20 on the NLS-containing cardiac specific *Camk2g* isoform in the embryonic heart, whereas the contribution of RBM20 increases in the adult heart.

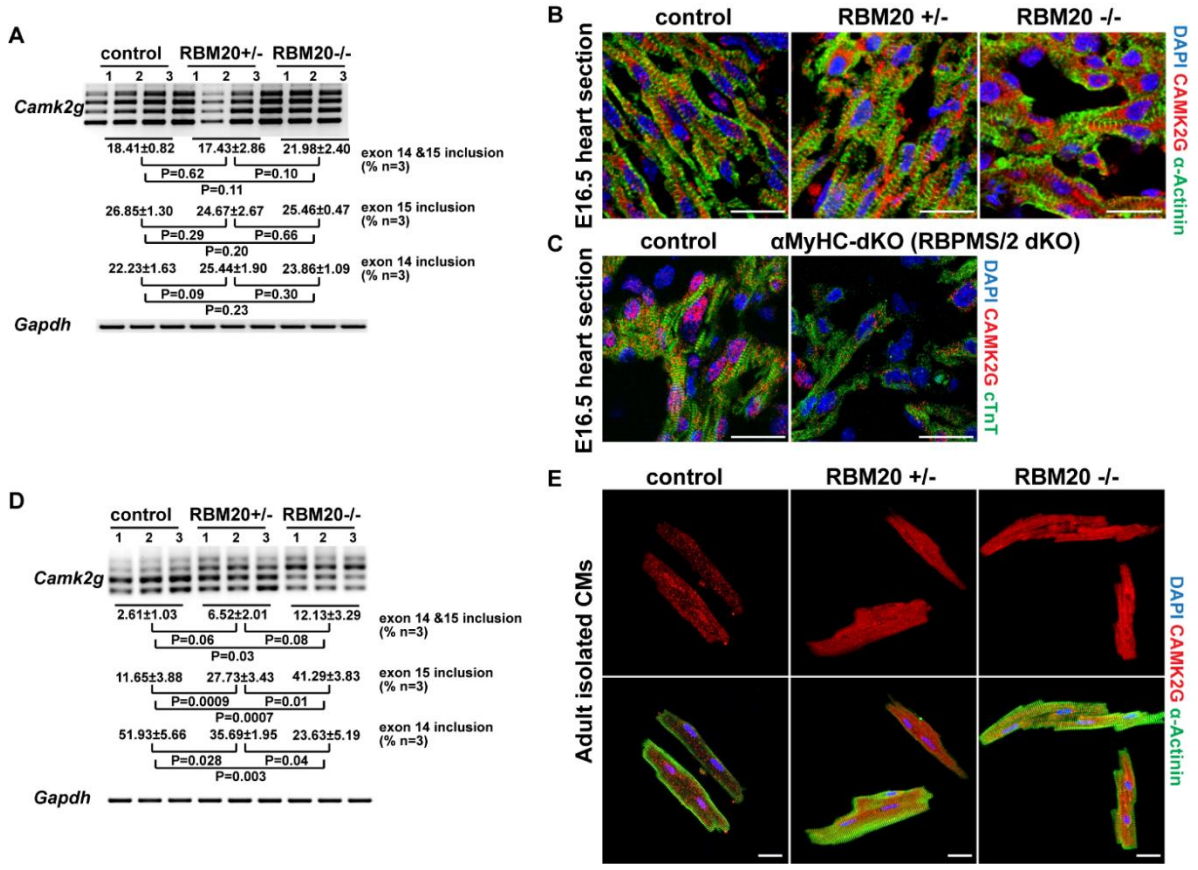

Figure 24. RBPMS/2 and RBM20 inactivation results in a stage specific reduction of the CM-specific Camk2g isoform harboring the NLS-encoding exon 14 and an alteration of the subcellular localization.

A. RT-PCR analysis of RBM20-dependent CM-specific *Camk2g* isoform alterations in the embryonic heart using mRNA from indicated RBM20 genotypes at E16.5, n=3 for each group. **B.** RBM20 inactivation has no effect on CAMK2G localization in embryonic cardiomyocytes. Immunofluorescence staining of CAMK2G, red, α-Actinin, green, and nuclei (DAPI, blue) of control (+/+), heterozygous (+/-) and homozygous (-/-) RBM20 mutant heart sections at E16.5.

Scale bar, 20 μm. **C.** RBPMS/2 inactivation results in nuclear-to-cytoplasmic mis-localization of CAMK2G in embryonic cardiomyocytes. Immunofluorescence staining of CAMK2G, red, cTnT, green, and nuclei (DAPI, blue) of control and *aMyHC-dKO* heart sections at E16.5. Scale bar, 20 μm. **D.** RT-PCR analysis of RBM20-dependent CM-specific *Camk2g* isoform alterations in adult heart using mRNA from isolated cardiomyocytes with indicated RBM20 genotypes, n=3 for each group. P-values were calculated using Student's t-test with significance set at $p \leq 0.05$. **E.** RBM20 inactivation results in a partial nuclear-to-cytoplasmic mis-localization of CAMK2G in the adult heart. Immunofluorescence staining of CAMK2G, red, α-Actinin, green, and nuclei (DAPI, blue) of isolated control (+/+), heterozygous (+/-) and homozygous (-/-) RBM20 mutant cardiomyocytes. Scale bar, 20 μm.

RBPMS/2 regulate granule formation in cardiomyocytes

The E26-related gene (ERG), a well-known transcription factor, was recently shown to have an additional function in regulating mRNA decay in higher eukaryotes (Xavier et al., 2016). Strikingly, ERG is recruited to mRNA via a physical interaction with RBPMS and CNOT2, a component of the CCR4–NOT deadenylation complex, thereby promoting mRNA decay. Co-immunostaining indicate that RBPMS/CNOT2 positive foci exactly co-localize with decapping protein1 A (DCP1A) and enhancer of mRNA decapping 4 (EDC4, HEDLS or GE-1), two well described markers for processing bodies (PBs). ERG also localizes to stress granules (SGs), a type of cytoplasmic granules, which form under stress conditions, thereby exchanging mRNP components with PBs in epithelium-derived HeLa cells. It was demonstrated that ERG triggers degradation of mRNAs associated with Aurora signaling, thereby indicating that transcription factors are directly involved in cytoplasmic mRNA decay (Rambout et al., 2016).

Since we found that RBPMS is localized in the nucleus and cytoplasm of cardiomyocytes (Figure 6 and 7) and RBPMS was previously shown to localize to PBs and SGs in Hela cells (Rambout et al., 2016), we were wondering whether RBPMS may also function in the formation of cytoplasmic granules in cardiomyocytes. Such a potential function may depend on different isoforms of RBPMS, which are either located in the nucleus and the cytoplasm (RBPMSA) or exclusively in the cytoplasm (RBPMSB) (Figure 9). To interrogate potential interactions of RBPMS with components of cytoplasmic granules, we stably overexpressed GFP-tagged RBPMSA in undifferentiated mouse embryonic stem cells and performed a GFP-based interaction screen. GO terms analysis of RBPMSA interactors revealed that enriched proteins are involved in splicing and RNA stability pathways (Figure 25A). Among the RBPMS-

interactors, we identified CCR4-NOT family members (typical PBs markers), the Ras GTPase-activating protein-binding protein (G3BP1 and 2) (typical SGs markers), as well as the DEAD-Box Helicase 6 (DDX6) (common marker for PBs and SGs) (Figure 25B) (Jonas and Izaurralde, 2015). The interaction between RBPMS and DDX6 was further validated by co-immunoprecipitation (co-IP) using N- and C-terminal GFP-tagged RBPMSA in undifferentiated mouse ES cells (Figure 25B and C) as a binding partner of RBPMSA. These results indicate a potential role of RBPMS in cytoplasmic RNP granules formation, in particular PBs and SGs.

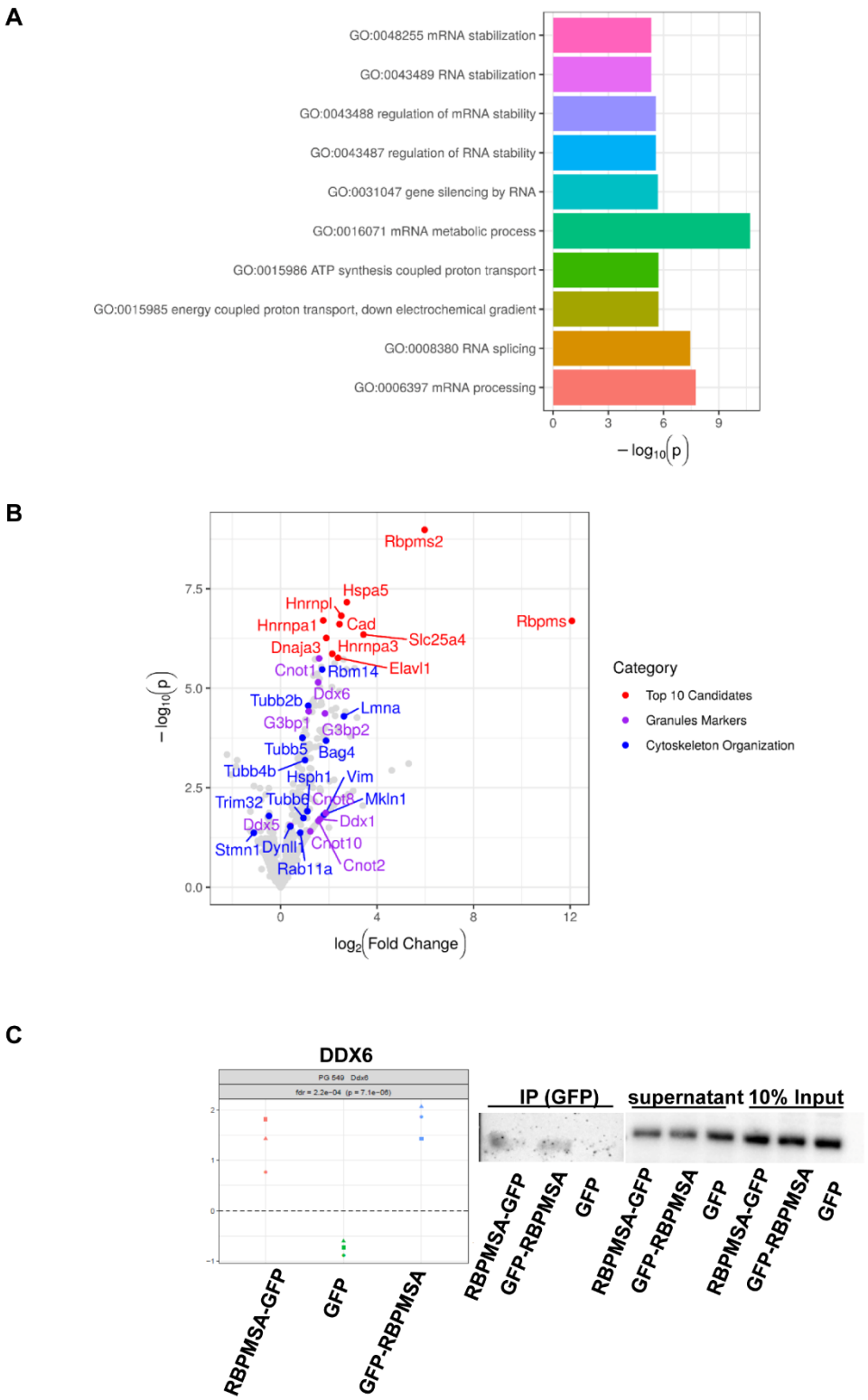

Figure 25. Enrichment analysis of RBPMSA-GFP protein interactome.

A. Barplots showing the top 10 enriched GO terms of protein-protein interaction of RBPMS-GFP (comparison of C- and N-terminal GFP tagged RBPMSA versus control GFP tags) in undifferentiated, proliferating mouse embryonic stem cells. **B.** Selected categories of the RBPMSA interactome are associated with splicing factors, red, granule markers, purple, and complex containing motor proteins (e.g., Dynll1) and cytoskeleton (eg. Tubulin) proteins, blue. **C.** RBPMSA co-factors (e.g., DDX6) identified by liquid chromatography-mass spectroscopy (LC-MS/MS) in undifferentiated mouse embryonic stem cells, left. Immunoblot analysis of anti-GFP precipitated lysates with anti-DDX6 antibody in stable RBPMSA-GFP and GFP-RBPMSA overexpression mouse ES cell lines, right. Input and IP fractions are shown.

In isolated embryonic cardiomyocytes, RBPMS predominantly localizes to the nucleus under physiological conditions, whereas a minor fraction also co-localizes to DCP1A-positive cytoplasmic PBs (Figure 26A). However, under cellular stress conditions, such as heat shock, high cellular density or myocardial infarction (Figure 6, 7 and 27), RBPMS undergoes a nuclear to cytoplasmic shift. Similarly, heat shock stress (46^{o} C/1h) initiates the translocation of RBPMS from the nucleus to the cytoplasm, where it co-localizes with G3BP1 in SGs (Figure 27A). Concomitant inactivation of RBPMS/2 in embryonic cardiomyocytes results in the formation of giant aberrant DCP1A-positive PBs under normoxic and hypoxic conditions (Figure 26B). Moreover, RBPMS/2 depleted embryonic cardiomyocytes fail to form G3BP1-positive SGs upon heat shock, indicated by reduced SG number and size (Figure 27B), indicating an essential role of RBPMS/2 in RNP-granule formation and dynamics.

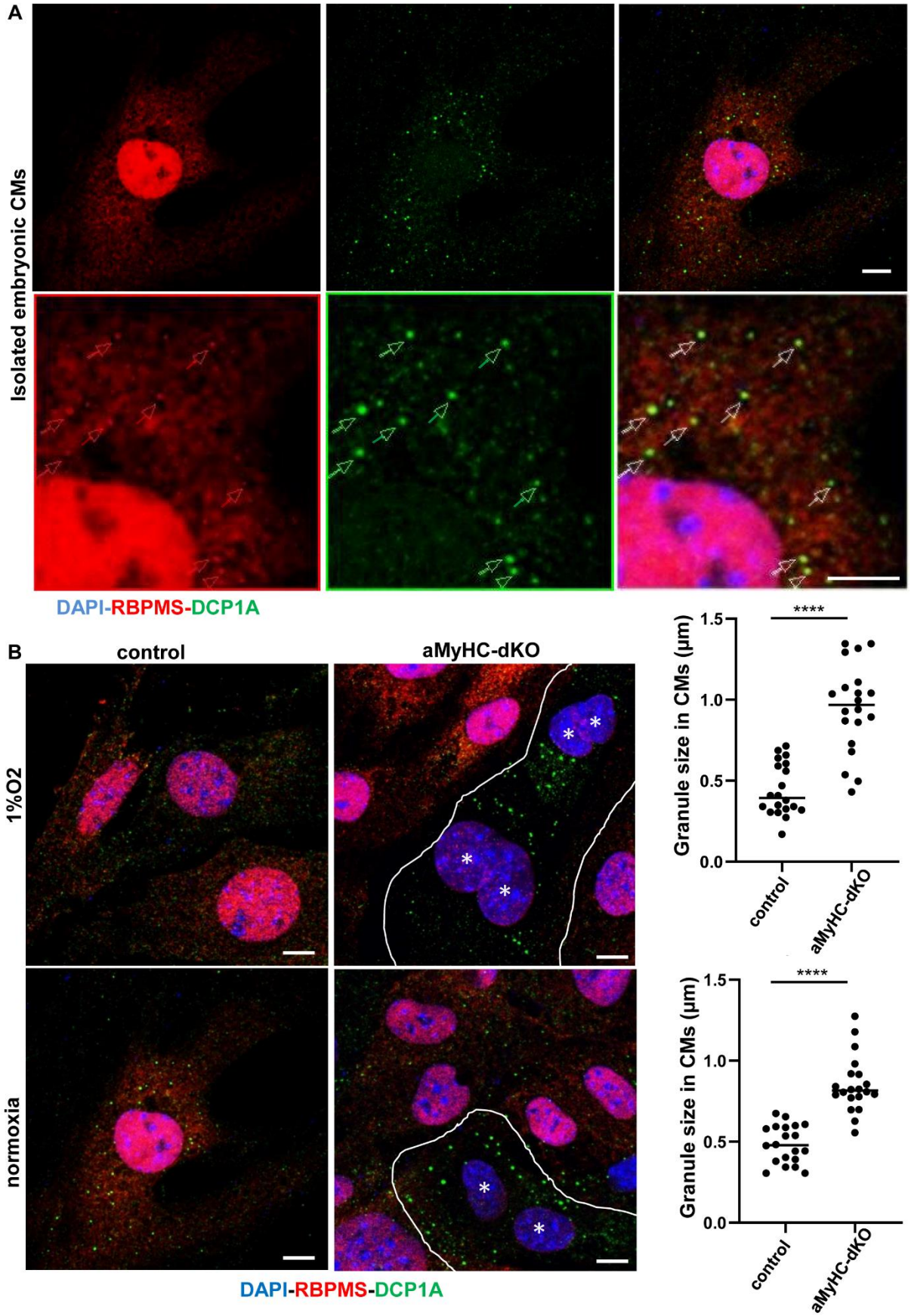
A
Isolated embryonic CMs
DAPI-RBPMS-DCP1A
B
control
aMyHC-dKO
1%O2
normoxia
DAPI-RBPMS-DCP1A
Granule size in CMs (µm)
1.5
1.0
0.5
0.0
****
control
aMyHC-dKO
Granule size in CMs (µm)
1.5
1.0
0.5
0.0
****
control
aMyHC-dKO

Figure 26. Concomitant inactivation of RBPMS/2 results in dynamic alterations of PBs.

A. Immunofluorescence staining of RBPMS, red, and DCP1A, green, in isolated wildtype embryonic cardiomyocytes (CMs) at E15.5. Scale bar =10 µm. Nuclei (DAPI, blue). Arrows highlight PBs. **B.** Immunofluorescence staining of RBPMS, red, and DCP1A, green, of isolated and cultured CMs of control and *αMyHC-dKO* at E15.5 under normoxic and hypoxic conditions. Scale bar, 10 µm. Measurement of granule diameters in cardiomyocytes, n = 20. Nuclei (DAPI, blue). Asterisks highlight RBPMS negative nuclei. Statistical significance was calculated by Student's t-test (****$p<0.0001$).

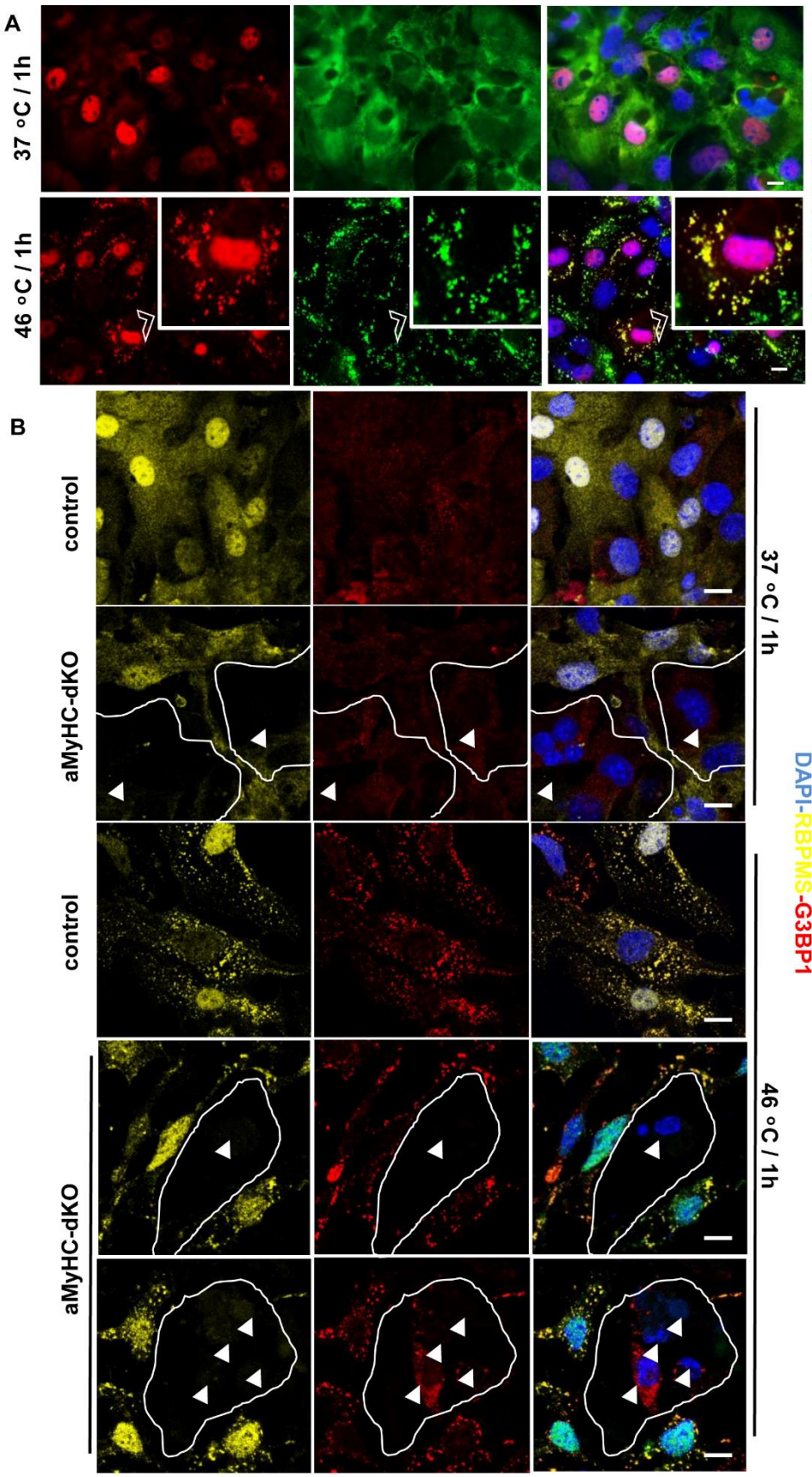
A
37 °C / 1h
46 °C / 1h
DAPI-RBPMS-G3BP1
B
control
aMyHC-dKO
control
aMyHC-dKO
37 °C / 1h
46 °C / 1h
DAPI-RBPMS-G3BP1

Figure 27. Concomitant inactivation of RBPMS/2 results in dynamic alterations of SGs formation.

A. Immunofluorescence staining of RBPMS, red, and G3BP1, green, in isolated wildtype embryonic cardiomyocytes at E15.5 under normal and heat shock stress conditions (46°C/1h). Scale bar, 10 µm. Nuclei (DAPI, blue). **B.** Immunofluorescence staining of RBPMS, red, and G3BP1, green of isolated and cultured cardiomyocytes of control and *αMyHC-dKO* hearts at E15.5 under normal and heat shock stress (46°C/1h). Arrowheads highlight RBPMS negative nuclei. Scale bar, 10µm. Nuclei (DAPI, blue).

In order to analyze the functional impact of the PB-protein DCP1A on RNP-granule formation and RBPMS inclusion, we generated a cardiomyocyte specific DCP1A knockout strain ($DCP1A^{flox/flox}$) using the constitutive active XMLC2-Cre driver (thereafter named as *DCP1A KO*). DCP1A KO mutants are viable and do not display gross morphological alterations of the heart under normal conditions (Figure 28A). Since inactivation of RBPMS/2 prevented formation of DCP1A-positive granules (Figure 26B), we also tested a potential reciprocal effect of DCP1A loss on RBPMS granules in cardiomyocytes. Apparently, loss of DCP1A in cardiomyocytes reduces levels of the RBPMS isoforms (A and B) (Figure 28B).

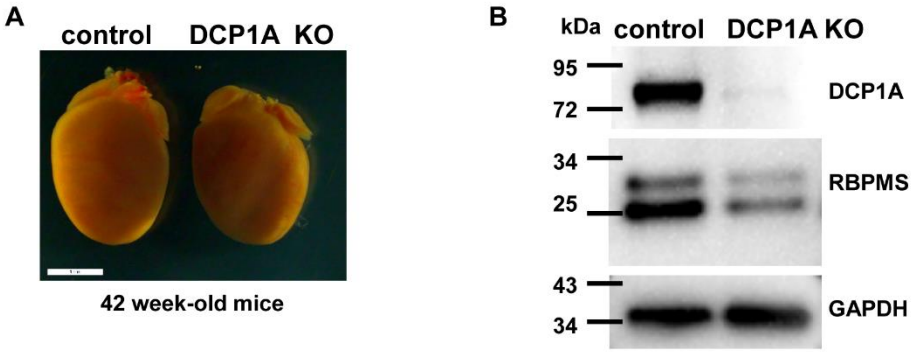

Figure 28. Cardiomyocyte specific DCP1A knockout are viable.

A. Images of dissected hearts from $DCP1A^{flox/flox}$ (control) and DCP1A KO mutant mice at 42 weeks, Scale bar, 1mm. **B.** Western blotting of control and DCP1A deficient isolated cardiomyocytes (4-week-old) using DCP1A and RBPMS specific antibodies. GAPDH was used as loading control.

Immunofluorescence staining of heart sections (Figure 29A) and isolated cardiomyocytes (Figure 29B) identified giant RBPMS-positive granules in DCP1A-deficient cardiomyocytes, which resembles the accumulation of giant DCP1A-positive granules in cardiomyocytes lacking RBPMS/2. To further characterize these giant RBPMS-positive granules, co-staining with an antibody against DDX6 was performed. Under physiological conditions, DDX6 localizes to discontinuous foci tethered to the inner membrane of adult cardiomyocytes (Figure 29A and B). In contrast, loss of DCP1A promoted a subcellular shift of DDX6 from the membrane fraction to the cytoplasm, where it partially co-localizes with RBPMS (Figure 29A and B). These findings suggest that loss of DCP1A in cardiomyocytes induces formation of giant granules in the cytoplasm that contain RBPMS and DDX6.

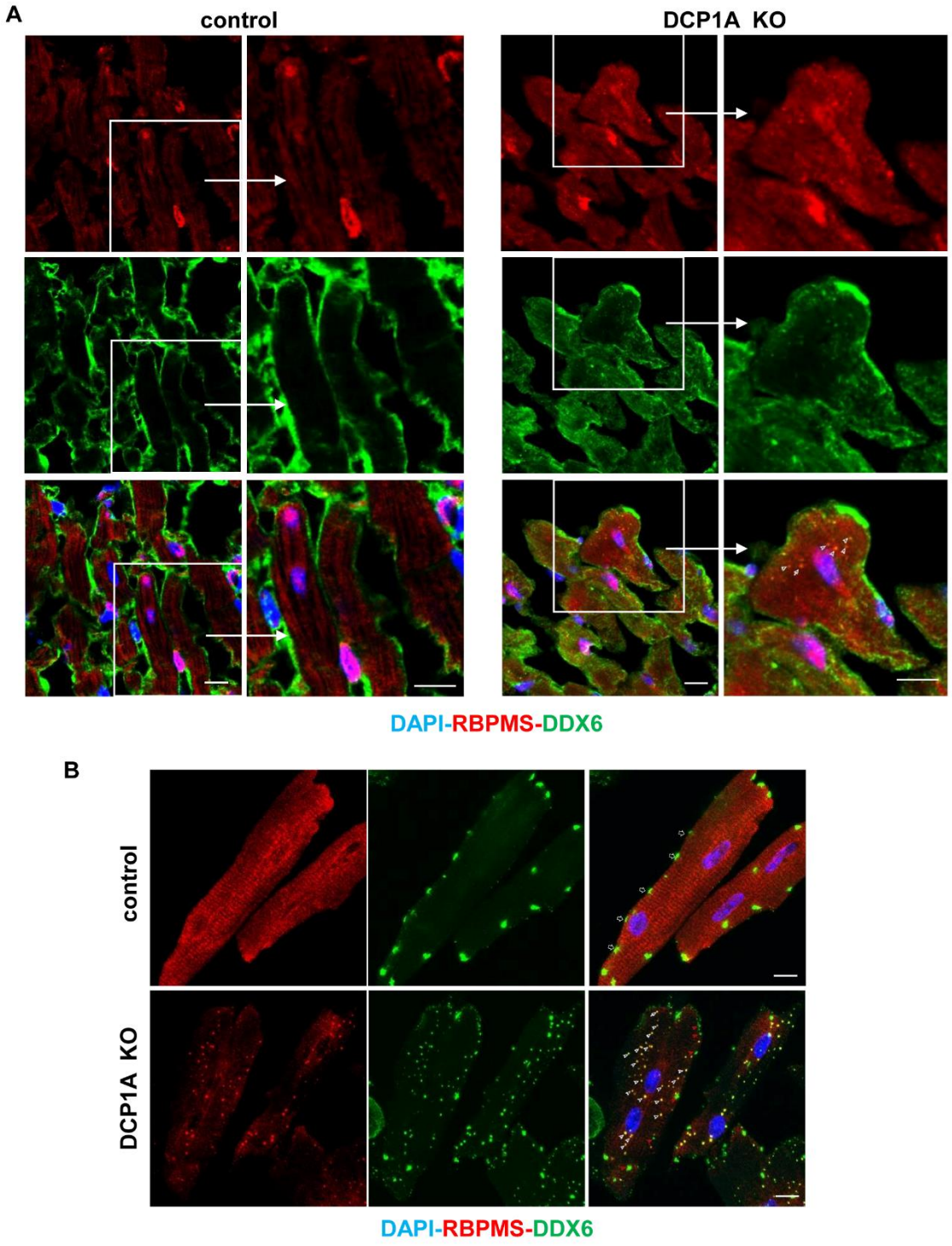

Figure 29. Aberrant giant RBPMS-positive granules co-localize with DDX6 in DCP1A deficient cardiomyocytes.

A. Immunofluorescence staining of RBPMS, red, and DDX6, green, on heart sections, 28 weeks old. Scale bar, 10 µm. Nuclei (DAPI, blue). White arrowheads highlight co-localization of DDX6 and RBPMS in DCP1A deficient cardiomyocytes. **B.** Immunofluorescence staining of RBPMS, red, and DDX6, green, of isolated control and DCP1A KO adult cardiomyocytes, 15

weeks old. Scale bar, 10 µm. Nuclei (DAPI, blue). White arrows highlight DDX6 in close vicinity to the cell membrane in control cardiomyocytes. White arrowheads highlight partial co-localizing of DDX6 and RBPMS in DCP1A deficient cardiomyocytes, red arrowheads highlight DDX6 fraction close to the cell membrane in DCP1A deficient cardiomyocytes.

In order to further characterize these atypical granules in DCP1A deficient cardiomyocytes, we performed immunofluorescence staining of isolated cardiomyocytes from control and DCP1A mutants for typical PBs (EDC4) (Figure 30A) and SGs marker (G3BP1) (Figure 30B). EDC4 is essential for decapping, providing a scaffold for DCP1A, DCP2 and XRN1 (Chang et al., 2014). The staining clearly indicated that the atypical giant RBPMS-positive granules do not contain the stress granule marker G3BP1, but the PB-marker EDC4 (Figure 30A and B). These findings suggest that DCP1A controls the composition of PBs under physiological conditions, whereas recruitment of SGs components to the atypical granules is not affected.

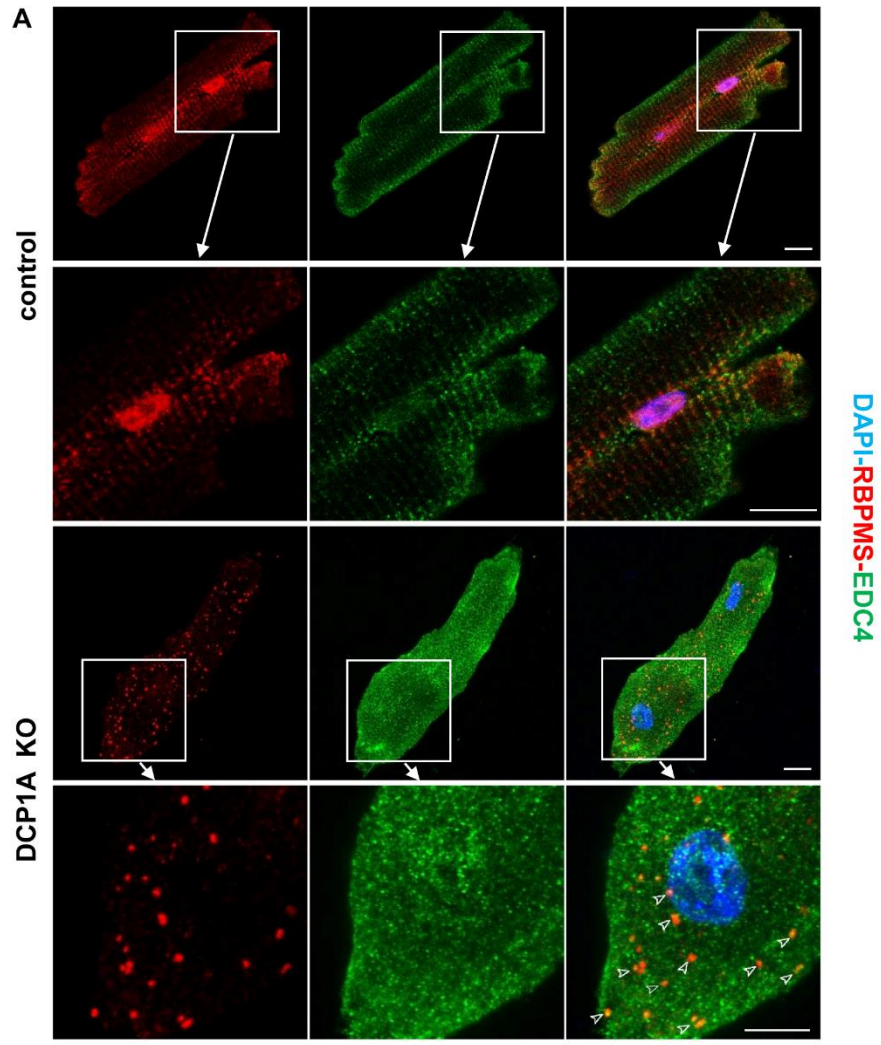
A
control
DCP1A KO
DAPI-RBPMS-EDC4

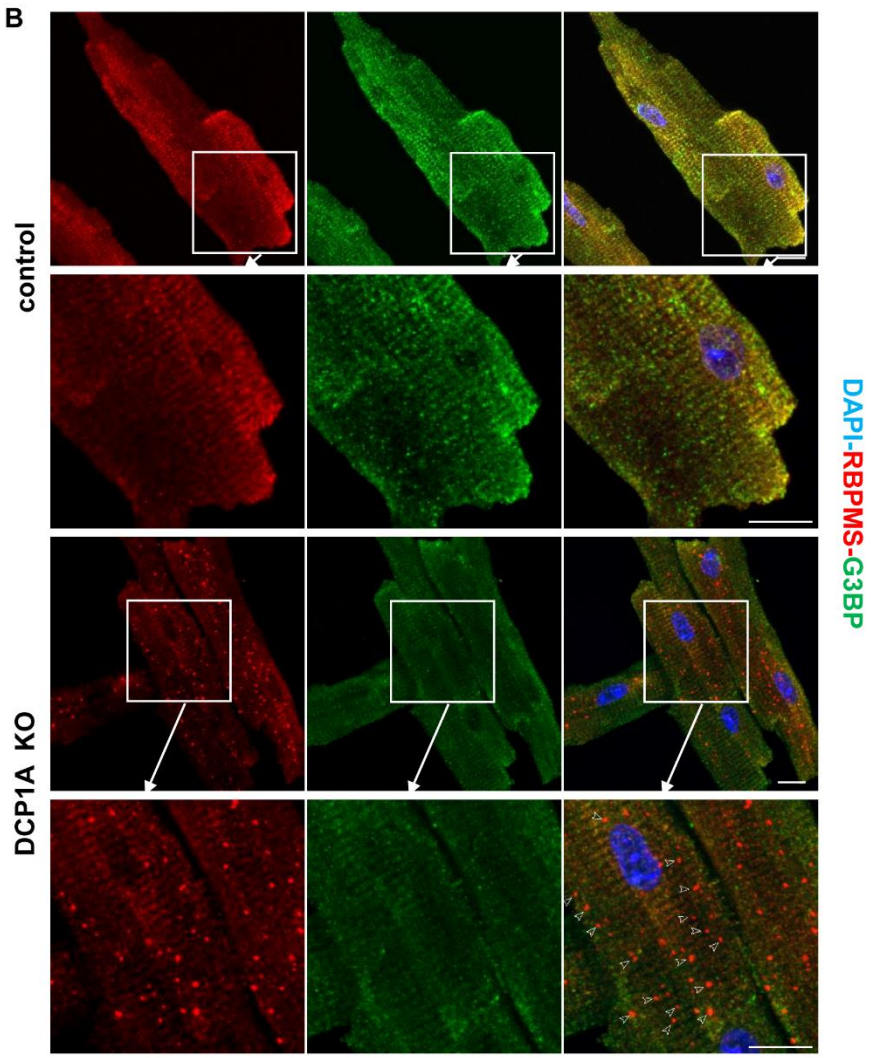

Figure 30. Altered RNP-granule composition in DCP1A deficient cardiomyocytes.

A. Immunofluorescence staining of RBPMS, red, and EDC4 (PBs marker), green, in isolated control and DCP1A KO adult cardiomyocytes. Scale bar, 10 µm. Nuclei (DAPI, blue). White arrowheads highlight co-localization of EDC4 and RBPMS in DCP1A deficient cardiomyocytes. **B.** Immunofluorescence staining of RBPMS, red, and G3BP1, green, in isolated control and DCP1A KO adult cardiomyocytes. Scale bar, 10 µm. Nuclei (DAPI, blue). White arrowheads highlight RBPMS-positive granules in DCP1A deficient cardiomyocytes.

The formation of giant PBs and the concomitant reduction of SGs, may rely on different reasons, including an altered flux of RNP granules components (Ohn et al., 2008). Directed movement of RNP granules is driven by motor proteins (Loschi et al., 2009) and involves the actin and microtubule network (Shao et al., 2017; Sweet et al., 2007). Absence of RBPMS may alter the

flux of components between the granules and the cytoplasmic pool, which is supported by the interaction of RBPMS with the motor protein Dynll1 and cytoskeleton proteins such as Tubb6 and Tubb2b (Figure 25B). Dynein and kinesin motor proteins localize to stress granules, and appear to facilitate assembly and disassembly of stress granules, respectively. IF staining clearly indicates that RBPMS aligns to the linear structure of sarcomeric actin (Figure 31A) and the tubulin cytoskeleton (Figure 31B) in isolated adult and embryonic cardiomyocytes, which further supports this hypothesis. Alternatively, RBPMS may directly affect recruitment of components to PBs and SGs, since it co-localizes with PBs and SGs (Figure 25-30). Taken together, the localization of RBPMS in PBs and SGs in cardiomyocytes as well as the interaction with motor and cytoskeleton proteins suggests that RBPMS might coordinate the interactions of motor proteins and the tubulin network to allow dynamic assembly and disassembly of RNP granules.

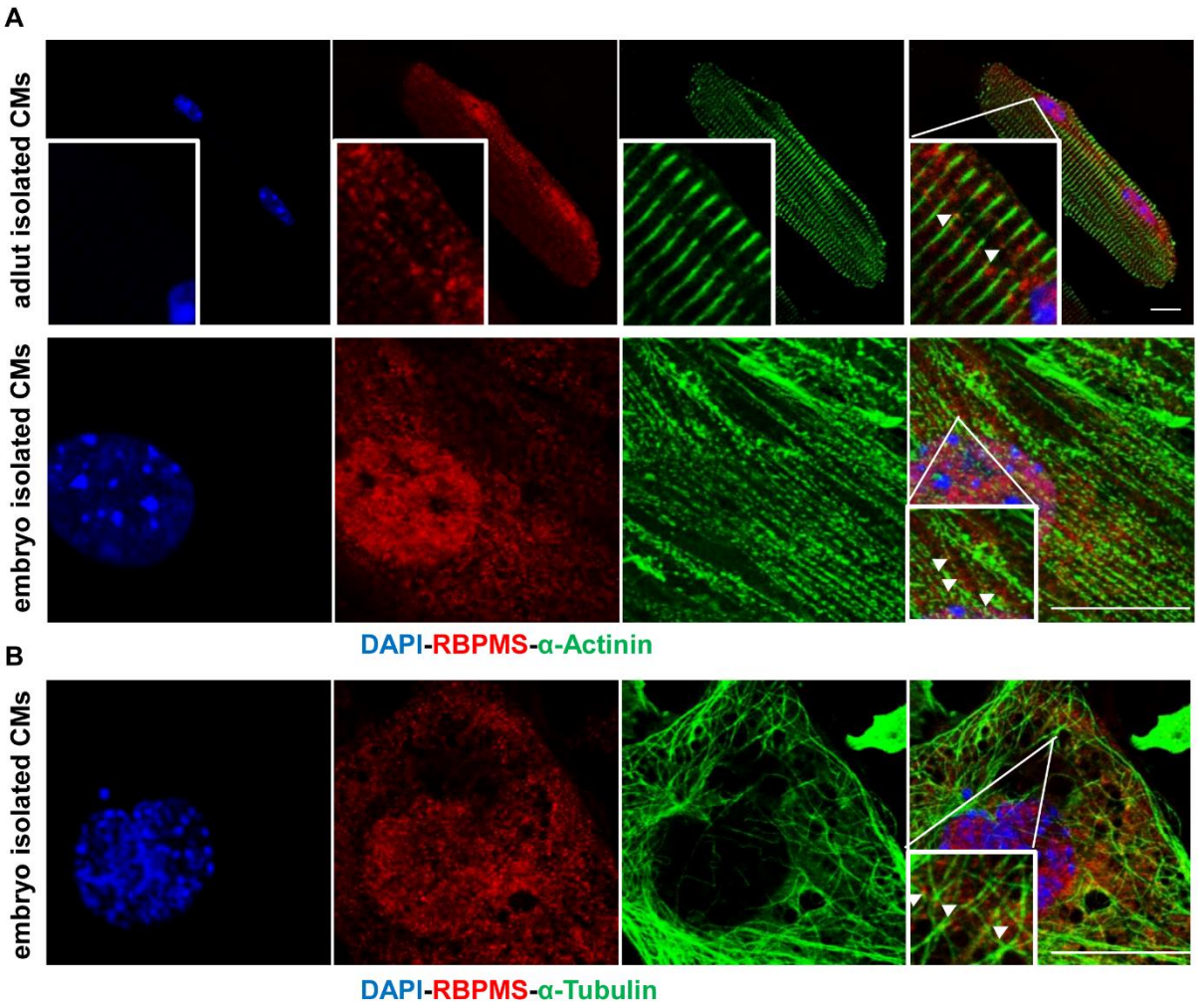

Figure 31. RBPMS-positive granules align along the cytoskeleton.

A. Immunofluorescence staining of RBPMS, red, and α-Actinin, green, of isolated and cultured adult, 15-week-old and embryonic (E11.5) cardiomyocytes. Scale bar, 10 μm. White arrowheads highlight RBPMS-positive granules aligned with α-Actinin (actin microfilament). **B.** Immunofluorescence staining of RBPMS, red, and α-Tubulin, green, of isolated embryonic cardiomyocytes at E11.5. Scale bar, 10 μm. The white arrowheads highlight the RBPMS-positive granules aligned with α-Tubulin (microtubule).

Discussion

RBPs coordinate complex alternative splicing networks during development. Since complex organs or tissues consist of multiple cell types, analysis and prediction of RBP-mediated splicing requires isolation of homogenous cell types, which sometimes is challenging due to difficulties in obtaining sufficient amounts of purified primary cells (Baralle and Giudice, 2017; Fu and Ares, 2014). During heart development, RNA splicing occurs in multiple cardiac genes (Castle et al., 2008). However only a few heart-specific splicing factors e.g., RBM20, MBNL1, RBM24, RBFOX1 and RBFOX2 as well as corresponding splicing targets have been described (Dixon et al., 2015; Gao et al., 2016; Guo et al., 2012; Kalsotra et al., 2008; Liu et al., 2019; Maatz et al., 2014; Wei et al., 2015; Yang et al., 2014). Recently, constitutive inactivation of RBPMS has been reported to regulate AS resulting in pre-mature binucleation and non-compaction cardiomyopathy (Gan et al., 2022). The results obtained in the present study are in part at odds with the report by Gan et al. Inactivation of RBPMS alone did not result in apparent cardiac defects. Conditional, concomitant inactivation of both RBPMS and RBPMS2 during heart development results in lethal cardiac defects accompanied by aberrant sarcomere organization and nuclear abnormalities, characterized by mitotic spindle and chromosome segregation defects. RBPMS/2 mutant hearts did not show typical characteristics of non-compaction cardiomyopathy, since also trabeculation was affected. Furthermore, the spindle defects in RBPMS/2 mutant cardiomyocytes did not only result in binucleation but caused genomic instability as indicated by formation of micronuclei. The analysis revealed that RBPMS/2 act both as activators and repressors of cardiac-specific splicing, depending on the localization of RBPMS/2 bindings sites in target pre-mRNAs.

Spindle organization coordinates with cytoarchitectural transitions in neonatal cardiomyocyte

Compared to embryonic stages, neonatal mouse cardiomyocytes undergo an extended S/G2/M phase (Hashimoto et al., 2014), probably due to the more rigid organization of neonatal sarcomeres (Ali et al., 2020). During the neonatal period, cardiomyocytes undergo cell cycle arrest, resulting in binucleation of up to 85% of all ventricular cardiomyocytes. Recent reports indicate that neonatal cardiomyocytes contain multiple and/or unpaired centrioles leading to multipolar spindle formation, which re-group to form pseudo-bipolar spindle, clearly different from proliferating embryonic cardiomyocytes (Becker et al., 2020; Leone and Engel, 2019). Cells containing extra centrosomes require more time for mitoses (Mercadante et al., 2019), suggesting that the extended S/G2/M phase in neonatal cardiomyocyte is determined by the

specific spindle morphology that forms during this time period. Currently, it is unclear how sarcomere maturation and multipolar spindle formation are coordinated in parallel in neonatal cardiomyocytes. In the present study, RBPMS/2 were identified as cardiac splicing factors that interconnect both processes. Mechanistically, we demonstrated that RBPMS/2 specifically regulate numerous stage-specific alternative splicing events in different pathways to safeguard the timing of cardiomyocyte structural remodelling and mitosis.

RBPMS/2 regulate AS of components of the actin cytoskeleton during heart development

Cardiac contractility is a hallmark of heart function. Abrogated cardiac contractility during development results in embryonic lethality (Sedmera et al., 2000; Waller et al., 1980). Mechanical force is generated by the motor protein myosin that slides along the actin filaments, anchored to the Z-discs at the ends of the sarcomere, thereby enabling contractile force transmission (Estigoy et al., 2009). The study reveals that RBPMS/2 play a dominant role in AS of genes coding for components of the contractile apparatus involved in sarcomere organization, actin binding as well as major cellular components of M-band, Z-discs and intercalated disc. Embryonic RBPMS/2 deficient hearts showed defects in AS of genes involved in cardiac contractile function such as *Tnnt2*, *Myom1*, *Pdlim5*, *Pdlim7*, *Ldb3*, *Tpm2*, *Sptan1*, *Popdc2* and *Myo9a*, strongly suggesting that dysregulated AS is causative for sarcomere disruption.

Troponin T (TNNT2) is the tropomyosin-binding subunit of the troponin complex, playing a key role in the interactions of actin and myosin mediating muscle contraction. During heart development, alternative splicing of *Tnnt2* switches from the embryonic isoform, characterized by inclusion of exon 5, to the adult isoform lacking exon 5 (Gomes et al., 2002; Townsend et al., 1995). The switch in AS occurs during a neonatal transition phase, in which both isoforms are co-expressed. In embryonic RBPMS/2-mutant hearts, inclusion of exon 5 into the mature mRNAs decreases dramatically, resulting in a shift to neonatal isoform ratios, indicating that RBPMS/2 act as pivotal splicing factors for the embryonic *Tnnt2* isoform. The embryonic isoform is characterized by a higher number of negatively charged residues at the N-terminus, resulting in higher Ca^{2+} sensitivity compared to the adult isoform. The isoform switches via AS are assumed to allow functional adaptations of *Tnnt2* for acquisition of physical requirements, necessary for morphogenesis and disease-related ventricular remodeling (Gomes et al., 2002; Huke and Knollmann, 2010).

Myomesin-1 (MYOM1) is an architectural component of the M-line in striated muscle, playing an important role to crosslink thick filaments with titin to the M-line and thereby maintaining structural integrity during contraction. The *Myom1* gene codes for a short and a large isoform, which includes an EH segment of about 100 amino acids in the center region, termed EH-myomesin. EH-myomesin is the predominant myomesin isoform in embryonic hearts, but rapidly declines around birth and is substituted by the short isoform lacking the EH domain (Agarkova et al., 2000). The EH domain acts as a molecular spring, similar to the PEVK domain in the long titin isoform N2BA in fetal hearts, and increases elasticity of the molecule. Around birth, myomesin and titin undergo a synchronized switch from the larger isoform to the shorter isoform, contributing to increased contraction efficiency (Agarkova and Perriard, 2005; Siedner et al., 2003). Embryonic RBPMS/2 dKO hearts show isoform ratios of *Myom1* normally only seen in neonatal hearts, which is in line with global alterations of the sarcomere structure of RBPMS/2 dKO mice.

Of note, two identified RBPMS/2 targets, namely *Tnnt2* and *Pdlim7*, bind to β-tropomyosin (TPM2), an actin binding protein essential for calcium-dependent thin filament function and muscle sarcomere contraction. *Tpm2* undergoes a mutually exclusive alternative splice event encompassing exon 6a and 6b (Dube et al., 2014; Gooding and Smith, 2008), which are dynamically regulated during the neonatal stage (Ye et al., 2013). Strikingly, RBPMS/2 deficient embryonic hearts display a global loss of exon 6a resulting in a concomitant increase of the *Tpm2* isoform containing exon 6b, thereby avoiding a premature termination codon. Cardiomyocyte specific transgenic overexpression of the *Tpm2* isoform with exon 6b causes physiological alterations in cardiac relaxation (Muthuchamy et al., 1995). Although the function of the *Tpm2* isoform comprising exon 6a and 6b still needs to be explored, our findings suggests that lack of RBPMS/2 results in a precocious switch of *Tpm2* isoforms characteristic for neonatal stages.

The mammalian genome contains ten genes**,** which contain both a PDZ domain and one or more LIM domains. These domains serve as modular protein-binding interfaces to facilitate dynamic interactions with the actin cytoskeleton and other structural components. In the study, 3 members of the Enigma subfamily identified, including *Pdlim5*, *Ldb3* and *Pdlim7*, which encode cardiac specific isoforms regulated by RBPMS/2. Mutations in the *Ldb3* gene, a well-characterized striated muscle PDZ-LIM protein, localized at Z-discs, have been previously implicated in dilated cardiomyopathy (DCM) in humans (Arimura et al., 2004; Vatta et al., 2003). Importantly, constitutive inactivation of LDB3 in mice is embryonic or perinatal lethal,

most likely due to functional failure of striated muscles, exemplified by disorganized and fragmented Z-lines in skeletal and cardiac muscles (Zhou et al., 2001). LDB3 exerts its function together with PDLIM5 at the Z-line and exists in two isoforms resulting from the mutual exclusive usage of exon 4 in cardiac muscle and exons 5–7 predominantly in skeletal muscle. However, the skeletal muscle characteristic *Ldb3* isoform is also expressed at low levels in cardiomyocytes from juvenile stage onwards. Strikingly, RBPMS/2 mutants showed a premature switch towards the skeletal muscle *Ldb3* isoform in embryonic hearts, comparable to the previously reported alterations of *Ldb3* isoforms in RBM20 (Guo et al., 2012; Maatz et al., 2014) and ASF/SF2 (Xu et al., 2005) deficient hearts. Exon 4 of LDB3 has been involved in binding to the glycolytic enzyme phosphoglucomutase 1 (PGM1). Mutations in exon 4 of LDB3 impair binding of PGM1 and result in DCM (Arimura et al., 2009).

Ablation of PDLIM5 in mouse leads to a destabilization of a protein complex at the Z line that also contains LDB3, eventually resulting in dilated cardiomyopathy (Cheng et al., 2010). A recent study by Gan et al. (2022) indicated that RBPMS regulates AS of *Pdlim5* by generating the long isoform of *Pdlim5*, thereby maintaining regular cardiomyocyte cytokinesis in the embryonic heart. Intriguingly, mis-expression of the short isoform of *Pdlim5* causes cytokinesis defects in embryonic cardiomyocytes, resulting in a premature onset of binucleation (Gan et al., 2022). Although this observation seems to indicate that defective splicing of *Pdlim5* is, at least in part, responsible for aberrant binucleation in RBPMS-mutant cardiomyocytes, several concerns remain. PDLIM5 binds to α-actinin through the PDZ domain and localizes in the Z-disk region of cardiomyocytes. PDLIM5 also interacts with the transcription factor CREB and acts as a scaffold protein for mediating PKCβ signals in cardiomyocytes. None of these functions point to a specific role in spindle formation. Thus, defective cytokinesis after overexpression of short isoform of *Pdlim5* might be secondary event and not directly caused by *Pdlim5*. In our study, the *Pdlim5* isoform switch in the embryonic heart observed by Gan et al. (2022) was found in RBPMS/2 compound mutants. However, we do not propose a direct role of *Pdlim5* in defective spindle formation but that aberrant splicing of *Camk2g* is responsible. It will be interesting to analyze whether inactivation of RBPMS alone, which in our hands does not induce defective spindle formation, is sufficient to lead to the accumulation of the short isoform of *Pdlim5*.

In addition, we identified a previously reported, functional uncharacterized mutually exclusive splicing event of *Pdlim7* exon 5 and 6 (Li et al., 2020; Yang et al., 2014), which is dramatically altered in RBPMS/2 mutant hearts. Global loss of *Pdlim7* in mouse does not disrupt cardiac

development, but causes mild cardiac dysfunction and structural valve defects in adults (Krcmery et al., 2013), indicating that this cardiac isoform of *Pdlim7* does not play a major role in cardiac development but rather fine tunes some processes.

αII spectrin (SPTAN1) is one out of two α spectrin family members, which encode cytoskeletal proteins, localized at the Z-line and intercalated discs, linking the actin-based cytoskeleton to the cell membrane (Lubbers et al., 2019). Cardiomyocyte specific SPTAN1 KO mice exhibit an age-dependent decrease in contractility, accompanied by enhanced cellular hypertrophy and fibrosis. Interestingly, these mutants show strong cardiac remodeling and increased mortality upon stimulation of cardiac hypertrophy (Lubbers et al., 2019). In our splicing analysis, we detected two isoforms, either including or excluding exon 51 at the C-terminus. In embryonic RBPMS/2 dKO hearts, the long isoform is almost completely lost, which is less pronounced in adult hearts (Zhang et al., 2010). The short isoform of *Sptan1* is characterized by a higher binding affinity to β spectrins, which restricts cardiomyocyte growth during development (Zhang et al., 2010).

Popeye domain containing (POPDC) gene family members are abundantly expressed in cardiac and skeletal muscles, encoding a distinct class of membrane-bound cyclic AMP effector proteins (Swan et al., 2019). POPDC2 localizes at the intercalated disks, near the Z-line of myofibrils and in T-tubules at the cardiac sarcolemma (Holt et al., 2020). Loss-of-function mutants develop a stress-induced sinus node bradycardia due to pacemaker dysfunction (Boukens and Christoffels, 2012; Froese et al., 2012). In juvenile DCM caused by PRMT1 deficiency, alternative splicing of *Popdc2* is deregulated (Murata et al., 2018), showing a 5`splicing site extension that normally occurs during heart development (Kalsotra et al., 2008). In embryonic RBPMS/2 mutant hearts, the developmental *Popdc2* isoform lacking the 5`splicing site extension of exon 3 is not detectable, whereas the mature *Popdc2* isoform is generated.

In addition to the RBPMS/2 splicing targets discussed above, several other cytoskeleton-related targets were identified, including MYO9A. Myosin-IXa (MYO9A), a family member of monomeric, unconventional myosins, is involved in cell polarization and in cell migration processes during development and morphogenesis (Saczko-Brack et al., 2016; Wood and Olson, 2012). In total, five alternative splicing events for *Myo9a* have been previously reported. One is located within the 5'-noncoding region, and two within the myosin head and the tail domain

region (Chieregatti et al., 1998). RBPMS/2 depleted embryonic hearts displayed an exclusion of *Myo9a* exon 27, encoding a non-defined region.

Nuclear RBPMSA isoform acts as a major regulator in AS of cardiomyocytes

RT-PCR profiling of RBPMS isoforms in different tissues and undifferentiated ES cells and ES derived cardiac bodies, identified six distinct isoforms, including two highly abundant protein isoforms (RBPMSA and RBPMSB) that share a common N-terminus, which encodes a single RNA recognition motif (RRM) domain, and a divergent short C-terminal sequence generated by alternative 3' exons. GFP-tagged RBPMS isoforms were predominantly located either in the nucleus (RBPMSA) or in the cytoplasm (RBPMSB). RBPMSB contains a predicted nuclear export signal (NES) sequence. RBPMS2, which is 70% identical to RBPMS, also contains a single RRM domain mediating RNA binding and dimerization (Sagnol et al., 2014; Teplova et al., 2016). Mice carrying only single mutation of RBPMS or RBPMS2 do not show any obvious phenotype, whereas double RBPMS/2 knockouts are embryonic lethal due to severe heart defects, indicating complementary function of both RBPs.

RBPMSA, located in the nucleus, is the predominant isoform of RBPMS in embryonic cardiomyocytes. However, RBPMSA and RBPMSB, predominantly located in the cytoplasm, are expressed at similar levels in smooth muscle cells (Nakagaki-Silva et al., 2019). Due to the nuclear localization, RBPMSA exerts most likely a predominant function in splicing, whereas RBPMSB is probably involved in RNA stability and trafficking. Future studies are necessary to explain why RBPMSA dominates in embryonic cardiomyocytes and the cytoplasmic RBPMSB form is less prominent. Comparison of RBPMS/2 loss of function mutants and RBPMSA overexpressing mice revealed that RBPMSA does not necessarily require additional heart-specific co-factors to accomplish cardiac-specific splicing. RBPMS/2 mutant hearts were defective for multiple cardiac-specific splicing events, including exon inclusion of *Tpm2* (exon 6a), *Map3k7* (exon 12), *Sptan1* (exon 51), *St7* (exon 7) as well as exon exclusion of *Camk2g* (exon 15) and *Bnip3l* (exon 6). Correspondingly, overexpression of RBPMSA was sufficient to induce all these cardiac-specific splicing events in various non-cardiac tissues during embryonic and juvenile stage. Of note, the limb and skeletal muscle are most receptive for acquisition of cardiac-specific AS events, suggesting that the efficiency of RBPMSA-directed splicing is supported by additional muscle specific RBPs, e.g., RBM20 or RBM24 (Guo et al., 2012; Yang et al., 2014).

Intriguingly, mice, in which RBPMSA is overexpressed in all tissues, are significantly smaller compared to littermate controls, accompanied by a massive reduction of the visceral white adipose tissue. Furthermore, RBPMSA expression in all cell lineages results in juvenile lethality, indicating that an induction of cardiomyocyte specific isoforms in non-cardiomyocytes is detrimental. This is in line with previous reports, demonstrating that altered splicing isoforms mediated by the enhanced expression of splicing factors promote multiple pathological changes in different cell types and tissues. For example, overexpression of SR protein family members, such as SRSF1 (Anczukow et al., 2012; Karni et al., 2007), SRSF3 (Jia et al., 2010) and SRSF6, which promote oncogenic splicing events, induces cell transformation and tumor formation (She et al., 2021). In order to identify a cell type, in which overexpression of RBPMSA generates adverse effects, we used several CRE driver strains for mediating RBPMSA overexpression in a cell lineage-specific manner. So far, none of the tested cell lineage specific RBPMSA overexpression lines, including lung and thyroid epithelium (Nkx2.1-Cre), neural crest and muscle (Pax3-Cre), blood endothelium (Tie2-Cre), muscle (Myf5-Cre and Myo-Cre), cardiomyocytes (XMLC2-Cre), kidney and thyroid epithelium and mid-hindbrain region (Pax8-Cre) as well as kidney and genitourinary epithelium (Ksp-Cre), showed obvious defects. These results suggest that juvenile lethality as well as reduction of the total body size and the visceral white adipose tissue originates from an additional cell type. Alternatively, it is also possible that minor defects occur in multiple organs, which can be compensated when present in a single but not when present in multiple tissues.

Global overexpression of RBPMSA prevented embryonic lethality and partially recuperated altered alternative splicing of exons in *RBPMS/2 dKO* mice. Notably, *RBPMSA*^{Res} mice show a reduced heart size and die prematurely during adulthood, indicating that RBPMSB and RBPMS2 exert additional posttranscriptional roles in the differentiation and maturation process of cardiomyocytes.

RBPMSA, RBPMSB and RBPMS2 showed profound differences in their ability to promote differential splicing. RBPMSA and RBPMS2 were more effective in exon inclusion compared to RBPMSB. In line with a previous study in smooth muscle cells (Nakagaki-Silva et al., 2019), RBPMS/2 regulate AS by tandem CAC motifs located in vicinity or within regulated exons. Downstream located tandem CAC motifs activate exon inclusion, whereas upstream motifs as well as motifs located in altered exons repress exon inclusion. Moreover, dispersed CAC motifs might regulate dynamic alternative splicing. In addition, we identified binding motifs of additional cardiac splicing factors adjacent to RBPMS/2 binding positions of RBPMS targeted

exons (data not show), which might recruit complexes containing additional splicing factors to alternative exons (Nakagaki-Silva et al., 2019). Analysis of RBPMS/2 loss- as well as gain-of-function mutants clearly indicate, that tight and precise regulation of cell type specific splicing factors is a requirement to establish and maintain cell type specific isoform expression serving different physiological functions.

Loss of the CAMK2G nuclear localization signal encoded by exon 14 causes mitotic defects and nuclear abnormalities in embryonic CMs

In addition to targets contributing to sarcomere structure and cytoskeleton formation, the calmodulin (CaM) binding pathway was a focus of the investigation, since CaM is highly concentrated at the mitotic spindle apparatus of dividing eukaryotic cells (Welsh et al., 1978, 1979). In budding yeast, CaM is required for the progression of nuclear division and the fidelity of chromosome segregation (Ohya and Anraku, 1989), mediated by spindle organization and spindle pole body functions (Sun et al., 1992). In addition, multifunctional Ca^{2+}/CaM-dependent protein kinases (CAMK) have been identified as mediators of cell cycle progression and implicated in every phase of the cell cycle. In particular CAMK1 regulates the G1 phase and CAMK2 mediates G2/M and metaphase-anaphase transition (Skelding et al., 2011). The *Camk2* gene family encodes four genes (a, b, d and g), which are expressed in virtually all tissues. Within the cardiovascular system, *Camk2d* and *Camk2g* have been implicated in the proliferation of vascular smooth muscle cells (House et al., 2007; Saddouk et al., 2016). Surprisingly, constitutive inactivation of either *Camk2d* or *Camk2g* does not result in an obvious phenotype in adult hearts (Kreusser et al., 2014), whereas concomitant inactivation of both genes exerts beneficial effects under pathological cardiac conditions (Cuello and Lorenz, 2016; Kreusser et al., 2014; Kreusser et al., 2016), indicating that cardiac proliferation and maturation is not affected in these mutants.

Calcium handling is crucial for optimal electrical and mechanical function of the heart and impaired when cardiac specific splicing factors are inactivated (Guo et al., 2012). *Camk2d* undergoes mutually exclusive alternative splicing utilizing three alternative exons (Exon 14, 15, and 16), which results in three isoforms containing exon 15 and 16 (*Camk2d-A*), exon 14 (*Camk2d-B*), and no alternative exons (*Camk2d-C*). It has been previously reported that the inclusion of an 11 amino acid nuclear localization signal encoded by exon 14 (*Camk2d-B* isoform) is mediated by 2 splicing factors, RBM20 as well as the general splicing factor ASF/SF2 (Guo et al., 2012; Xu et al., 2005). Inactivation of one of the two splicing factors results in *Camk2d* isoforms lacking a nuclear localization signal, which are therefore

mistargeted to the sarcolemma, causing excitation-contraction coupling defects (Guo et al., 2012; Xu et al., 2005) as well as arrhythmias (Wagner et al., 2006). Xu and co-worker (2005) demonstrated that transgenic overexpression of CAMK2D-A results in an enhanced excitation-contraction coupling by targeting T-tubules and thereby activating various Ca^{2+} channels (Xu et al., 2005). Furthermore, re-expression of CAMK2D-C in a background of global *Camk2d* deletion increases the infarct size and systolic dysfunction (Zhang et al., 2002a). In contrast, CAMK2D-B overexpression results in smaller infarct size suggesting protective effects of this isoform (Zhang et al., 2002b). RBPMS/2 deficient embryonic cardiomyocytes completely loose the nuclear isoform *Camk2d-B,* indicating subcellular localization might participate in *Camk2d* isoform-specific pathophysiological roles.

Notably, members of the CAMK2 family exert multiple functions to achieve spatial regulation of cellular activities (Xu et al., 2005). CAMK2 functions as a multimeric holoenzyme consisting of 12 subunits (Braun and Schulman, 1995), which enables fractional isoform change to influence features of the enzymatic complex (Xu et al., 2005). Indeed, we observed that murine *Camk2g* utilizes two alternative exons (exon 14 & 15) in a tissue-specific manner, eventually resulting in four isoforms in heart, which either lack or contain both exons or include either exon 14 or exon 15 (Takeuchi and Fujisawa, 1998). RBPMS/2 deficient hearts lose both heart enriched *Camk2g* isoforms containing exon 14, which contains the nuclear localization sequence, thereby resulting in nuclear-to-cytoplasmic mis-localization of CAMK2G, potentially causing mitotic defects. Of note, *Camk2g* isoforms are dynamical regulated during heart development and maturation, suggesting stage-specific functions.

To our best knowledge, the specific functions of different *Camk2g* isoforms in cardiomyocytes have not been addressed yet (Kreusser et al., 2014). In particular, the role of CAMK2G for suppressing the depolymerase activity of the mitotic centromere associated kinesin (MCAK) has not been analyzed in cardiomyocytes, although depletion of *Camk2g* in human leukemia cells results in disorganized multipolar spindles (Holmfeldt et al., 2005). MCAK is a member of the kinesin/13 family, which is required for proper chromosome segregation (Holmfeldt et al., 2005; Maney et al., 1998). The results from the study demonstrate that loss of RBPMS/2 results in exclusion of exon 14 of the *Camk2g* gene, which contains the nuclear localization signal, causing a nuclear to cytoplasmic translocation of CAMK2G and multipolar spindle defects as well as chromosome mis-segregation (e.g., unaligned / polar chromosomes). The siRNA mediated knockdown of both exon 14 containing isoforms in isolated embryonic cardiomyocytes partially phenocopies the altered nuclear morphology and defective spindle

apparatus of RBPMS/2 deficient cardiomyocytes, indicating that proper isoform composition of the CAMK2G holoenzyme is indispensable for accurate mitotic spindle formation and chromosome segregation in embryonic cardiomyocytes. The specific loss of CAMK2G in nuclei differs substantially from the complete loss of the *Camk2g* gene, which leads to a relatively mild phenotype (Kreusser et al., 2014). Apparently, accumulation of CAMK2G in the cytoplasm, parallel to depletion in nuclei has devastating effects on spindle formation, which does not happen when CAMK2G is absent throughout the cell. Of course, it is of outmost interest to perform additional studies to understand the underlying mechanisms.

It is well established, that complex and dynamic alternative splicing events, in particular mutually exclusive exons, are co-regulated by different specific splicing factors, which are expressed either permanently or dynamically. Although RBM20 is expressed during early embryonic heart development, deletion of RBM20 deficient only causes a partial loss of the *Camk2g* isoforms containing exon 14 in adult hearts. Compared to the early lethality of cardiomyocyte specific RBPMS/2 dKOs, *Rbm20* mutant mice survive until adulthood without severe abnormalities (van den Hoogenhof et al., 2018), which may be explained by unaltered inclusion of *Camk2g* exon 14 in proliferating embryonic cardiomyocytes. In contrast, RNA binding proteins of the CELF family as well as MBNL are more dynamically expressed, either from embryonic to neonatal stages (CELF1 and 2) or starting after birth (MBNL) (Kalsotra et al., 2008). A well-balanced combinatorial interplay of permanently and dynamically expressed splicing factors are the driving force for the complex and dynamic landscape of isoforms during transitions from embryonic to fetal, from fetal to neonatal, and neonatal for adult.

In summary, the study uncovered that the majority of RBPMS/2 mediated alternative splicing events are cardiomyocyte specific and / or cardiac development-related, thereby altering isoform ratios from embryonic to adult stages. The results highlight a complex RBPMS/2-orchestrated regulatory AS network that ensures maturation of the contractile apparatus and fidelity of mitosis and cytokinesis in proliferating embryonic cardiomyocytes. Concomitant loss of RBPMS and RBPMS2 results in precocious expression of dynamically regulated developmental and/or maturation-specific isoforms, thereby leading to sarcomere and proliferation defects (Figure 32). Despite these new insights, the interplay of RBPMS/2 with additional cardiomyocyte specific splicing factors for regulating isoform switches is still poorly understood and requires further attention.

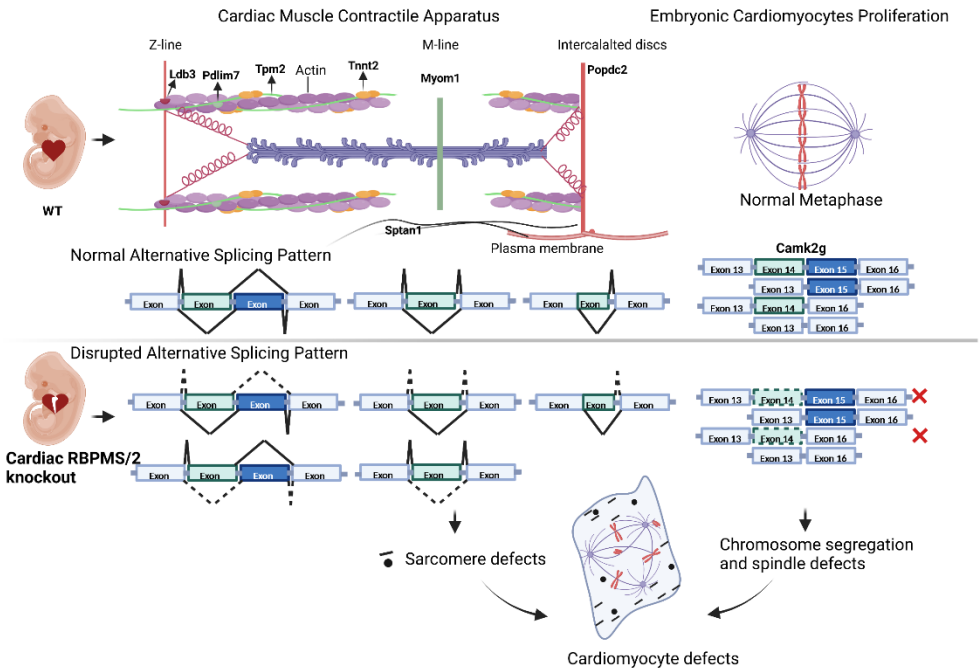

Figure 32. RBPMS/2-orchestrated regulatory AS network ensuring concomitant fidelity of the contractile apparatus as well as mitosis and cytokinesis in proliferating embryonic cardiomyocytes.

RBPMS functions in RNP-granule formation under normal and stress condition

The study mainly focused on the role of RBPMS/2 for alternative splicing in embryonic cardiomyocytes, for which RBPMS/2 play a decisive role. However, expression of the nuclear RBPMSA isoform in RBPMS/2 mutants clearly indicate, that the cytoplasmic isoform RBPMSB exerts additional functions, which are not directly related to alternative splicing.

Several RNA binding proteins play important roles in the transport, stabilization and degradation of RNAs. This includes function during assembly and disassembly of RNP granules, which employs liquid-liquid phase separation processes. Typical examples of RBPs with function in RNA splicing and RNP turnover are TDP43, RBM20, RBFOX1 and RBFOX2. TDP-43 is a component of stress-induced RNP granules, which form as cytoplasmic inclusions, representing a key pathological hallmark of degenerating neurons. The role of TDP-43 in the regulation of splicing has been attributed to either phase separation dependent or independent

mechanisms (Harrison and Shorter, 2017; Schmidt et al., 2019). Recently, a DCM-causing point mutation in RBM20, which affects the nuclear export signal of RBM20, has been implicated in the formation of cytoplasmic RBM20-positive granules (Schneider et al., 2021). This mutant version of RBM20 results in accumulation of RBM20 in DDX6-positive cytoplasmic P-bodies and in stress granules (G3BP1) during basal conditions and following acute stress, respectively (Fenix et al., 2021). In contrast, constitutive loss of RBM20 only leads to a mild phenotype in mice, which differs from the situation in rats and humans (van den Hoogenhof et al., 2018).

Other well-characterized cardiac splicing factors, such as RBFOX1 and RBFOX2 (Gao et al., 2016; Nutter et al., 2016) have also been implicated with accumulation of cytoplasmic RNP granules under stress in $S2R^{+}$ Drosophila and Hela cells, respectively, although reports for cardiomyocytes are still pending (Kucherenko and Shcherbata, 2018; Park et al., 2017). RBPs involved in the formation of aberrant cytoplasmic granules contain a prion-like or low-complexity domain (LCD), which is predicted to form intrinsically disordered regions (IDR) (Li et al., 2018). Intriguingly, RBPMS and RBPMS2 carry a putative LCD−IDR domain, in addition to the RNA recognition motif, suggesting a role in the assembly of RNP granules. Interestingly, RBPMS localizes to cytoplasmic SGs under stress conditions (Farazi et al., 2014) and to PBs under normal conditions (Rambout et al., 2016). In line with their study, we also observed that RBPMS co-localizes in isolated cardiomyocytes with the typical PB marker (DCP1A) under normal and SGs marker (G3BP1) under stress conditions.

Loss of RBPMS/2 results in formation of giant PBs in embryonic cardiomyocytes under normal conditions and even more intriguingly to a complete loss of SG formation under heat shock stress, indicating disruption of dynamic RNP granule assembly and disassembly. These observations correspond to a previous study, demonstrating that knockdown of the cyclophilin-binding protein PRPF18 (Pre-mRNA-splicing factor 18) inhibits SG formation and causes assembly of giant PBs, which blocks the directional flux of mRNA between SGs and PBs (Ohn et al., 2008).

We also demonstrated that DCP1A deficient cardiomyocytes form giant cytoplasmic RBPMS-positive granules, which contain DDX6. In control cardiomyocytes, DDX6 is specifically localized to the cardiomyocyte membrane, in areas of the intercalated discs, indicating that loss of critical RNP granule components such as RBPMS or DCP1A disrupt granule formation and affects compartmentalization of RBP, as indicated by abnormal localization of DDX6. So far,

the data suggests interactions of RBPMS with typical PBs markers, which affects the composition of RNA-containing cytoplasmic granules.

Assembly and disassembly of RNA-containing granules is associated with the cytoskeleton and related motor proteins. Live-cell imaging revealed that PBs anchor generally to microtubules. Disruption of microtubule reduces cellular motility, but also increases the size of P-Bodies and blocks formation of large SGs (Aizer et al., 2008; Kwon et al., 2007; Loschi et al., 2009; Sweet et al., 2007). In contrast to microtubules, actin bundles are less flexible, counteracting movement of PBs (Aizer et al., 2008). Dynein and kinesin motor proteins appear to facilitate assembly and disassembly of SGs, respectively. In addition, dynein proteins increase assembly of PBs under stress (Loschi et al., 2009). We found that RBPMS/2 play a key role for maintaining integrity of actin microfilaments by regulating alternative splicing of cytoskeleton components but this does not seems to be the only functions of RBPMS/2. RBPMS also binds directly to microtubules and is associated with motor proteins, suggesting pleiotropic function of RBPMS in RNP granule assembly. The alignment of RBPMS-positive granules on microtubule or actin microfilaments might be a prerequisite for the transport of RNAs or granule components to maintain a dynamic balance.

Expression of the nuclear RBPMSA isoform restored CMs-specific AS in RBPMS/2 deficient mouse cardiomyocytes (*RBPMSA*^{Res} mice), indicating that the nuclear isoform RBPMSA is the predominant mediator of AS. However, *RBPMSA*^{Res} mice show a reduced heart size and die at around 20 weeks of age, suggesting that other RBPMS isoforms, in particular the RBPMSB isoform, which contains a nuclear export signal, exerts important cytoplasmic functions independent from the regulation of alternative splicing. Comparable to the fetal stage, postnatal hearts are exposed to more physiological and environmental stressors, suggesting that stress-related processes that involve RNA-containing granules in an RBPMS-dependent manner are critical to maintain cardiomyocyte function. Such processes are disrupted in *RBPMSA*^{Res} mice, leading to precocious lethality after birth.

The increase of PB size and the loss of SGs in RBPMS/2 deficient cardiomyocytes as well as the formation of giant RBPMS-positive granules in cardiomyocytes lacking DCP1A raises many interesting questions, which need to be addressed in the future. Which functions do cytoplasmic RBPMS/2 and DCP1A exert in cardiomyocytes under normal and stress conditions? Does the loss of these components abrogate a directed flux of granule associated RNA or

protein components? What are the roles of microtubule and motor proteins in anchoring and transport of RBP-containing granules?

References

Agah, R., Frenkel, P.A., French, B.A., Michael, L.H., Overbeek, P.A., and Schneider, M.D. (1997). Gene recombination in postmitotic cells. Targeted expression of Cre recombinase provokes cardiac-restricted, site-specific rearrangement in adult ventricular muscle in vivo. J Clin Invest *100*, 169-179.

Agarkova, I., Auerbach, D., Ehler, E., and Perriard, J.C. (2000). A novel marker for vertebrate embryonic heart, the EH-myomesin isoform. J Biol Chem *275*, 10256-10264.

Agarkova, I., and Perriard, J.C. (2005). The M-band: an elastic web that crosslinks thick filaments in the center of the sarcomere. Trends Cell Biol *15*, 477-485.

Aizer, A., Brody, Y., Ler, L.W., Sonenberg, N., Singer, R.H., and Shav-Tal, Y. (2008). The Dynamics of Mammalian P Body Transport, Assembly, and Disassembly In Vivo. Molecular Biology of the Cell *19*, 4154-4166.

Ali, H., Braga, L., and Giacca, M. (2020). Cardiac regeneration and remodelling of the cardiomyocyte cytoarchitecture. FEBS J *287*, 417-438.

An, H.Y., Tan, J.T., and Shelkovnikova, T.A. (2019). Stress granules regulate stress-induced paraspeckle assembly. Journal of Cell Biology *218*, 4127-4140.

Anczukow, O., Rosenberg, A.Z., Akerman, M., Das, S., Zhan, L.X., Karni, R., Muthuswamy, S.K., and Krainer, A.R. (2012). The splicing factor SRSF1 regulates apoptosis and proliferation to promote mammary epithelial cell transformation. Nature Structural & Molecular Biology *19*, 220-228.

Anderson, P., Kedersha, N., and Ivanov, P. (2015). Stress granules, P-bodies and cancer. Biochim Biophys Acta *1849*, 861-870.

Arimura, T., Hayashi, T., Terada, H., Lee, S.Y., Zhou, Q., Takahashi, M., Ueda, K., Nouchi, T., Hohda, S., Shibutani, M., *et al.* (2004). A Cypher/ZASP mutation associated with dilated cardiomyopathy alters the binding affinity to protein kinase C. J Biol Chem *279*, 6746-6752.

Arimura, T., Inagaki, N., Hayashi, T., Shichi, D., Sato, A., Hinohara, K., Vatta, M., Towbin, J.A., Chikamori, T., Yamashina, A., *et al.* (2009). Impaired binding of ZASP/Cypher with phosphoglucomutase 1 is associated with dilated cardiomyopathy. Cardiovascular Research *83*, 80-88.

Ash, P.E., Vanderweyde, T.E., Youmans, K.L., Apicco, D.J., and Wolozin, B. (2014). Pathological stress granules in Alzheimer's disease. Brain Res *1584*, 52-58.

Ashburner, M., Ball, C.A., Blake, J.A., Botstein, D., Butler, H., Cherry, J.M., Davis, A.P., Dolinski, K., Dwight, S.S., Eppig, J.T., *et al.* (2000). Gene Ontology: tool for the unification of biology. Nature Genetics *25*, 25-29.

Ayache, J., Benard, M., Ernoult-Lange, M., Minshall, N., Standart, N., Kress, M., and Weil, D. (2015). P-body assembly requires DDX6 repression complexes rather than decay or Ataxin2/2L complexes. Molecular Biology of the Cell *26*, 2579-2595.

Bairoch, A., Bougueleret, L., Altairac, S., Amendolia, V., Auchincloss, A., Puy, G.A., Axelsen, K., Baratin, D., Blatter, M.C., Boeckmann, B., *et al.* (2007). The universal protein resource (UniProt). Nucleic Acids Research *35*, D193-D197.

Balcerak, A., Trebinska-Stryjewska, A., Konopinski, R., Wakula, M., and Grzybowska, E.A. (2019). RNA-protein interactions: disorder, moonlighting and junk contribute to eukaryotic complexity. Open Biol *9*, 190096.

Banani, S.F., Lee, H.O., Hyman, A.A., and Rosen, M.K. (2017). Biomolecular condensates: organizers of cellular biochemistry. Nat Rev Mol Cell Biol *18*, 285-298.

Baralle, F.E., and Giudice, J. (2017). Alternative splicing as a regulator of development and tissue identity. Nat Rev Mol Cell Biol *18*, 437-451.

Barry, S.P., Davidson, S.M., and Townsend, P.A. (2008). Molecular regulation of cardiac hypertrophy. Int J Biochem Cell Biol *40*, 2023-2039.

Baudoin, N.C., and Cimini, D. (2018). A guide to classifying mitotic stages and mitotic defects in fixed cells. Chromosoma *127*, 215-227.

Becker, R., Leone, M., and Engel, F.B. (2020). Microtubule Organization in Striated Muscle Cells. Cells *9*.

Bennett, V., and Baines, A.J. (2001). Spectrin and ankyrin-based pathways: Metazoan inventions for integrating cells into tissues. Physiological Reviews *81*, 1353-1392.

Bergeron-Sandoval, L.P., Safaee, N., and Michnick, S.W. (2016). Mechanisms and Consequences of Macromolecular Phase Separation. Cell *165*, 1067-1079.

Boukens, B.J., and Christoffels, V.M. (2012). Popeye proteins: muscle for the aging sinus node. J Clin Invest *122*, 810-813.

Brar, S.S., Watson, M., and Diaz, M. (2004). Activation-induced cytosine deaminase (AID) is actively exported out of the nucleus but retained by the induction of DNA breaks. J Biol Chem *279*, 26395-26401.

Brauch, K.M., Karst, M.L., Herron, K.J., de Andrade, M., Pellikka, P.A., Rodeheffer, R.J., Michels, V.V., and Olson, T.M. (2009). Mutations in Ribonucleic Acid Binding Protein Gene Cause Familial Dilated Cardiomyopathy. J Am Coll Cardiol *54*, 930-941.

Braun, A.P., and Schulman, H. (1995). The Multifunctional Calcium Calmodulin-Dependent Protein-Kinase - from Form to Function. Annu Rev Physiol *57*, 417-445.

Breckenridge, R., Kotecha, S., Towers, N., Bennett, M., and Mohun, T. (2007). Pan-myocardial expression of Cre recombinase throughout mouse development. Genesis *45*, 135-144.

Castle, J.C., Zhang, C., Shah, J.K., Kulkarni, A.V., Kalsotra, A., Cooper, T.A., and Johnson, J.M. (2008). Expression of 24,426 human alternative splicing events and predicted cis regulation in 48 tissues and cell lines. Nat Genet *40*, 1416-1425.

Chang, C.T., Bercovich, N., Loh, B., Jonas, S., and Izaurralde, E. (2014). The activation of the decapping enzyme DCP2 by DCP1 occurs on the EDC4 scaffold and involves a conserved loop in DCP1. Nucleic Acids Res *42*, 5217-5233.

Cheng, H.Q., Kimura, K., Peter, A.K., Cui, L., Ouyang, K.F., Shen, T., Liu, Y.J., Gu, Y.S., Dalton, N.D., Evans, S.M., *et al.* (2010). Loss of Enigma Homolog Protein Results in Dilated Cardiomyopathy. Circulation Research *107*, 348-U365.

Chieregatti, E., Gartner, A., Stoffler, H.E., and Bahler, M. (1998). Myr 7 is a novel myosin IX-RhoGAP expressed in rat brain. J Cell Sci *111 (Pt 24)*, 3597-3608.

Chow, L.T., Gelinas, R.E., Broker, T.R., and Roberts, R.J. (2000). An amazing sequence arrangement at the 5 ' ends of adenovirus 2 messenger RNA (Reprinted from Cell, vol 12, pg 1-12, 1977). Rev Med Virol *10*, 362-369.

Cooper, T.A., and Ordahl, C.P. (1985). A single cardiac troponin T gene generates embryonic and adult isoforms via developmentally regulated alternate splicing. J Biol Chem *260*, 11140-11148.

Corley, M., Burns, M.C., and Yeo, G.W. (2020). How RNA-Binding Proteins Interact with RNA: Molecules and Mechanisms. Mol Cell *78*, 9-29.

Cox, J., and Mann, M. (2008). MaxQuant enables high peptide identification rates, individualized p.p.b.-range mass accuracies and proteome-wide protein quantification. Nature Biotechnology *26*, 1367-1372.

Cox, J., Neuhauser, N., Michalski, A., Scheltema, R.A., Olsen, J.V., and Mann, M. (2011). Andromeda: A Peptide Search Engine Integrated into the MaxQuant Environment. J Proteome Res *10*, 1794-1805.

Cuello, F., and Lorenz, K. (2016). Inhibition of cardiac CaMKII to cure heart failure: step by step towards translation? Basic Research in Cardiology *111*.

de Lange, F.J., Moorman, A.F., Anderson, R.H., Manner, J., Soufan, A.T., de Gier-de Vries, C., Schneider, M.D., Webb, S., van den Hoff, M.J., and Christoffels, V.M. (2004). Lineage and morphogenetic analysis of the cardiac valves. Circ Res *95*, 645-654.

Derti, A., Garrett-Engele, P., Macisaac, K.D., Stevens, R.C., Sriram, S., Chen, R., Rohl, C.A., Johnson, J.M., and Babak, T. (2012). A quantitative atlas of polyadenylation in five mammals. Genome Res *22*, 1173-1183.

Deutschmeyer, V., Breuer, J., Walesch, S.K., Sokol, A.M., Graumann, J., Bartkuhn, M., Boettger, T., Rossbach, O., and Richter, A.M. (2019). Epigenetic therapy of novel tumour suppressor ZAR1 and its cancer biomarker function. Clin Epigenetics *11*.

Ding, J.H., Xu, X., Yang, D., Chu, P.H., Dalton, N.D., Ye, Z., Yeakley, J.M., Cheng, H., Xiao, R.P., Ross, J., *et al.* (2004). Dilated cardiomyopathy caused by tissue-specific ablation of SC35 in the heart. EMBO J *23*, 885-896.

Dixon, D.M., Choi, J., El-Ghazali, A., Park, S.Y., Roos, K.P., Jordan, M.C., Fishbein, M.C., Comai, L., and Reddy, S. (2015). Loss of muscleblind-like 1 results in cardiac pathology and persistence of embryonic splice isoforms. Sci Rep *5*, 9042.

Dodt, M., Roehr, J.T., Ahmed, R., and Dieterich, C. (2012). FLEXBAR-Flexible Barcode and Adapter Processing for Next-Generation Sequencing Platforms. Biology (Basel) *1*, 895-905.

Dube, D.K., McLean, M.D., Dube, S., and Poiesz, B.J. (2014). Translational control of tropomyosin expression in vertebrate hearts. Anat Rec (Hoboken) *297*, 1585-1595.

Estigoy, C.B., Ponten, F., Odeberg, J., Herbert, B., Guilhaus, M., Charleston, M., Ho, J.W.K., Cameron, D., and Dos Remedios, C.G. (2009). Intercalated discs: multiple proteins perform multiple functions in non-failing and failing human hearts. Biophys Rev *1*, 43.

Farazi, T.A., Leonhardt, C.S., Mukherjee, N., Mihailovic, A., Li, S., Max, K.E., Meyer, C., Yamaji, M., Cekan, P., Jacobs, N.C., *et al.* (2014). Identification of the RNA recognition element of the RBPMS family of RNA-binding proteins and their transcriptome-wide mRNA targets. RNA *20*, 1090-1102.

Faustino, N.A., and Cooper, T.A. (2003). Pre-mRNA splicing and human disease. Genes Dev *17*, 419-437.

Fenix, A.M., Miyaoka, Y., Bertero, A., Blue, S.M., Spindler, M.J., Tan, K.K.B., Perez-Bermejo, J.A., Chan, A.H., Mayerl, S.J., Nguyen, T.D., *et al.* (2021). Gain-of-function cardiomyopathic mutations in RBM20 rewire splicing regulation and re-distribute ribonucleoprotein granules within processing bodies. Nature Communications *12*.

Froese, A., Breher, S.S., Waldeyer, C., Schindler, R.F., Nikolaev, V.O., Rinne, S., Wischmeyer, E., Schlueter, J., Becher, J., Simrick, S., *et al.* (2012). Popeye domain containing proteins are essential for stress-mediated modulation of cardiac pacemaking in mice. J Clin Invest *122*, 1119-1130.

Fu, X.D., and Ares, M., Jr. (2014). Context-dependent control of alternative splicing by RNA-binding proteins. Nat Rev Genet *15*, 689-701.

Gan, P., Wang, Z., Morales, M.G., Zhang, Y., Bassel-Duby, R., Liu, N., and Olson, E.N. (2022). RBPMS is an RNA-binding protein that mediates cardiomyocyte binucleation and cardiovascular development. Dev Cell *57*, 959-973 e957.

Gao, C., Ren, S., Lee, J.H., Qiu, J., Chapski, D.J., Rau, C.D., Zhou, Y., Abdellatif, M., Nakano, A., Vondriska, T.M., *et al.* (2016). RBFox1-mediated RNA splicing regulates cardiac hypertrophy and heart failure. J Clin Invest *126*, 195-206.

Gerber, W.V., Vokes, S.A., Zearfoss, N.R., and Krieg, P.A. (2002). A role for the RNA-binding protein, hermes, in the regulation of heart development. Dev Biol *247*, 116-126.

Gerber, W.V., Yatskievych, T.A., Antin, P.B., Correia, K.M., Conlon, R.A., and Krieg, P.A. (1999). The RNA-binding protein gene, hermes, is expressed at high levels in the developing heart. Mech Dev *80*, 77-86.

Gilks, N., Kedersha, N., Ayodele, M., Shen, L., Stoecklin, G., Dember, L.M., and Anderson, P. (2004). Stress granule assembly is mediated by prion-like aggregation of TIA-1. Molecular Biology of the Cell *15*, 5383-5398.

Glisovic, T., Bachorik, J.L., Yong, J., and Dreyfuss, G. (2008). RNA-binding proteins and post-transcriptional gene regulation. FEBS Lett *582*, 1977-1986.

Godt, R.E., Fogaca, R.T., Silva, I.K., and Nosek, T.M. (1993). Contraction of developing avian heart muscle. Comp Biochem Physiol Comp Physiol *105*, 213-218.

Gohr, A., and Irimia, M. (2019). Matt: Unix tools for alternative splicing analysis. Bioinformatics *35*, 130-132.

Gomes, A.V., Guzman, G., Zhao, J., and Potter, J.D. (2002). Cardiac troponin T isoforms affect the Ca2+ sensitivity and inhibition of force development. Insights into the role of troponin T isoforms in the heart. J Biol Chem *277*, 35341-35349.

Gooding, C., and Smith, C.W. (2008). Tropomyosin exons as models for alternative splicing. Adv Exp Med Biol *644*, 27-42.

Grajevskaja, V., Camerota, D., Bellipanni, G., Balciuniene, J., and Balciunas, D. (2018). Analysis of a conditional gene trap reveals that tbx5a is required for heart regeneration in zebrafish. Plos One *13*.

Gumy, L.F., Katrukha, E.A., Kapitein, L.C., and Hoogenraad, C.C. (2014). New Insights into mRNA Trafficking in Axons. Dev Neurobiol *74*, 233-244.

Guo, W., Schafer, S., Greaser, M.L., Radke, M.H., Liss, M., Govindarajan, T., Maatz, H., Schulz, H., Li, S., Parrish, A.M., *et al.* (2012). RBM20, a gene for hereditary cardiomyopathy, regulates titin splicing. Nat Med *18*, 766-773.

Haas, J., Frese, K.S., Peil, B., Kloos, W., Keller, A., Nietsch, R., Feng, Z., Muller, S., Kayvanpour, E., Vogel, B., *et al.* (2015). Atlas of the clinical genetics of human dilated cardiomyopathy. Eur Heart J *36*, 1123-U1143.

Harrison, A.F., and Shorter, J. (2017). RNA-binding proteins with prion-like domains in health and disease. Biochem J *474*, 1417-1438.

Hashimoto, H., Yuasa, S., Tabata, H., Tohyama, S., Hayashiji, N., Hattori, F., Muraoka, N., Egashira, T., Okata, S., Yae, K., *et al.* (2014). Time-lapse imaging of cell cycle dynamics during development in living cardiomyocyte. Journal of Molecular and Cellular Cardiology *72*, 241-249.

Hermesh, O., and Jansen, R.P. (2013). Take the (RN)A-train: Localization of mRNA to the endoplasmic reticulum. Bba-Mol Cell Res *1833*, 2519-2525.

Holland, A.J., and Cleveland, D.W. (2012). Losing balance: the origin and impact of aneuploidy in cancer. EMBO Rep *13*, 501-514.

Holmfeldt, P., Zhang, X., Stenmark, S., Walczak, C.E., and Gullberg, M. (2005). CaMKIIgamma-mediated inactivation of the Kin I kinesin MCAK is essential for bipolar spindle formation. EMBO J *24*, 1256-1266.

Holt, I., Fuller, H.R., Schindler, R.F.R., Shirran, S.L., Brand, T., and Morris, G.E. (2020). An interaction of heart disease-associated proteins POPDC1/2 with XIRP1 in transverse tubules and intercalated discs. BMC Mol Cell Biol *21*, 88.

House, S.J., Ginnan, R.G., Armstrong, S.E., and Singer, H.A. (2007). Calcium/calmodulin-dependent protein kinase II-delta isoform regulation of vascular smooth muscle cell proliferation. Am J Physiol-Cell Ph *292*, C2276-C2287.

Huang, C., Zhou, Q., Liang, P., Hollander, M.S., Sheikh, F., Li, X., Greaser, M., Shelton, G.D., Evans, S., and Chen, J. (2003). Characterization and in vivo functional analysis of splice variants of cypher. J Biol Chem *278*, 7360-7365.

Hudmon, A., and Schulman, H. (2002). Neuronal Ca2+/calmodulin-dependent protein kinase II: The role of structure and autoregulation in cellular function. Annu Rev Biochem *71*, 473-510.

Huke, S., and Knollmann, B.C. (2010). Increased myofilament Ca2+-sensitivity and arrhythmia susceptibility. J Mol Cell Cardiol *48*, 824-833.

Jia, R., Li, C.L., Mccoy, J.P., Deng, C.X., and Zheng, Z.M. (2010). SRp20 is a proto-oncogene critical for cell proliferation and tumor induction and maintenance. Int J Biol Sci *6*, 806-826.

Johnson, B.S., Snead, D., Lee, J.J., McCaffery, J.M., Shorter, J., and Gitler, A.D. (2009). TDP-43 is intrinsically aggregation-prone, and amyotrophic lateral sclerosis-linked mutations accelerate aggregation and increase toxicity. J Biol Chem *284*, 20329-20339.

Jonas, S., and Izaurralde, E. (2015). Towards a molecular understanding of microRNA-mediated gene silencing. Nat Rev Genet *16*, 421-433.

Kalsotra, A., Xiao, X., Ward, A.J., Castle, J.C., Johnson, J.M., Burge, C.B., and Cooper, T.A. (2008). A postnatal switch of CELF and MBNL proteins reprograms alternative splicing in the developing heart. Proc Natl Acad Sci U S A *105*, 20333-20338.

Kanehisa, M., Goto, S., Sato, Y., Furumichi, M., and Tanabe, M. (2012). KEGG for integration and interpretation of large-scale molecular data sets. Nucleic Acids Research *40*, D109-D114.

Karni, R., de Stanchina, E., Lowe, S.W., Sinha, R., Mu, D., and Krainer, A.R. (2007). The gene encoding the splicing factor SF2/ASF is a proto-oncogene. Nature Structural & Molecular Biology *14*, 185-193.

Kaufman, O.H., Lee, K., Martin, M., Rothhamel, S., and Marlow, F.L. (2018). rbpms2 functions in Balbiani body architecture and ovary fate. PLoS Genet *14*, e1007489.

Kedersha, N., Chen, S., Gilks, N., Li, W., Miller, I.J., Stahl, J., and Anderson, P. (2002). Evidence that ternary complex (eIF2-GTP-tRNA(i)(Met))-deficient preinitiation complexes are core constituents of mammalian stress granules. Mol Biol Cell *13*, 195-210.

Kedersha, N., Stoecklin, G., Ayodele, M., Yacono, P., Lykke-Andersen, J., Fritzler, M.J., Scheuner, D., Kaufman, R.J., Golan, D.E., and Anderson, P. (2005). Stress granules and processing bodies are dynamically linked sites of mRNP remodeling. J Cell Biol *169*, 871-884.

Kim, E., Goren, A., and Ast, G. (2008). Alternative splicing: current perspectives. Bioessays *30*, 38-47.

Kindler, S., Wang, H., Richter, D., and Tiedge, H. (2005). RNA transport and local control of translation. Annu Rev Cell Dev Biol *21*, 223-245.

King, O.D., Gitler, A.D., and Shorter, J. (2012). The tip of the iceberg: RNA-binding proteins with prion-like domains in neurodegenerative disease. Brain Research *1462*, 61-80.

Krcmery, J., Gupta, R., Sadleir, R.W., Ahrens, M.J., Misener, S., Kamide, C., Fitchev, P., Losordo, D.W., Crawford, S.E., and Simon, H.G. (2013). Loss of the cytoskeletal protein Pdlim7 predisposes mice to heart defects and hemostatic dysfunction. PLoS One *8*, e80809.

Kreusser, M.M., Lehmann, L.H., Keranov, S., Hoting, M.O., Oehl, U., Kohlhaas, M., Reil, J.C., Neumann, K., Schneider, M.D., Hill, J.A., *et al.* (2014). Cardiac CaM Kinase II genes delta and gamma contribute to adverse remodeling but redundantly inhibit calcineurin-induced myocardial hypertrophy. Circulation *130*, 1262-1273.

Kreusser, M.M., Lehmann, L.H., Wolf, N., Keranov, S., Jungmann, A., Grone, H.J., Muller, O.J., Katus, H.A., and Backs, J. (2016). Inducible cardiomyocyte-specific deletion of CaM kinase II protects from pressure overload-induced heart failure. Basic Research in Cardiology *111*.

Kucherenko, M.M., and Shcherbata, H.R. (2018). Stress-dependent miR-980 regulation of Rbfox1/A2bp1 promotes ribonucleoprotein granule formation and cell survival. Nature Communications *9*.

Kwon, S., Zhang, Y., and Matthias, P. (2007). The deacetylase HDAC6 is a novel critical component of stress granules involved in the stress response. Genes Dev *21*, 3381-3394.

Kyburz, A., Friedlein, A., Langen, H., and Keller, W. (2006). Direct interactions between subunits of CPSF and the U2 snRNP contribute to the coupling of pre-mRNA 3' end processing and splicing. Mol Cell *23*, 195-205.

Lahmers, S., Wu, Y., Call, D.R., Labeit, S., and Granzier, H. (2004). Developmental control of titin isoform expression and passive stiffness in fetal and neonatal myocardium. Circ Res *94*, 505-513.

Langmead, B., and Salzberg, S.L. (2012). Fast gapped-read alignment with Bowtie 2. Nat Methods *9*, 357-359.

Leone, M., and Engel, F.B. (2019). Pseudo-bipolar spindle formation and cell division in postnatal binucleated cardiomyocytes. J Mol Cell Cardiol *134*, 69-73.

Lewis, B.P., Green, R.E., and Brenner, S.E. (2003). Evidence for the widespread coupling of alternative splicing and nonsense-mediated mRNA decay in humans. P Natl Acad Sci USA *100*, 189-192.

Li, D., Morales, A., Gonzalez-Quintana, J., Norton, N., Siegfried, J.D., Hofmeyer, M., and Hershberger, R.E. (2010). Identification of novel mutations in RBM20 in patients with dilated cardiomyopathy. Clin Transl Sci *3*, 90-97.

Li, L.Y., McGinnis, J.P., and Si, K. (2018). Translational Control by Prion-like Proteins. Trends in Cell Biology *28*, 494-505.

Li, M., Zhuang, Y., Batra, R., Thomas, J.D., Li, M., Nutter, C.A., Scotti, M.M., Carter, H.A., Wang, Z.J., Huang, X.S., *et al.* (2020). HNRNPA1-induced spliceopathy in a transgenic mouse model of myotonic dystrophy. Proc Natl Acad Sci U S A *117*, 5472-5477.

Li, Y.R., King, O.D., Shorter, J., and Gitler, A.D. (2013). Stress granules as crucibles of ALS pathogenesis. Journal of Cell Biology *201*, 361-372.

Liao, Y., Castello, A., Fischer, B., Leicht, S., Foehr, S., Frese, C.K., Ragan, C., Kurscheid, S., Pagler, E., Yang, H., *et al.* (2016). The Cardiomyocyte RNA-Binding Proteome: Links to Intermediary Metabolism and Heart Disease. Cell Rep *16*, 1456-1469.

Lipshitz, H.D., Claycomb, J.M., and Smibert, C.A. (2017). Post-transcriptional regulation of gene expression. Methods *126*, 1-2.

Liu, J., Kong, X., Zhang, M., Yang, X., and Xu, X. (2019). RNA binding protein 24 deletion disrupts global alternative splicing and causes dilated cardiomyopathy. Protein Cell *10*, 405-416.

Long, J.C., and Caceres, J.F. (2009). The SR protein family of splicing factors: master regulators of gene expression. Biochem J *417*, 15-27.

Lopez-Bigas, N., Audit, B., Ouzounis, C., Parra, G., and Guigo, R. (2005). Are splicing mutations the most frequent cause of hereditary disease? Febs Letters *579*, 1900-1903.

Loschi, M., Leishman, C.C., Berardone, N., and Boccaccio, G.L. (2009). Dynein and kinesin regulate stress-granule and P-body dynamics. Journal of Cell Science *122*, 3973-3982.

Lubbers, E.R., Murphy, N.P., Musa, H., Huang, C.Y., Gupta, R., Price, M.V., Han, M., Daoud, E., Gratz, D., El Refaey, M., *et al.* (2019). Defining new mechanistic roles for alphaII spectrin in cardiac function. J Biol Chem *294*, 9576-9591.

Lundquist, E.A., Herman, R.K., Rogalski, T.M., Mullen, G.P., Moerman, D.G., and Shaw, J.E. (1996). The mec-8 gene of C. elegans encodes a protein with two RNA recognition motifs and regulates alternative splicing of unc-52 transcripts. Development *122*, 1601-1610.

Maatz, H., Jens, M., Liss, M., Schafer, S., Heinig, M., Kirchner, M., Adami, E., Rintisch, C., Dauksaite, V., Radke, M.H., *et al.* (2014). RNA-binding protein RBM20 represses splicing to orchestrate cardiac pre-mRNA processing. J Clin Invest *124*, 3419-3430.

Makarenko, I., Opitz, C.A., Leake, M.C., Neagoe, C., Kulke, M., Gwathmey, J.K., del Monte, F., Hajjar, R.J., and Linke, W.A. (2004). Passive stiffness changes caused by upregulation of compliant titin isoforms in human dilated cardiomyopathy hearts. Circ Res *95*, 708-716.

Man, J., Barnett, P., and Christoffels, V.M. (2018). Structure and function of the Nppa-Nppb cluster locus during heart development and disease. Cell Mol Life Sci *75*, 1435-1444.

Maney, T., Hunter, A.W., Wagenbach, M., and Wordeman, L. (1998). Mitotic centromere-associated kinesin is important for anaphase chromosome segregation. Journal of Cell Biology *142*, 787-801.

Maris, C., Dominguez, C., and Allain, F.H.T. (2005). The RNA recognition motif, a plastic RNA-binding platform to regulate post-transcriptional gene expression. Febs Journal *272*, 2118-2131.

Mayr, C., and Bartel, D.P. (2009). Widespread Shortening of 3 ' UTRs by Alternative Cleavage and Polyadenylation Activates Oncogenes in Cancer Cells. Cell *138*, 673-684.

McAuliffe, J.J., Gao, L.Z., and Solaro, R.J. (1990). Changes in myofibrillar activation and troponin C Ca2+ binding associated with troponin T isoform switching in developing rabbit heart. Circ Res *66*, 1204-1216.

Mercadante, D.L., Crowley, E.A., and Manning, A.L. (2019). Live Cell Imaging to Assess the Dynamics of Metaphase Timing and Cell Fate Following Mitotic Spindle Perturbations. Jove-J Vis Exp.

Millevoi, S., Loulergue, C., Dettwiler, S., Karaa, S.Z., Keller, W., Antoniou, M., and Vagner, S. (2006). An interaction between U2AF 65 and CFIm links the splicing and 3 ' end processing machineries. Embo Journal *25*, 4854-4864.

Murata, K., Lu, W., Hashimoto, M., Ono, N., Muratani, M., Nishikata, K., Kim, J.D., Ebihara, S., Ishida, J., and Fukamizu, A. (2018). PRMT1 Deficiency in Mouse Juvenile Heart Induces Dilated Cardiomyopathy and Reveals Cryptic Alternative Splicing Products. iScience *8*, 200-213.

Muthuchamy, M., Grupp, I.L., Grupp, G., O'Toole, B.A., Kier, A.B., Boivin, G.P., Neumann, J., and Wieczorek, D.F. (1995). Molecular and physiological effects of overexpressing striated muscle beta-tropomyosin in the adult murine heart. J Biol Chem *270*, 30593-30603.

Muzumdar, M.D., Tasic, B., Miyamichi, K., Li, L., and Luo, L. (2007). A global double-fluorescent Cre reporter mouse. Genesis *45*, 593-605.

Nagueh, S.F., Shah, G., Wu, Y., Torre-Amione, G., King, N.M., Lahmers, S., Witt, C.C., Becker, K., Labeit, S., and Granzier, H.L. (2004). Altered titin expression, myocardial stiffness, and left ventricular function in patients with dilated cardiomyopathy. Circulation *110*, 155-162.

Nakagaki-Silva, E.E., Gooding, C., Llorian, M., Jacob, A.G., Richards, F., Buckroyd, A., Sinha, S., and Smith, C.W. (2019). Identification of RBPMS as a mammalian smooth muscle master splicing regulator via proximity of its gene with super-enhancers. Elife *8*.

Neagoe, C., Kulke, M., del Monte, F., Gwathmey, J.K., de Tombe, P.P., Hajjar, R.J., and Linke, W.A. (2002). Titin isoform switch in ischemic human heart disease. Circulation *106*, 1333-1341.

Nutter, C.A., Jaworski, E.A., Verma, S.K., Deshmukh, V., Wang, Q., Botvinnik, O.B., Lozano, M.J., Abass, I.J., Ijaz, T., Brasier, A.R., *et al.* (2016). Dysregulation of RBFOX2 Is an Early Event in Cardiac Pathogenesis of Diabetes. Cell Rep *15*, 2200-2213.

O'Connell, T.D., Rodrigo, M.C., and Simpson, P.C. (2007). Isolation and culture of adult mouse cardiac myocytes. Methods Mol Biol *357*, 271-296.

Ohn, T., Kedersha, N., Hickman, T., Tisdale, S., and Anderson, P. (2008). A functional RNAi screen links O-GlcNAc modification of ribosomal proteins to stress granule and processing body assembly. Nature Cell Biology *10*, 1224-1231.

Ohya, Y., and Anraku, Y. (1989). A Galactose-Dependent Cmd1 Mutant of Saccharomyces-Cerevisiae - Involvement of Calmodulin in Nuclear Division. Curr Genet *15*, 113-120.

Oka, T., Xu, J., and Molkentin, J.D. (2007). Re-employment of developmental transcription factors in adult heart disease. Semin Cell Dev Biol *18*, 117-131.

Olson, E.N. (2006). Gene regulatory networks in the evolution and development of the heart. Science *313*, 1922-1927.

Pagani, F., and Baralle, F.E. (2004). Genomic variants in exons and introns: identifying the splicing spoilers. Nature Reviews Genetics *5*, 389-U382.

Park, C., Choi, S., Kim, Y.E., Lee, S., Park, S.H., Adelstein, R.S., Kawamoto, S., and Kim, K.K. (2017). Stress Granules Contain Rbfox2 with Cell Cycle-related mRNAs. Sci Rep-Uk *7*.

Park, J.Y., Li, W., Zheng, D., Zhai, P., Zhao, Y., Matsuda, T., Vatner, S.F., Sadoshima, J., and Tian, B. (2011). Comparative analysis of mRNA isoform expression in cardiac hypertrophy and development reveals multiple post-transcriptional regulatory modules. PLoS One *6*, e22391.

Parker, R., and Sheth, U. (2007). P bodies and the control of mRNA translation and degradation. Mol Cell *25*, 635-646.

Poon, K.L., Tan, K.T., Wei, Y.Y., Ng, C.P., Colman, A., Korzh, V., and Xu, X.Q. (2012). RNA-binding protein RBM24 is required for sarcomere assembly and heart contractility. Cardiovascular Research *94*, 418-427.

Prabhu, S.D., and Frangogiannis, N.G. (2016). The Biological Basis for Cardiac Repair After Myocardial Infarction From Inflammation to Fibrosis. Circulation Research *119*, 91-112.

Rajabi, M., Kassiotis, C., Razeghi, P., and Taegtmeyer, H. (2007). Return to the fetal gene program protects the stressed heart: a strong hypothesis. Heart Fail Rev *12*, 331-343.

Rambout, X., Detiffe, C., Bruyr, J., Mariavelle, E., Cherkaoui, M., Brohee, S., Demoitie, P., Lebrun, M., Soin, R., Lesage, B., *et al.* (2016). The transcription factor ERG recruits CCR4-NOT to control mRNA decay and mitotic progression. Nat Struct Mol Biol *23*, 663-672.

Ray, D., Kazan, H., Cook, K.B., Weirauch, M.T., Najafabadi, H.S., Li, X., Gueroussov, S., Albu, M., Zheng, H., Yang, A., *et al.* (2013). A compendium of RNA-binding motifs for decoding gene regulation. Nature *499*, 172-177.

Ritchie, M.E., Phipson, B., Wu, D., Hu, Y.F., Law, C.W., Shi, W., and Smyth, G.K. (2015). limma powers differential expression analyses for RNA-sequencing and microarray studies. Nucleic Acids Research *43*.

Ruzicka, D.L., and Schwartz, R.J. (1988). Sequential activation of alpha-actin genes during avian cardiogenesis: vascular smooth muscle alpha-actin gene transcripts mark the onset of cardiomyocyte differentiation. J Cell Biol *107*, 2575-2586.

Saczko-Brack, D., Warchol, E., Rogez, B., Kross, M., Heissler, S.M., Sellers, J.R., Batters, C., and Veigel, C. (2016). Self-organization of actin networks by a monomeric myosin. Proc Natl Acad Sci U S A *113*, E8387-E8395.

Saddouk, F.Z., Sun, L.Y., Liu, Y.F., Jiang, M., Singer, D.V., Backs, J., Van Riper, D., Ginnan, R., Schwarz, J.J., and Singer, H.A. (2016). Ca2+/calmodulin-dependent protein kinase II-gamma (CaMKII gamma) negatively regulates vascular smooth muscle cell proliferation and vascular remodeling. Faseb Journal *30*, 1051-1064.

Sagnol, S., Yang, Y.S., Bessin, Y., Allemand, F., Hapkova, I., Notarnicola, C., Guichou, J.F., Faure, S., Labesse, G., and de Santa Barbara, P. (2014). Homodimerization of RBPMS2 through a new RRM-interaction motif is necessary to control smooth muscle plasticity. Nucleic Acids Research *42*, 10173-10184.

Schmidt, H.B., Barreau, A., and Rohatgi, R. (2019). Phase separation-deficient TDP43 remains functional in splicing. Nature Communications *10*.

Schneider, J.W., Oommen, S., Qureshi, M.Y., Goetsch, S.C., Pease, D.R., Sundsbak, R.S., Guo, W., Sun, M., Sun, H., Kuroyanagi, H., *et al.* (2021). Author Correction: Dysregulated ribonucleoprotein granules promote cardiomyopathy in RBM20 gene-edited pigs. Nat Med *27*, 1309.

Schoenauer, R., Emmert, M.Y., Felley, A., Ehler, E., Brokopp, C., Weber, B., Nemir, M., Faggian, G.G., Pedrazzini, T., Falk, V., *et al.* (2011). EH-myomesin splice isoform is a novel marker for dilated cardiomyopathy. Basic Res Cardiol *106*, 233-247.

Schukken, K.M., and Foijer, F. (2018). CIN and Aneuploidy: Different Concepts, Different Consequences. Bioessays *40*.

Sedmera, D., Pexieder, T., Vuillemin, M., Thompson, R.P., and Anderson, R.H. (2000). Developmental patterning of the myocardium. Anat Rec *258*, 319-337.

Sergeeva, I.A., Hooijkaas, I.B., Ruijter, J.M., van der Made, I., de Groot, N.E., van de Werken, H.J., Creemers, E.E., and Christoffels, V.M. (2016). Identification of a regulatory domain controlling the Nppa-Nppb gene cluster during heart development and stress. Development *143*, 2135-2146.

Shao, J., Gao, F., Zhang, B.B., Zhao, M., Zhou, Y.L., He, J.Y., Ren, L., Yao, Z., Yang, J., Su, C., *et al.* (2017). Aggregation of SND1 in Stress Granules is Associated with the Microtubule Cytoskeleton During Heat Shock Stimulus. Anatomical Record-Advances in Integrative Anatomy and Evolutionary Biology *300*, 2192-2199.

She, W.T., Shao, J., and Jia, R. (2021). Targeting Splicing Factor SRSF6 for Cancer Therapy. Front Cell Dev Biol *9*.

Shen, S., Park, J.W., Lu, Z.X., Lin, L., Henry, M.D., Wu, Y.N., Zhou, Q., and Xing, Y. (2014). rMATS: robust and flexible detection of differential alternative splicing from replicate RNA-Seq data. Proc Natl Acad Sci U S A *111*, E5593-5601.

Shimamoto, A., Kitao, S., Ichikawa, K., Suzuki, N., Yamabe, Y., Imamura, O., Tokutake, Y., Satoh, M., Matsumoto, T., Kuromitsu, J., *et al.* (1996). A unique human gene that spans over 230 kb in the human chromosome 8p11-12 and codes multiple family proteins sharing RNA-binding motifs. Proc Natl Acad Sci U S A *93*, 10913-10917.

Shin, Y., and Brangwynne, C.P. (2017). Liquid phase condensation in cell physiology and disease. Science *357*.

Siedner, S., Kruger, M., Schroeter, M., Metzler, D., Roell, W., Fleischmann, B.K., Hescheler, J., Pfitzer, G., and Stehle, R. (2003). Developmental changes in contractility and sarcomeric proteins from the early embryonic to the adult stage in the mouse heart. J Physiol *548*, 493-505.

Skelding, K.A., Rostas, J.A.P., and Verrills, N.M. (2011). Controlling the cell cycle The role of calcium/calmodulin-stimulated protein kinases I and II. Cell Cycle *10*, 631-639.

Soufari, H., and Mackereth, C.D. (2017). Conserved binding of GCAC motifs by MEC-8, couch potato, and the RBPMS protein family. RNA *23*, 308-316.

Srinivas, S., Watanabe, T., Lin, C.S., William, C.M., Tanabe, Y., Jessell, T.M., and Costantini, F. (2001). Cre reporter strains produced by targeted insertion of EYFP and ECFP into the ROSA26 locus. BMC Dev Biol *1*, 4.

Sun, G.H., Hirata, A., Ohya, Y., and Anraku, Y. (1992). Mutations in Yeast Calmodulin Cause Defects in Spindle Pole Body Functions and Nuclear Integrity. Journal of Cell Biology *119*, 1625-1639.

Swan, A.H., Gruscheski, L., Boland, L.A., and Brand, T. (2019). The Popeye domain containing gene family encoding a family of cAMP-effector proteins with important functions in striated muscle and beyond. J Muscle Res Cell M *40*, 169-183.

Sweet, T.J., Boyer, B., Hu, W.Q., Baker, K.E., and Coller, J. (2007). Microtubule disruption stimulates P-body formation. Rna *13*, 493-502.

Taegtmeyer, H., Sen, S., and Vela, D. (2010). Return to the fetal gene program: a suggested metabolic link to gene expression in the heart. Ann N Y Acad Sci *1188*, 191-198.

Takeuchi, M., and Fujisawa, H. (1998). New alternatively spliced variants of calmodulin-dependent protein kinase II from rabbit liver. Gene *221*, 107-115.

Teplova, M., Farazi, T.A., Tuschl, T., and Patel, D.J. (2016). Structural basis underlying CAC RNA recognition by the RRM domain of dimeric RNA-binding protein RBPMS. Q Rev Biophys *49*, e1.

Tourriere, H., Chebli, K., Zekri, L., Courselaud, B., Blanchard, J.M., Bertrand, E., and Tazi, J. (2003). The RasGAP-associated endoribonuclease G3BP assembles stress granules. J Cell Biol *160*, 823-831.

Townsend, P.J., Barton, P.J., Yacoub, M.H., and Farza, H. (1995). Molecular cloning of human cardiac troponin T isoforms: expression in developing and failing heart. J Mol Cell Cardiol *27*, 2223-2236.

Valverde, R., Edwards, L., and Regan, L. (2008). Structure and function of KH domains. Febs Journal *275*, 2712-2726.

van den Hoogenhof, M.M., Pinto, Y.M., and Creemers, E.E. (2016). RNA Splicing: Regulation and Dysregulation in the Heart. Circ Res *118*, 454-468.

van den Hoogenhof, M.M.G., Beqqali, A., Amin, A.S., van der Made, I., Aufiero, S., Khan, M.A.F., Schumacher, C.A., Jansweijer, J.A., van Spaendonck-Zwarts, K.Y., Remme, C.A., *et al.* (2018). RBM20 Mutations Induce an Arrhythmogenic Dilated Cardiomyopathy Related to Disturbed Calcium Handling. Circulation *138*, 1330-1342.

Vanderweyde, T., Yu, H., Varnum, M., Liu-Yesucevitz, L., Citro, A., Ikezu, T., Duff, K., and Wolozin, B. (2012). Contrasting pathology of the stress granule proteins TIA-1 and G3BP in tauopathies. J Neurosci *32*, 8270-8283.

Vatta, M., Mohapatra, B., Jimenez, S., Sanchez, X., Faulkner, G., Perles, Z., Sinagra, G., Lin, J.H., Vu, T.M., Zhou, Q., *et al.* (2003). Mutations in Cypher/ZASP in patients with dilated cardiomyopathy and left ventricular non-compaction. J Am Coll Cardiol *42*, 2014-2027.

Wagner, S., Dybkova, N., Rasenack, E.C., Jacobshagen, C., Fabritz, L., Kirchhof, P., Maier, S.K., Zhang, T., Hasenfuss, G., Brown, J.H., *et al.* (2006). Ca2+/calmodulin-dependent protein kinase II regulates cardiac Na+ channels. J Clin Invest *116*, 3127-3138.

Wahl, M.C., Will, C.L., and Luhrmann, R. (2009). The Spliceosome: Design Principles of a Dynamic RNP Machine. Cell *136*, 701-718.

Waller, B.F., Smith, E.R., Blackbourne, B.D., Arce, F.P., Sarkar, N.N., and Roberts, W.C. (1980). Congenital hypoplasia of portions of both right and left ventricular myocardial walls. Clinical and necropsy observations in two patients with parchment heart syndrome. Am J Cardiol *46*, 885-891.

Wang, A., Conicella, A.E., Schmidt, H.B., Martin, E.W., Rhoads, S.N., Reeb, A.N., Nourse, A., Ramirez Montero, D., Ryan, V.H., Rohatgi, R., *et al.* (2018a). A single N-terminal phosphomimic disrupts TDP-43 polymerization, phase separation, and RNA splicing. EMBO J *37*.

Wang, B., Zhang, L., Dai, T., Qin, Z., Lu, H., Zhang, L., and Zhou, F. (2021). Liquid-liquid phase separation in human health and diseases. Signal Transduct Target Ther *6*, 290.

Wang, E.T., Sandberg, R., Luo, S., Khrebtukova, I., Zhang, L., Mayr, C., Kingsmore, S.F., Schroth, G.P., and Burge, C.B. (2008). Alternative isoform regulation in human tissue transcriptomes. Nature *456*, 470-476.

Wang, G.S., and Cooper, T.A. (2007). Splicing in disease: disruption of the splicing code and the decoding machinery. Nat Rev Genet *8*, 749-761.

Wang, H., Chen, Y., Li, X., Chen, G., Zhong, L., Chen, G., Liao, Y., Liao, W., and Bin, J. (2016). Genome-wide analysis of alternative splicing during human heart development. Sci Rep *6*, 35520.

Wang, J., Choi, J.M., Holehouse, A.S., Lee, H.O., Zhang, X., Jahnel, M., Maharana, S., Lemaitre, R., Pozniakovsky, A., Drechsel, D., *et al.* (2018b). A Molecular Grammar Governing the Driving Forces for Phase Separation of Prion-like RNA Binding Proteins. Cell *174*, 688-699 e616.

Weeland, C.J., van den Hoogenhof, M.M., Beqqali, A., and Creemers, E.E. (2015). Insights into alternative splicing of sarcomeric genes in the heart. J Mol Cell Cardiol *81*, 107-113.

Wei, C., Qiu, J., Zhou, Y., Xue, Y., Hu, J., Ouyang, K., Banerjee, I., Zhang, C., Chen, B., Li, H., *et al.* (2015). Repression of the Central Splicing Regulator RBFox2 Is Functionally Linked to Pressure Overload-Induced Heart Failure. Cell Rep *10*, 1521-1533.

Welsh, M.J., Dedman, J.R., Brinkley, B.R., and Means, A.R. (1978). Calcium-Dependent Regulator Protein - Localization in Mitotic Apparatus of Eukaryotic Cells. P Natl Acad Sci USA *75*, 1867-1871.

Welsh, M.J., Dedman, J.R., Brinkley, B.R., and Means, A.R. (1979). Tubulin and Calmodulin - Effects of Microtubule and Microfilament Inhibitors on Localization in the Mitotic Apparatus. Journal of Cell Biology *81*, 624-634.

Wood, J.M., and Olson, M.F. (2012). Collective migration: spatial tension relief. Curr Biol *22*, R125-127.

Woodcock-Mitchell, J., Mitchell, J.J., Low, R.B., Kieny, M., Sengel, P., Rubbia, L., Skalli, O., Jackson, B., and Gabbiani, G. (1988). Alpha-smooth muscle actin is transiently expressed in embryonic rat cardiac and skeletal muscles. Differentiation *39*, 161-166.

Xiao, R., Sun, Y., Ding, J.H., Lin, S.R., Rose, D.W., Rosenfeld, M.G., Fu, X.D., and Li, X. (2007). Splicing regulator SC35 is essential for genomic stability and cell proliferation during mammalian organogenesis. Mol Cell Biol *27*, 5393-5402.

Xu, X., Yang, D., Ding, J.H., Wang, W., Chu, P.H., Dalton, N.D., Wang, H.Y., Bermingham, J.R., Jr., Ye, Z., Liu, F., *et al.* (2005). ASF/SF2-regulated CaMKIIdelta alternative splicing temporally reprograms excitation-contraction coupling in cardiac muscle. Cell *120*, 59-72.

Yang, J., Hung, L.H., Licht, T., Kostin, S., Looso, M., Khrameeva, E., Bindereif, A., Schneider, A., and Braun, T. (2014). RBM24 is a major regulator of muscle-specific alternative splicing. Dev Cell *31*, 87-99.

Ye, J., Llorian, M., Cardona, M., Rongvaux, A., Moubarak, R.S., Comella, J.X., Bassel-Duby, R., Flavell, R.A., Olson, E.N., Smith, C.W., *et al.* (2013). A pathway involving HDAC5, cFLIP and caspases regulates expression of the splicing regulator polypyrimidine tract binding protein in the heart. J Cell Sci *126*, 1682-1691.

Zhang, T., Dalton, N., Maier, L.S., Gu, Y.S., Bers, D.M., Ross, J., and Brown, J.H. (2002a). The delta(c) isoform of CaMKII is activated in cardiac hypertrophy and induces dilated cardiomyopathy and heart failure. Circulation *106*, 255-255.

Zhang, T., Johnson, E.N., Gu, Y.S., Morissette, M.R., Sah, V.P., Gigena, M.S., Belke, D.D., Dillmann, W.H., Rogers, T.B., Schulman, H., *et al.* (2002b). The cardiac-specific nuclear delta(B) isoform of Ca2+/calmodulin-dependent protein kinase II induces hypertrophy and dilated cardiomyopathy associated with increased protein phosphatase 2A activity. Journal of Biological Chemistry *277*, 1261-1267.

Zhang, Y., Resneck, W.G., Lee, P.C., Randall, W.R., Bloch, R.J., and Ursitti, J.A. (2010). Characterization and expression of a heart-selective alternatively spliced variant of alpha II-spectrin, cardi+, during development in the rat. J Mol Cell Cardiol *48*, 1050-1059.

Zhou, H.L., Mangelsdorf, M., Liu, J.H., Zhu, L., and Wu, J.Y. (2014). RNA-binding proteins in neurological diseases. Sci China Life Sci *57*, 432-444.

Zhou, Q., Chu, P.H., Huang, C., Cheng, C.F., Martone, M.E., Knoll, G., Shelton, G.D., Evans, S., and Chen, J. (2001). Ablation of Cypher, a PDZ-LIM domain Z-line protein, causes a severe form of congenital myopathy. J Cell Biol *155*, 605-612

List of tables

List of figures

List of abbreviation

µm	Micrometer
%	Percent
3D	Three-dimensional
aa	Amino acids
A5SS	alternative 5’ splice site
A3SS	alternative 3’ splice site
ACTA1	actin alpha 1, skeletal muscle
ACTA2	actin alpha 2, skeletal muscle
Ad	Adenovirus
AD	Alzheimer’s disease
ALS	Amyotrophic lateral sclerosis
ATP	Adenosine 5′-triphosphate
APS	Ammoniumperoxodisulfat
AS	Alternative splicing
ASF/SF2	SR protein family member alternative splicing factor 2
bp	Base pairs
BSA	Bovine serum albumin
BW	Body weight
°C	Degrees celcius
C57bl/6	C57 black 6 mice
CAMK2D	calcium/calmodulin dependent kinase II delta
CAMK2G	calcium/calmodulin dependent kinase II gamma
cDNA	Complementary deoxyribonucleic acid
CMV	Cytomegalovirus
CO2	Carbon dioxide
DAPI	4’,6-diamidino-2-phenylindole
DCM	Dilated cardiomyopathy
ddH2O	Double distilled water
DMEM	Dulbecco Modified Eagle Medium

DMSO	Dimethyl sulfoxide
DNA	Deoxyribonucleic acid
dNTPs	Nucleoside triphosphate
DTA	Subunit of the diphtheria toxin gene
DTT	1,4-Dithiothreit
E	Exon
E11.5	Embryonic day 11.5
E14.5	Embryonic day 14.5
EBs	Embryonic stem cell drived bodies
EDTA	Ethylenediaminetetraacetic acid
eGFP	Enhanced green fluorescent protein
EM	Electron microscopy
ER	Endoplasmic reticulum
ES	Exon skipping
ES cell	Embryonic stem cell
EtOH	Ethanol
FC	Fold change
FCS	Fetal calf serum
For	Forward
GAPDH	Glyceraldehyde 3-phosphate dehydrogenase
GO	Gene Ontology
KH	K homology
H&E	Hematoxylin & eosin
H1299	Human non-small cell lung carcinoma cell line derived from the lymph node
HEK293	Human embryonic kidney cells 293
hnRNPK	Heterogeneous nuclear ribonucleoprotein K
Hs	Human
ID	Intercalated disk
IgG	Immunoglobulin G
IP	Immunoprecipitation
kDa	Kilo Dalton

kg	Kilogram
LC-MS/MS	Liquid chromatography–mass spectrometry
mg	Milligrams
min	Minutes
MBNL1	Muscle blind like splicing regulator
MTOC	Microtubule-organizing center
MXE	Mutually exclusive exon
NaCl	Sodium chloride
NB	Nuclear body
Neo	Neomycin
NMD	Nonsense-mediated mRNA decay
nm	Nanometers
ORF	Open reading frame
P0	Postnatal day 0
PB	Processing body
PBS	Phosphate-buffered saline
PCR	Polymerase chain reaction
PFA	Paraformaldehyde
PMSF	Phenylmethylsulfonyl fluoride
pre-mRNA	precursor messenger RNA
qRT-PCR	Quantitative reverse transcription PCR
RBPMS	RNA binding protein with multiple splicing
Rev	Reverse
RNA	Ribonucleic acid
RNP	Ribonucleoprotein
RI	Retained intron
RRM	RNA recognition motif
RT	Room temperature
RT-PCR	Reverse transcription PCR
ssRNA	Single-stranded RNA
S	Second

SE	Skipped exon
SDS	Sodium dodecyl sulfate
snRNAs	Small nuclear RNAs
sqRT-PCR	Semi-quantitative reverse transcription PCR
SG	Stress granules
TAE	Tris-acetate-EDTA
TBS	Tris-buffered saline
TBS-T	Tris-buffered saline / Tween-20
TE	Tris-EDTA
TEMED	Tetramethylethylenediamine
TNNI3	Troponin I, cardiac muscle
TNNT2	Cardiac muscle troponin T
TPM2	Tropomyosin alpha-2 chain
Ttn	Titin
UTRs	Untranslated regions
UV	Ultraviolet
WT	Wildtype
XMLC2	Xenopus laevis light chain 2
α-MyHC	α-Myosin heavy chain